2016

FRP Shear Transfer Reinforcement for Composite Concrete Construction

Jehad Alkatan
University of Windsor

FRP Shear Transfer Reinforcement for Composite Concrete Construction

By

Jehad Alkatan

A Thesis
Submitted to the Faculty of Graduate Studies
through the Department of Civil & Environmental Engineering
in Partial Fulfillment of the Requirements for
the Degree of Master of Applied Science at the
at the University of Windsor

Windsor, Ontario, Canada

2016

FRP Shear Transfer Reinforcement for Composite Concrete Construction

By

Jehad Alkatan

APPROVED BY:

_____

N. Zamani, Outside Dept. Reader
Department of Mechanical, Automotive & Materials Engineering

_____

S. Cheng, Dept. Reader
Department of Civil and Environmental Engineering

_____

F. Ghrib, Principal Advisor
Department of Civil and Environmental Engineering

_____

A. El Ragaby, Co-Advisor
Department of Civil and Environmental Engineering

June 13, 2016

DECLARATION OF ORIGINALITY

I hereby certify that I am the sole author of this thesis and that no part of this thesis has been published or submitted for publication.

I certify that, to the best of my knowledge, my thesis does not infringe upon anyone's copyright nor violate any proprietary rights and that any ideas, techniques, quotations, or any other material from the work of other people included in my thesis, published or otherwise, are fully acknowledged in accordance with the standard referencing practices. Furthermore, to the extent that I have included copyrighted material that surpasses the bounds of fair dealing within the meaning of the Canada Copyright Act, I certify that I have obtained a written permission from the copyright owner(s) to include such material(s) in my thesis and have included copies of such copyright clearances to my appendix.

I declare that this is a true copy of my thesis, including any final revisions, as approved by my thesis committee and the Graduate Studies office, and that this thesis has not been submitted for a higher degree to any other University or Institution.

ABSTRACT

Composite precast concrete girders supporting cast-in-place slabs are widely used in Accelerated Bridge Construction. The steel reinforcement provided across the interface, to ensure full composite action, is susceptible to sever corrosion especially when de-icing chemicals are used. This research project is exploring an innovative and sustainable application of the non-corrodible Glass Fiber Reinforced Polymer (GFRP) as shear transfer reinforcement in composite elements. Twenty large scale push-off specimens, each consists of two L-shaped concrete blocks cast at different times, were constructed and tested to investigate the effects of the axial stiffness and shape of the GFRP reinforcement in addition to the concrete compressive strength. The ultimate strength, relative slip, lateral separation and reinforcement strain were reported in this study. Test results showed the effectiveness of the GFRP shear friction reinforcement compared to steel. A new shear friction model for the ultimate shear transfer of interfaces intersected by GFRP reinforcement is introduced.

ACKNOWLEDGEMENTS

I am very thankful to my supervisors, Dr. Amr El Ragaby and Dr. Faouzi Ghrib for their guidance and constant help and support during the entire course of this program.

I would like to thank my committee members, Dr. Nader Zamani and Dr. Shaohong Cheng.

The help received from the technical staff of the Structural Laboratory of the Department of Civil and Environmental Engineering at the University of Windsor is also acknowledged.

Thanks are to all of my fellow graduate students in the Department of Civil and Environmental Engineering for their help in the test program.

The support of GFRP materials provided by Pultrall Inc. is gratefully appreciated and acknowledged.

I am very much grateful to my parents and brothers for their continuous help and support.

I would like to express my sincere and deepest appreciation to my wife who has shown constant encouragement, support and patience without which I would not have taken up and completed this study.

TABLE OF CONTENTS

LIST OF TABLES

LIST OF FIGURES

LIST OF SYMBOLS

A_{cv} = area of the concrete section resisting shear transfer

A_{vf} = area of the reinforcement crossing the shear plane

A_{vmin} = minimum area of shear transfer reinforcement

b_v = width of the cross section at the level under consideration

c = cohesion stress of the interface surface in MPa

C_f = total factored compressive force in the cast-in-place slab along the considered beam segment

d = effective depth of the beam cross section

E_F = modulus of elasticity of GFRP reinforcement

E_s = modulus of elasticity of steel reinforcement

f_c' = concrete compressive strength

f_{ctd} = design tensile strength of the concrete (Eurocode 2, 2004)

f_{cd} = design compressive strength of the concrete (Eurocode 2, 2004)

f_r = modulus of rupture of concrete

f_y = yield strength of the steel reinforcement crossing the shear plane

f_{Fu} = ultimate tensile strength of GFRP reinforcement

I = moment of inertia of the entire uncracked cross section

I_{ct} = moment of inertia of the cracked transformed section

k = constant in Loov's parabolic equation (Loov, 1978)

k = constant in Andersons' equation (Anderson, 1960)

k = constant in Loov and Patnaik's equation (Anderson, 1960)

K_1 = equation parameter (Mattock, 2001)

K_2 = equation parameter (Mattock, 2001)

K_3 = equation parameter (Mattock, 2001)

l_v = length of the interface of the horizontal shear transfer

N = unfactored permanent load perpendicular to the shear plane (positive if compression and negative if tension)

Q = first moment of the area above or below the level of the cross section under

		consideration with respect to the natural axis of the section
Q_{ct}	=	Q for cracked transformed section
T_f	=	total factored tensile force in the longitudinal reinforcement
v_h	=	horizontal shear stress
v_u	=	ultimate shear transfer strength
v_{ud}	=	ultimate design shear transfer strength
v_0	=	parameter in Anderson's equation (Anderson, 1960)
V	=	shear force at the section under consideration
V_f	=	factored shear force at the section under consideration
V_h	=	horizontal shear force
V_{nh}	=	nominal horizontal shear strength
α_f	=	angle between the shear plane and the shear friction reinforcement
ε_F	=	strain in the GFRP reinforcement at ultimate shear transfer load
ε_{Fu}	=	ultimate tensile strain of GFRP reinforcement
θ	=	angle between the shear plane and the reinforcement crossing the shear plane (Mattock, 1974)
λ	=	factor to account for low-density concrete
μ	=	coefficient of friction ($\tan \emptyset$)
μ_e	=	effective coefficient of friction
ρ_v	=	reinforcement ratio of the reinforcement crossing the shear plane (A_v/A_{cv})
$\rho_{v,min}$	=	minimum ratio of the reinforcement crossing the shear plane
$\rho_v f_y$	=	reinforcement parameter
σ	=	total compressive stress to the shear plane ($\rho_v f_y + \sigma_n$)
σ_n	=	externally applied normal stress (N/A_{cv})
$\emptyset$	=	angle of internal friction.
$\emptyset_c$	=	resistance factor for concrete
$\emptyset_s$	=	resistance factor for steel reinforcement
ν	=	strength ratio factor (Eurocode 2, 2004)

CHAPTER 1

INTRODUCTION

1.1 General

Composite construction is being used extensively, particularly, in bridge engineering for long time. In earlier applications, a composite beam was referred to a concrete slab provided on top of a steel beam along with shear keys at the junction of the slab and the beam as shown in Figure 1.1. However, composite concrete beams, which consists of cast-in-place slabs and precast girders, are widely used nowadays (Figure 1.2). Precast girders are usually fabricated in industrial facilities before they are moved to their final forecasted position. The slab is then cast on top of the precast girder with its form supported by a fixed base in the case of shored construction or supported by the precast girder in unshored construction. This accelerated construction method has proven to save time and minimize traffic disruption. Since the girder and the flange are cast at different times, also known as a cold-joint condition, the joint between these interconnected members becomes an inevitable concern to ensure the continuity of composite concrete beams. When the composite action and full strain compatibility of the cast-in-place and the precast parts are ensured by a strong connection capable of transferring the longitudinal, horizontal, shear stresses at the interface, the overall strength and stiffness of the composite section can be utilized. Therefore, lighter and shallower beams can be used leading to an efficient and economical construction method.

Reinforcement intersecting concrete-to-concrete interfaces of composite concrete beams remain the main key parameter that allows for the whole process of the shear transfer

to occur along these interfaces. Up to date, steel reinforcement crossing the shear plane between prefabricated girders and their cast-in-place flanges is being utilized and designed according to various design models. However, deterioration of the deck slab caused by the environmental and loading conditions results in extensive corrosion of the steel reinforcement between the slab and the girder, especially when de-icing salt is used. This results in gradual loss of the monolithic behaviour and the strength of the composite concrete beams. For this reason, epoxy coated steel reinforcement (ECR) was proposed as a substitute of black steel at the joints. Yet, it was shown to be ineffective in providing the desired corrosion resistance or in reducing the long-term maintenance cost (Pianca et al. 2005).

Fiber Reinforced Polymer (FRP) reinforcement, bars and stirrups, have shown to be an effective alternative to conventional steel as a flexural and shear reinforcement, particularly Glass FRP. In addition to their non-corrodible nature, the superior high tensile and bond strength as well as the ease of handling of the FRP reinforcement due to its lightweight, promoted their applications in reinforced concrete structures. Also, based on practical applications, using FRP reinforcement, was found to represent a life-cycle cost saving of 15 to 25%, relative to traditional steel reinforcement and up to 30%, comparing to epoxy coated steel reinforcement. Moreover, the initial cost associated with GFRP reinforcement was shown not to exceed 10% of that of steel (V-ROD, 2016)

Accordingly, this research project aims to extend the application of the GFRP to be used as a shear transfer reinforcement across interfaces with concretes cast at different times (cold-joint condition).

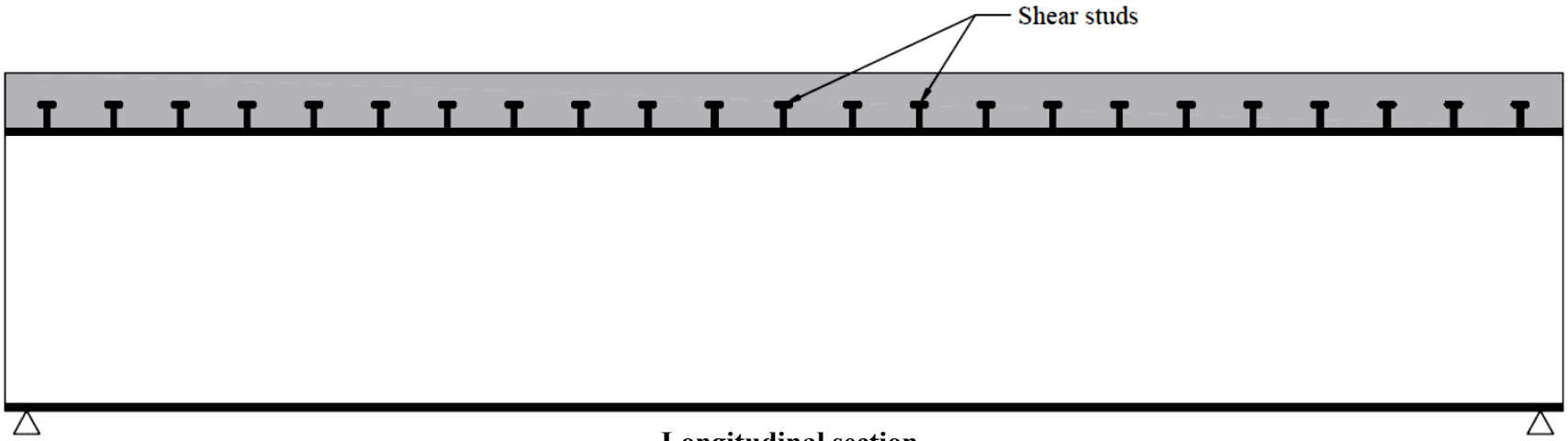

Longitudinal section

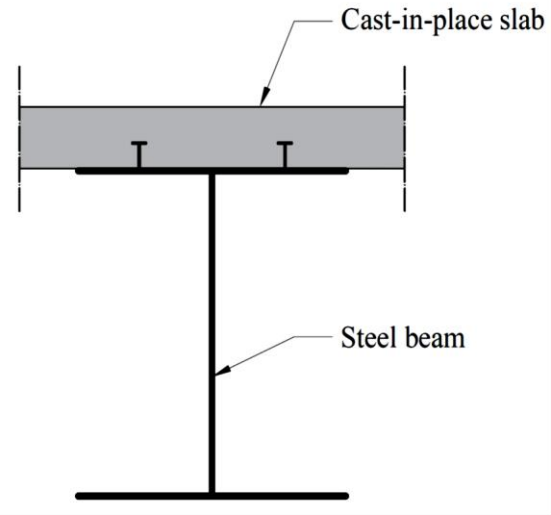

Cross section

Figure 1.1 Composite beam

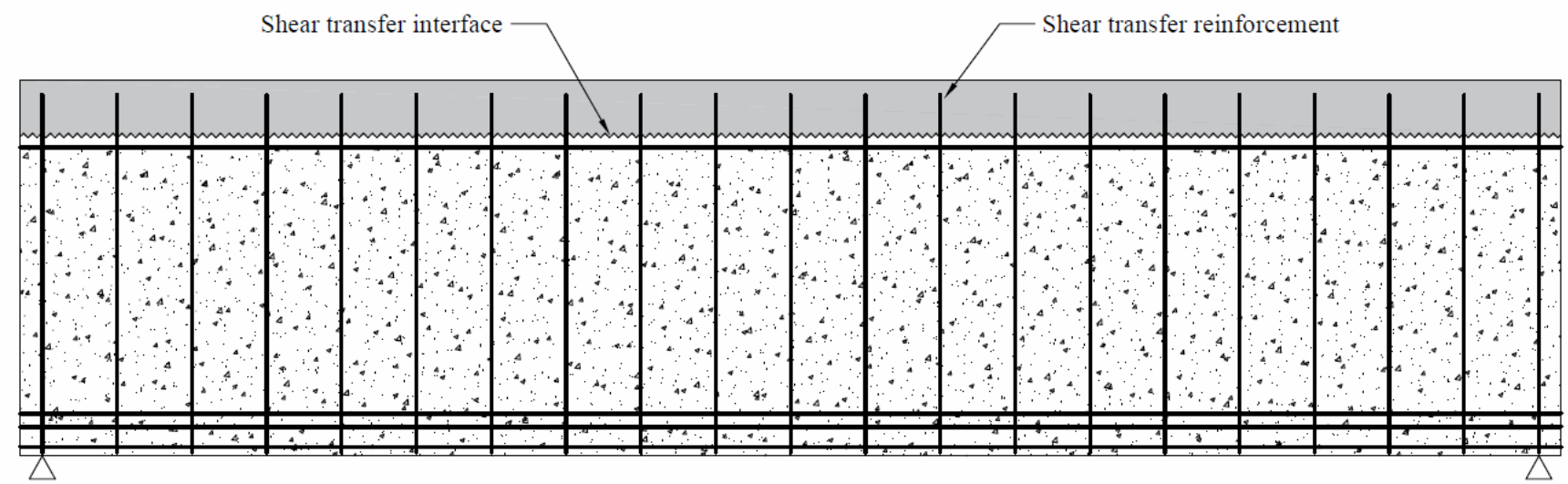

Figure 1.2 Typical composite concrete beam

1.2 Motivation

The Ministry of Transportation of Ontario, in a memo released in 2013, eliminated the use of epoxy coated reinforcing (ECR) steel. This reinforcement was shown to be ineffective to add significantly to the service life compared to black steel, in addition to its high cost relative to the black steel. This reinforcement was also found to significantly limit the repair and investigation techniques that can be used (Pianca et al. 2005).

Glass Fiber Reinforced Polymer (GFRP) is a new construction material that is strong, light and most importantly, resistant to corrosion. It has been emerged over the past two decades in structural applications and has been increasingly used in an effort to provide a corrosion free reinforcement. GFRP was shown to be an effective alternative to conventional steel as a flexural and shear reinforcement. Accordingly, the design and construction requirements of reinforced with Fiber Reinforced Polymer (FRP) reinforcement were provided in distinct and specially prepared design codes and guidelines such as the Canadian standard of the design and construction of building structures with Fiber-Reinforced Polymers (CSA S806-12) and, the American guide for the design and construction of structural concrete reinforced with Fiber-Reinforced Polymers (ACI 440.1R-15). However, no previous research, codes provisions or applications were found concerning the shear transfer strength of concrete-to-concrete interfaces reinforced by GFRP reinforcement. Therefore, the objective of this research is to study the behaviour of Glass Fiber Reinforced Polymers (GFRP) reinforcement as a shear transfer reinforcement along the junctions of precast girders and cast-in-place slabs and provide the associated design guidelines, equations and recommendations.

1.3 Objective

The overall objective of this study is to investigate and evaluate the shear transfer strength and the behaviour of the concrete cold-jointed interfaces when GFRP is utilized as a shear transfer reinforcement. The specific objectives are:

1. Asses the feasibility of GFRP as a shear friction reinforcement in cold-jointed concrete interfaces.
2. Investigate the influence of different parameters such as, the axial stiffness and the shape of the GFRP reinforcement as well as the concrete compressive strength.
3. Develop an understanding of the shear transfer mechanism associated with GFRP reinforcement.
4. Establish the design equations and recommendations.

1.4 Scope

To investigate the capacity and performance of the proposed Glass FRP shear friction reinforcement and to optimize the effect of different design parameters, large scale double L-shaped push-off tests were conducted. The test specimens were divided into two series. The first series with specimens made of a concrete of 50 MPa and the second series includes specimens made of 30 MPa concrete. Three different shapes of the GFRP reinforcement were used, namely: (a) stirrup; (b) headed bar; and (c) angle. The nominal modulus of elasticity was 50 GPa for GFRP stirrups and angles, and 60 GPa for headed bars. The data collected from the tests included the relative slip between the interconnected members, the strain of the reinforcement crossing the shear plane, and the lateral dilation of the interface

were discussed in details. Based on the test results, a description of the shear transfer mechanism along interfaces with cold-joint condition intersected by GFRP reinforcement was introduced along with an equation for the shear transfer strength.

1.5 Thesis Organization

Chapter 2 discuses and summarizes the details and findings of the previous research and current design codes related to the horizontal shear transfer in steel reinforced concrete interfaces. Chapter 3 provides a full description of the experimental program Including the details of the push-off specimens, the test matrix, the test setup, material properties and the instrumentations. Chapter 4 presents a critical analysis of the test results and observations. The conclusions and recommendations are listed in chapter 5.

CHAPTER 2

PREVIOUS RESEARCH AND LITERATURE REVIEW

2.1 Overview

In reinforced concrete structures, there are instances where the transfer of shear stresses along a definite plane needs to be considered. Such cases include Connections between concrete layers cast at different times, which exist in wide range of structural applications, such as composite construction of precast and cast-in-situ concrete structures (Figure 2.1). There are also other situations where the transfer of shear forces along a definitive plane of a potential crack has to be considered in monolithic casting, such as in corbels and at the bearing shoes, as shown in Figures 2.2 and 2.3, respectively. The main requirement of the joint between any two components in composite construction, i.e. the precast girder and the cast-in-place slab, is to assure adequate shear strength to resist and transfer the longitudinal (horizontal) shear stresses that develop at the interface under the gravity loads.

When transvers loads are applied to a beam, normal and shear stresses develop at any cross section of that beam. In order for any element of the cross section to be in a static equilibrium, the shear stresses in the transversal and the longitudinal directions of that element must be equal. Therefore, when a beam member is subjected to transverse loading, longitudinal shear stresses must exist along that member (Beer et al. 2011). This concept can be further visualized from the case shown in Figure 2.4 in which the beam is made of separate planks of timber with smooth frictionless surfaces. Upon loading, these planks tend to slide relative to each other [Figure 2.4(b)].

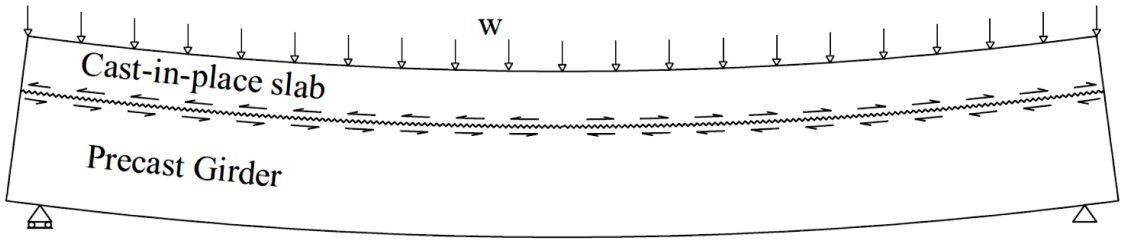

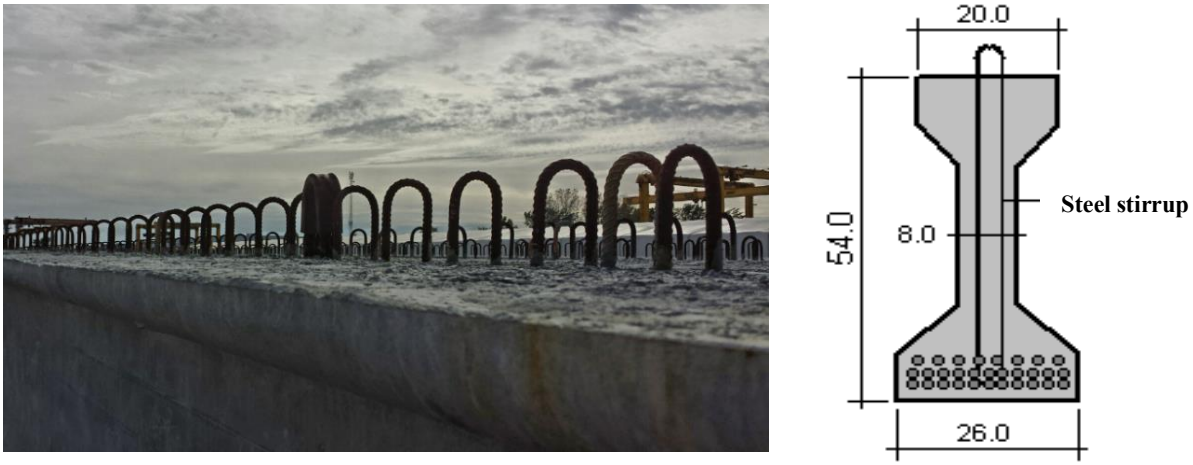

Figure 2.1 Composite concrete beam (shear transfer reinforcement)

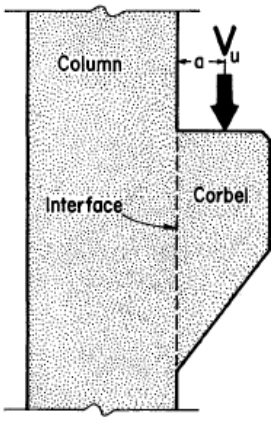

Figure 2.2 Typical corbel

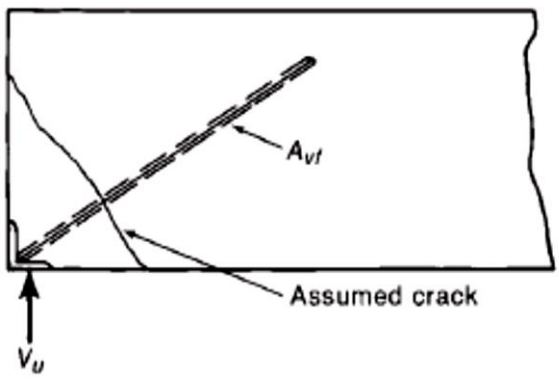

Figure 2.3 Precast beam bearing

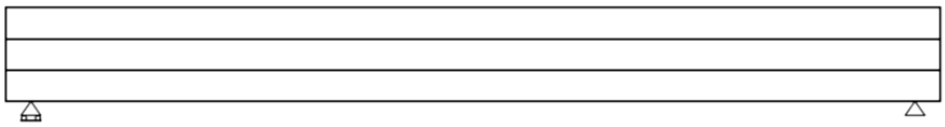

(a) Beam made of separate planks of timber

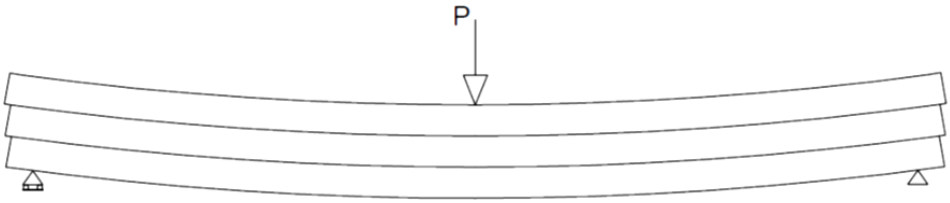

(b) Behavior when the planks are not bonded

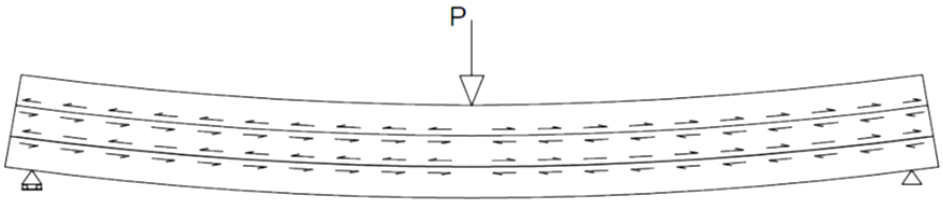

(c) Behavior when the planks are firmly bonded together

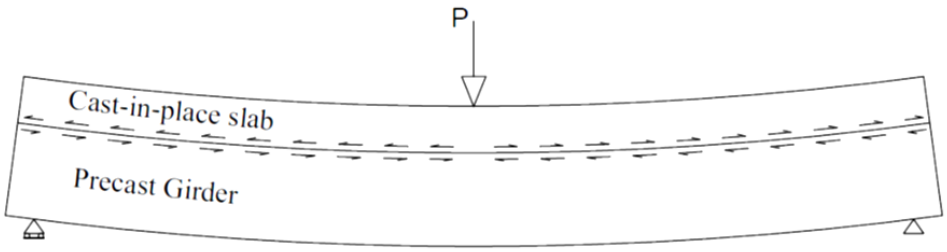

(d) Composite concrete beam

Figure 2.4 The concept of horizontal shear in composite beams

Each plank of timber would act individually and independently as a single beam with its compression zone above its natural axis and tension zone below its natural axis. However, if these planks are perfectly bonded or clamped together so that relative slips are prevented, the resulted composite section would act as a one element as if it is made from one piece of timber with the same cross section [Figure 2.4(c)]. In this case, the tendency to slipping caused by the horizontal shear is resisted by the proper bond between the planks. Similarly, joints between precast girders and cast-in-place slabs in composite concrete beams must be strong enough to resist the tendency of the slab to slide relative to the web and to transmit, efficiently, the longitudinal shear stresses from the web to the flange, and vice versa as shown in Figure 2.4(d).

2.2 The Horizontal Shear

Despite of several benefits resulting from the use of composite concrete beams, the performance of such a system largely depends on the ability of the precast girder and the cast-in-place to act together as a single unit. The monolithic behaviour becomes only possible if the shear stresses resulting from the imposed gravity loads on the beam are effectively transferred between the interconnected members at their interface as shown in Figure 2.5(a). If the joint capacity is not adequate to transfer the horizontal shear stresses, the beam will be partially composite or noncomposite where the slab and the girder tend to work separately as an individual beam [Figure 2.5(b)].

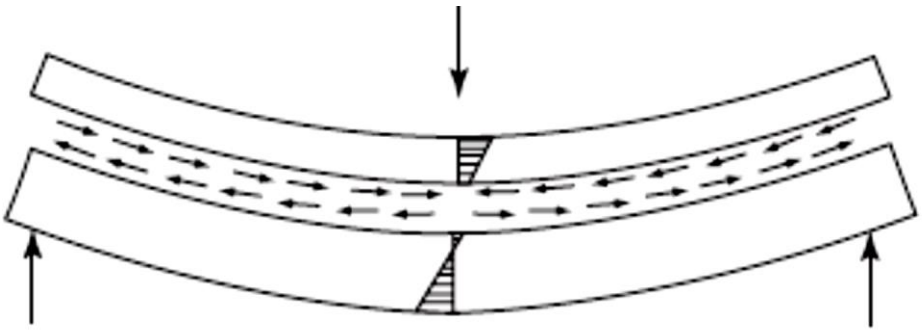

(a) Composite

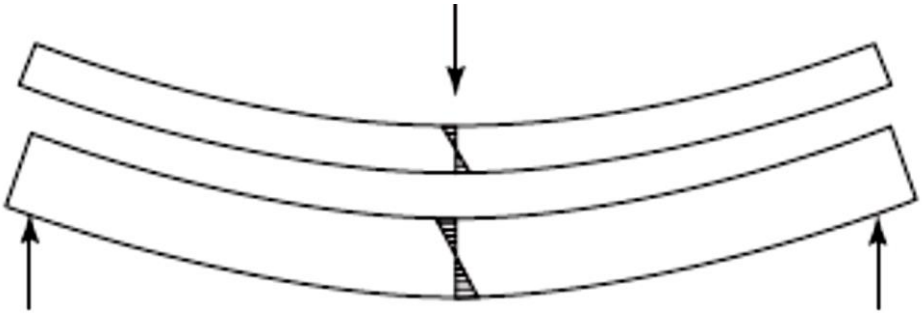

(b) Non-Composite

Figure 2.5 Horizontal shear transfer in composite concrete beams

For an Elastic and uncracked composite concrete beam, the longitudinal shear stresses along the contact surface between the precast girder and its cast-in-place slab can be expressed by:

$$\boldsymbol{v_h = \frac{VQ}{Ib_v}} \tag{2.1}$$

This is expression is also valid for a cracked cross section, only if the properties of the cracked and transformed of that cross section are used (i.e. Q_{ct}, I_{ct}). Although this expression (Eq. 2.1) is only valid for a linearly elastic condition of a cross section of a

composite concrete beam, it was used in most of the previous research and in design practices to evaluate the horizontal shear stresses for cracked concrete beams at various loading stages including those at which the stress distribution is not linear and near the ultimate. However, it was realized that this equation gives only an approximate estimation of the horizontal shear at the ultimate load and provides a good basis for comparison when the cracked and transformed properties of the cross section are used (Saemann and Washa, 1964; Hanson 1960; Loov and Patnaik, 1994; Gohnert, 2003). This equation was also used in clause 2505 of the ACI 318 (1963).

Both of the ACI 318 14 (2014) and the CSA A23.3 (2004) permit the evaluation of the longitudinal shear stresses at the web-slab interface based on the longitudinal stress equilibrium condition at the ultimate load. This implies, that the horizontal shear can be determined by computing the actual change in the compressive (C_f) or the tensile force (T_f) between any two segments of the beam, as shown in Figure 2.6. This condition can be expressed by:

$$\boldsymbol{v_h = \frac{C_f}{b_v l_v}} \tag{2.2}$$

This expression is more appropriate than Eq. 2.1 to be used at loading stages where the beam behaviour is not linear and at the ultimate state. Nonetheless, whenever this equation is to be used between two sections at l_v distant, the distribution of the normal stresses along the cross section must be known at each of these segments. Moreover, it provides an average value of the longitudinal shear stress over the length of the beam segment under consideration and it does not reflect the variation of the horizontal shear stresses over that length when the beam is loaded by a distributed load. It should be noted that in the case when the natural axis is within the flange (i.e. above the shear plane), the

tensile force in the longitudinal reinforcement T_f may be used instead of C_f in Eq. 2.2 according to the design manual of the Canadian Precast Prestressed Concrete Institute (CPCI, 2007).

The present codes; ACI 318-14 (ACI, 2014) and CSA A23.3-04 (CSA, 2004) require the factored horizontal shear strength at any section equals to the factored vertical shear force at that section, at the ultimate state. This condition suggests the following expression to calculate the horizontal shear stresses at ultimate:

$$\boldsymbol{v_h = \frac{V_f}{b_v d}} \tag{2.3}$$

In fact, Eqs. 2.1, 2.2 and 2.3 are closely related. The term VQ/I in Eq. 2.1 represents the horizontal shear force per unit length along the interface between the girder and the slab (shear flow). Since $V_h = C_f$ in Eq. 2.2, the term C_f/l_v also represents the longitudinal (horizontal) shear force per unit length between a section at distance l_v from the section of zero moment ($C_f = 0$). Eq. 2.3 is similar to the others because $V_f = \partial M_f/\partial x$ is the rate of change of the moment. If the compression zone is entirely within the flange, and the small variation in the depth of the stress block is ignored, the compression force, over a deferential element of the beam length, ∂C_f will be equal to $\partial M_f/(d - a/2)$, where a is the depth of the equivalent rectangular stress block. The horizontal shear force per unit length will be $V_f/(d - a/2)$. Therefore, V_f/d in Eq. 2.3 is a non-conservative simplification. It should be highlighted that, theoretically, Eq. 2.3 predicts the shear stresses in the cracked zone of the beam where the shear flow is constant (Park and Paulay, 1974). Consequently, this equation is best utilized to estimate the horizontal shear stresses at the web-flange interface of composite concrete beams when this interface lies in the cracked

zone, i.e. when the natural axis is located within the flange.

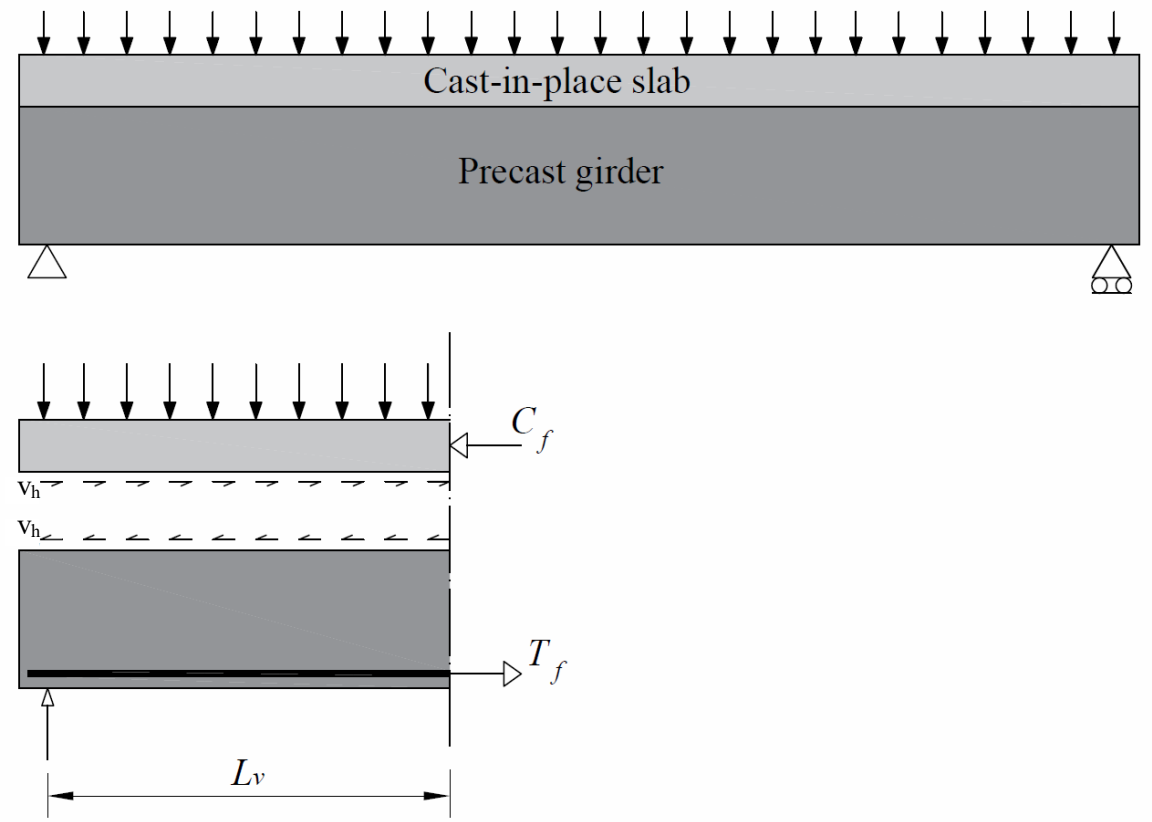

Figure 2.6 Evaluation of the interface longitudinal shear by equilibrium condition

2.3 Shear Transfer Mechanisms

The shear friction is the first, simplest and the most popular hypothesis that describes the shear transfer mechanism along concrete-to-concrete interfaces where the slip is not restrained, such as interfaces between precast girders and cast-in-place slabs in composite concrete beams. The first investigation that explained, in details, the shear friction analogy was proposed by Birkeland and Birkeland (1966). This theory was adopted by many design codes of reinforced concrete structures, including the Canadian standard of the design of the concrete structures, CAN/CSA A23.3 (2004), the Canadian highway bridge design code,

CAN/CSA S6 (2014), the American building code requirements for structural concrete, ACI 318 (2014), the Eurocode standard of the design of concrete structures, Eurocode 2 (2004), the precast and Prestressed Concrete Institute, PCI Design Handbook (2004), AASHTO LFRD Bridge Design Specifications (2007), and AASHTO standard specifications for highway bridges (2002).

The shear friction theory, in it is original form (Birkeland and Birkeland, 1966), assumes that the shear forces parallel to the concrete-to-concrete interfaces are transmitted by friction only. If a crack is postulated along the shear plane, and reinforcement across that shear plane is provided, the roughness of the crack faces would force the interconnected concrete elements to separate when slip occurs. This separation would place the steel across the interface in tension, which in return creates a balancing compressive, clamping, stress on the crack faces. Owing to the friction between the rough and irregular faces of the crack, this clamping stress provides a frictional shear resistance as shown in Figure 2.7. It is hypnotized that if the steel reinforcement is sufficiently provided and well anchored on both sides of the shear plane, the ultimate frictional shear resistance is achieved upon the yielding of the steel.

The shear transfer across initially uncracked shear planes in monolithic concrete was first investigated by Hofbeck et al. (1969) and Mattock and Hawkins (1972). In contrary to the shear friction theory, these authors proposed a shear transfer by a truss action after diagonal tension cracking occur across the interface (Figure 2.8). Based on this model, the failure is caused by yielding of the steel reinforcement if concrete crushing failure did not occur first.

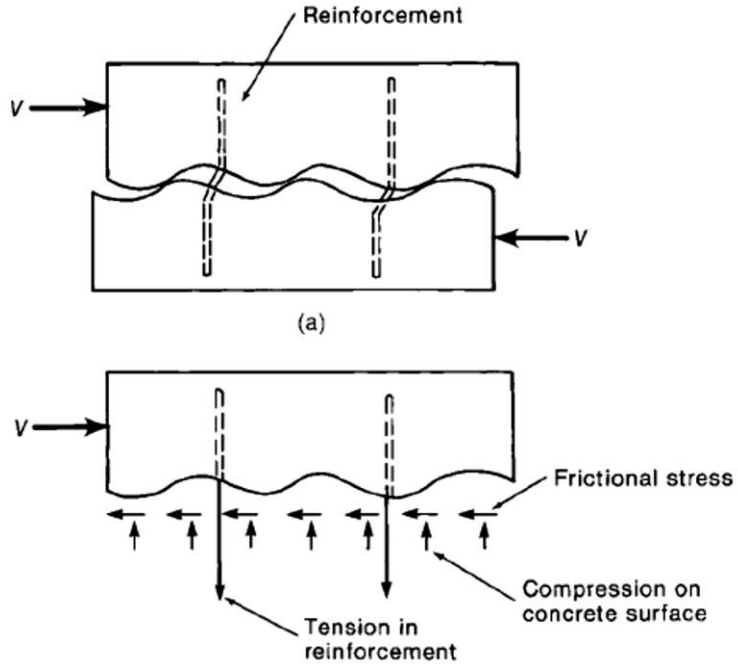

Figure 2.7 Shear transfer by friction (Wight and Macgregor, 2011)

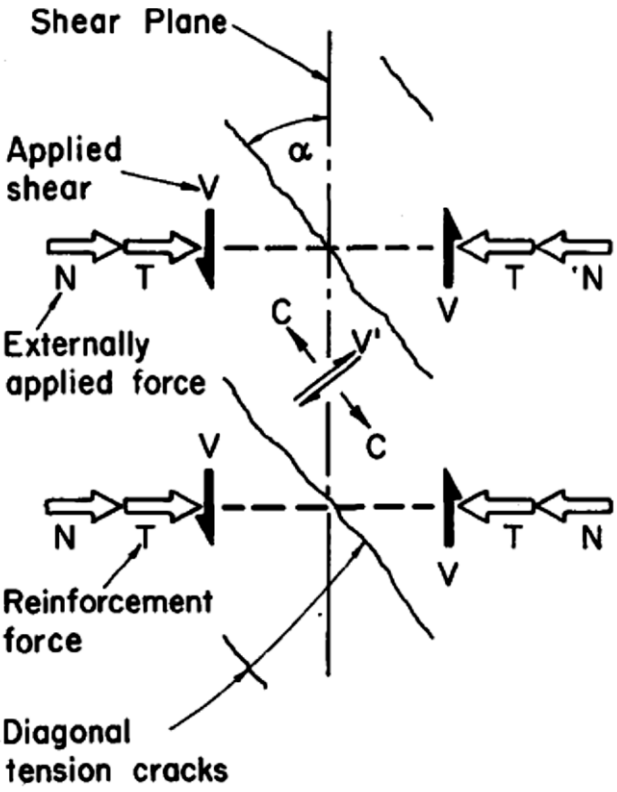

Figure 2.8 Shear transfer in initially uncracked concrete (Mattock and Hawkins, 1972)

Hsu et al. (1987) proposed a similar shear transfer mechanism for uncracked shear planes based on a truss model, where the failure is caused by the crushing of the concrete struts. This theory considers the reinforcement parallel to the shear plane to contribute to the shear transfer. Hwang et al. (2000) suggested a comparable theory based on the "softened strut-and-tie" model. It was proposed that the failure will occur due to the crushing o the concrete in the compression struts parallel to the direction of the diagonal cracks that have formed in a direction inclined to the shear plane. This model was claimed to be applicable to both initially cracked and uncracked interfaces (see Figure 2.9).

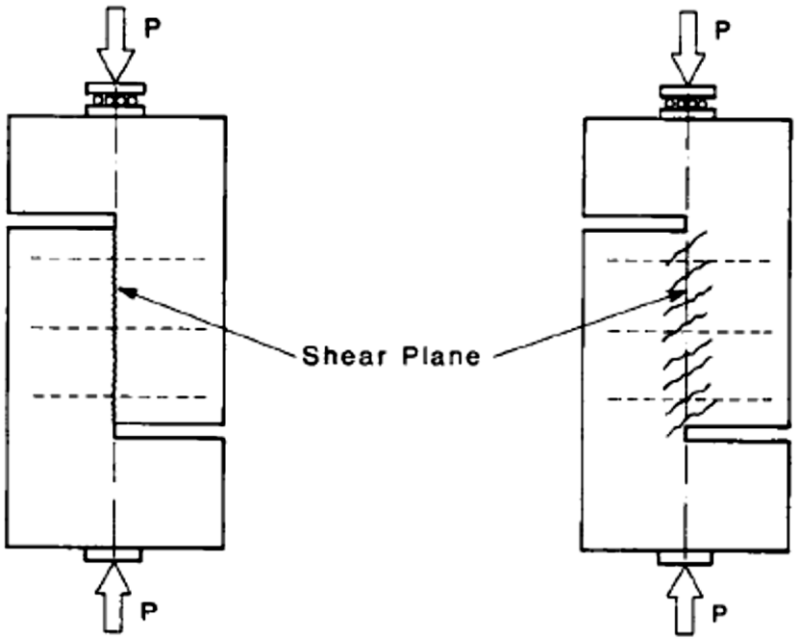

Figure 2.9 Initially cracked (left) and initially uncracked (right) shear transfer push-off specimens (Hsu et al. 1987)

However, joints with concrete cast at different times (cold-joints) were not given much interest until the recent studies such as Loov and Patnaik (1994), Kahn and Mitchell (2002), Harries et al. (2012) and Shaw and Sneed (2014) by which test specimens with cold-joint conditions at their interfaces were used in the investigation of the shear transfer problem.

The shear strength of Concrete-to-concrete interfaces was described by Zilch and Reinecke (2001) as combination of three load carrying mechanisms, which are: 1) adhesion bond, τ_{adh}; 2) shear-friction, τ_{sf}; and 3) shear reinforcement (dowel action), τ_{sr}. Figure 2.10 shows the contribution of each mechanism to the shear transfer strength. The shear strength by adhesion may be defined as the transference of stress throughout the chemical bond connections between the particles of the new concrete and the existing one. The adhesive bond is a rigid type of connection, which is the main difference between this mechanism and the shear friction and dowel action.

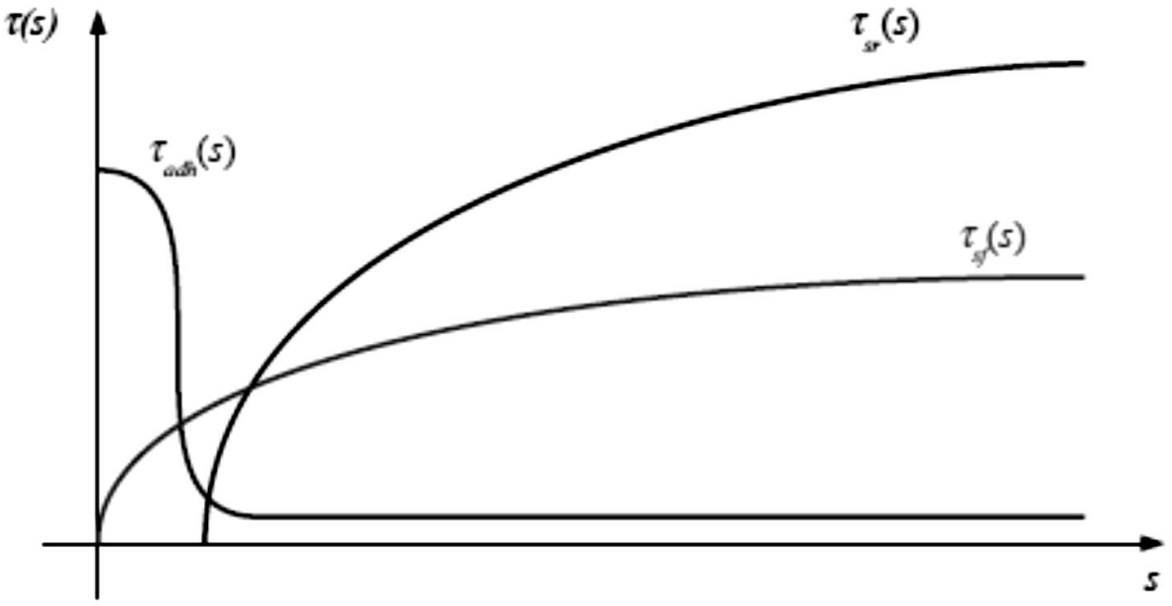

Figure 2.10 Contribution of adhesion, shear-friction and dowel action (Zilch & Reinecke, 2001)

When the maximum shear capacity of the adhesive bond is achieved, debonding of the concrete-to-concrete interface faces occurs and the shear stress will be transferred by the mechanical interlocking. However, if the interface is subjected to external compressive forces or/and provided with adequate and well anchored reinforcement across it, the shear

stress will then be transferred by shear-friction. Due to slippage, the reinforcement across a joint would be subjected to shear at the interface level, which is usually referred to as the dowel action. The dowel action effect was investigated primarily by Hanson (1960), Hofbeck et al. (1969), Paulay et al. (1974) and Walraven and Reinhardt (1981). These authors showed that significant shearing resistance can be developed by the dowel action only if large slip occurs along the joint. This slip may be in excess of what could be considered acceptable within the limits of structural efficiency, and hence, the dowel action cannot be considered a feasible shear resistance component along concrete-to-concrete joints (Paulay et al. 1974).

2.4 Shear Transfer Models

There exists a large amount of research devoted to study the shear transfer mechanism and to evaluate the shear transfer strength of interfaces between interconnected reinforced concrete elements; the significant and most relevant research, since the 1960's, will be discussed herein. The corresponding design expressions are also presented. Some of these expressions were originally proposed in imperial units, while others were expressed in SI units. However, a single SI unit format is adopted in the following. Some expressions were modified to follow the notation of this thesis.

2.4.1 Anderson (1960)

In this study, the author discussed the design of composite concrete beams. Push-off tests were performed (Figure 2.11). A satisfactory shear connection was believed to be possible if the interface surface was roughened to an amplitude of 6.4 mm (0.25 in) before

casting the new concrete of the slab against the hardened concrete of the girder. It was suggested that if the roughened surface of the hardened concrete was coated with a cement slurry immediately before casting the new concrete would greatly enhance the bond at the interface. The ultimate shear transfer resistance was assumed to vary linearly with the amount of the reinforcement crossing the interface, and the following expression was proposed:

$$\boldsymbol{v_u = v_0 + k\rho_v} \tag{2.4}$$

where v_0 and k are experimentally calibrated parameters:

$v_0 = 4.41$ MPa and $k = 229$ for $f_c' = 20.7$ MPa

$v_0 = 5.52$ MPa and $k = 276$ for $f_c' = 51.7$ MPa

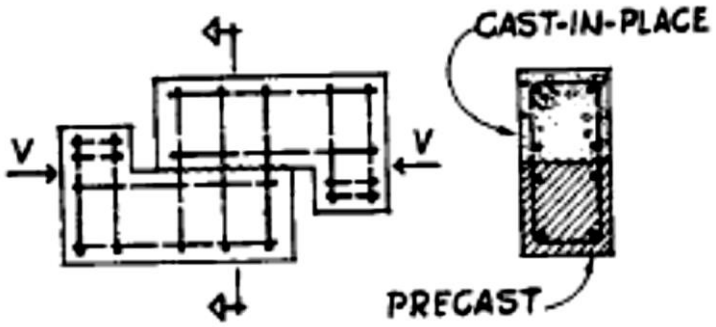

Figure 2.11 Push-off specimen (Anderson, 1960)

2.4.2 Hanson (1960)

This was a systematic study that provided the first major development in the area of composite construction. Ten simply supported composite T-beams, assorted into two series, with four-point bending loading condition and a span of 3.7 m for the first series and 6 m for the second series, in addition to 62 push-off specimens were tested (Figure 2.12). Different amount of steel reinforcement was provided in addition to various types of

preparations of the contact surface between the girder and the slab were used. The effect of the bond between the girder and the slab was also investigated. The influence of the shear keys on the shear transfer strength was also explored. It was shown that shear keys were ineffective unless the bond at the interface was initially destroyed. Although, the concrete compressive strength influence was not investigated in this study, it was suggested that it has a possible effect on the shear transfer strength and further investigations are needed to determine that. For test specimens in which the bond at the interface was utilized, the initial shear stress peak developed at a small slip followed by an increase in the shear resistance with increasing slip depending on the amount of the reinforcement existent in the joint. The ultimate strength was noted at the initial peak at a slip of approximately 0.13 mm (0.005 in). It was concluded that this slip is a critical slip value after which the composite action is rapidly lost.

The reported maximum shear stress resistance was of 3.45 MPa (500 psi) for rough and bonded contact surface and a maximum of 2.07 MPa (300 psi) for smooth bonded surface when the concrete strength varied between 20.7 to 34.5 MPa (3000 to 5000 psi). An extra 1.21 MPa of shear resistance was proposed for an additional one percent of steel reinforcement crossing the shear plane.

It was pointed out that the shear-slip behaviour of push-off specimens was similar to that of the interfaces of composite girders. Therefore, push-off tests were considered a valuable aid in evaluating of the horizontal shear strength of composite beams.

The elastic shear equation (Eq. 2.1) was used to evaluate the horizontal shear stresses for the cracked and transformed sections of the tested composite concrete beams. However, it was mentioned that this equation only gives an approximate estimation and provides a

good basis for comparison.

Based on his test results, Hanson proposed the following equation for the ultimate shear transfer stress for rough and bonded interfaces.

$$v_u = 3.45 + 121\rho_v \quad \text{(MPa)} \tag{2.5}$$

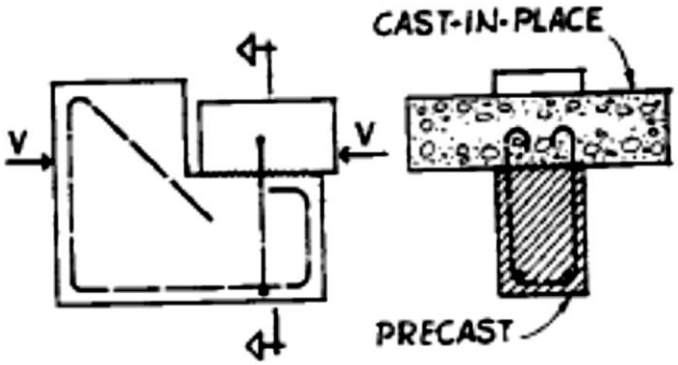

Figure 2.12 Push-off specimen (Hanson, 1960)

2.4.3 Birkeland (1966, 1968)

The shear friction hypothesis was explained in details. The joint and the interface roughness were idealized as shown in Figure 2.13. The roughness of the interface was modeled as a series of saw-tooth ramps with a slope of $tan\,\emptyset$, Owing to the roughness of the interface faces, the horizontal slippage, along the plane m-m shown in Figure 2.13(b), is accompanied by a separation δ of the connected parts. This separation would put the reinforcement crossing the shear plane in tension, resulting in a balancing compressive stresses across the joint interface, and hence, a frictional shear resistance will be developed.

At ultimate, the shear friction theory assumes that the separation of the shear plane is sufficient enough to stress the reinforcement across this plane to its yield point. The proposed shear friction equation is as follows:

$$v_u = \rho_v f_y \tan \emptyset = \rho_v f_y \mu \tag{2.6}$$

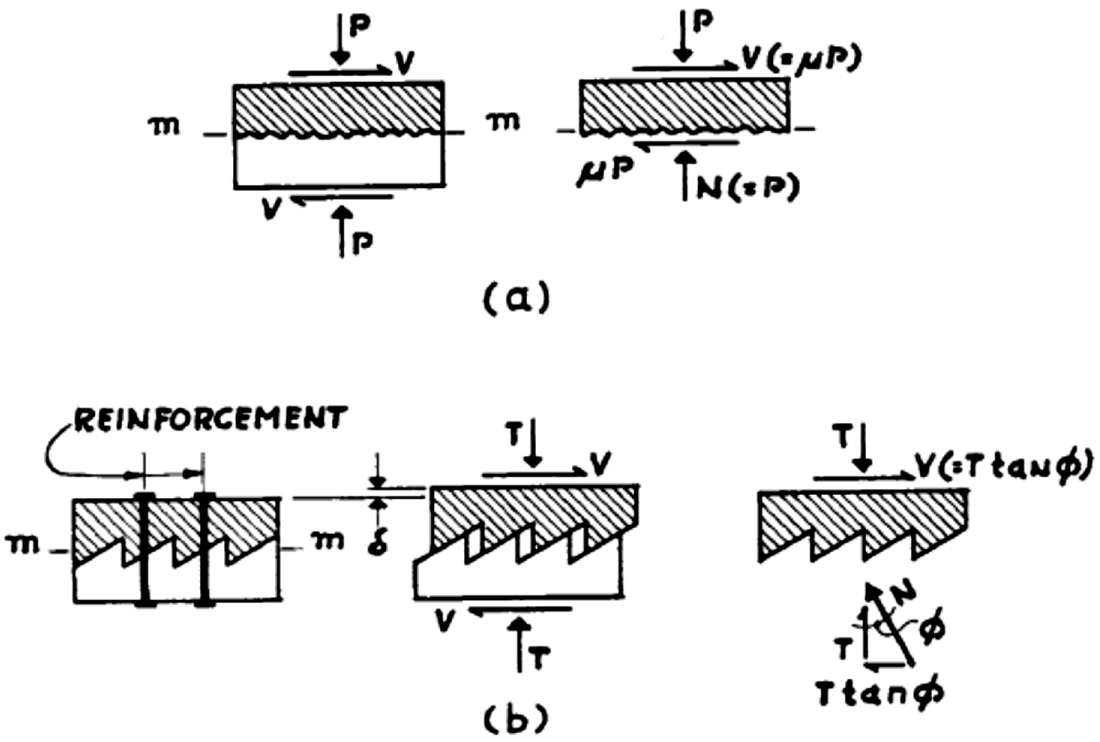

Figure 2.13 Shear friction hypothesis (Birkeland and Birkeland, 1966)

This expression was proposed for a crack in monolithic concrete and was extended to include smooth concrete surfaces, intentionally roughened interfaces and concrete-to-steel interfaces. The coefficient of friction was empirically determined and was defined for the following situations: a) μ = 1.7, for a crack in monolithic concrete; b) $\mu = 1.4$, for artificially roughened construction joints; and c) $\mu = 0.8 - 1$, for ordinary construction joints and concrete-to-steel interfaces. The yield strength of the reinforcement crossing the interface should not exceed 414 MPa (60 ksi). This expression was limited to: $\rho_v \leq 1.5\%$; $v_u \leq 5.52$ MPa (800 psi) and $f_c' \geq 27.6$ MPa (4000 psi).

Birkeland (1968) was the first to introduce the following nonlinear expression for the shear transfer strength along the junctions of the concrete members that are cast at different times. His equation was developed based on the best fit of the available tests data at that time.

$$\boldsymbol{v_u = 2.78\sqrt{\rho_v f_y}} \quad \text{(MPa)} \tag{2.7}$$

This equation was not published and was only handed out as class notes for the following reasons: 1) the apparent friction coefficient will vary with clamping stress from less than one to infinity depending on the clamping stress and, hence, it has no physical meaning; 2) it does not present the designer with the visual impact and simplicity of the concept which is embodied in the linear equation of the shear friction (Eq. 2.6); and 3) the coefficient 2.78 (33.5 in psi units) has an awkward unit of $\sqrt{\text{MPa}}$ or ($\sqrt{\text{psi}}$).

2.4.4 Mast (1968)

This research provided more insight into the shear friction hypothesis. The shear friction proposed by Birkeland and Birkeland (1966) was adopted by Mast. The limit of ($0.15f_c'$) for the reinforcement index ($\rho_v f_y$) was granted and the values of the shear coefficient were firmed up as: (a) $\mu = 1.4$ for concrete-to-concrete rough interfaces; (b) $\mu = 1.0$, for concrete-to-steel interfaces in composite beams; (c) $\mu = 0.7$, for concrete-to-steel, field welded inserts; (d) $\mu = 0.7$, for concrete-to-concrete smooth interfaces.

The limitations of the shear friction equation (Eq. 2.9**)** were emphasized as follows:

1) When tensile stresses act across the crack, extra reinforcement should be provided for these stresses in addition to the reinforcement required by the shear friction model.

2) The shear transfer reinforcement should be anchored on both sides of the interface in order to develop the yield strength of steel at the ultimate load, but a finite slip and consequent separation of both of the connected elements on each side of the interface must take place.

3) The angle of internal friction ϕ shall be assumed to be independent of the concrete strength and the shear stress level.

2.4.5 Mattock et al. (1969 – 2001)

Dr. Alan H. Mattock who was a professor at the University of Washington and his coworkers conducted a series of research through which they investigated the shear friction analogy proposed by Birkeland and Birkeland (1966) and Mast (1968) for various conditions of the concrete joints.

Hofbeck, Ibrahim and Mattock (1969) developed an experimental program included a total of 38 push-off tests to explore the influence of the pre-existing crack along the shear plane, the concrete strength, the dowel action; and the reinforcement ratio and yield strength.

In both the pre-cracked heavily reinforced specimens and initially uncracked (monolithic) specimens, diagonal cracks across the joint developed prior to failure. Shear strengths of initially uncracked specimens were generally higher than those of pre-cracked specimens. However, the difference in the strengths between the two types decreased at

higher values of the reinforcement index ($\rho_v f_y$). The dowel action effect of the reinforcement crossing the shear plane was shown to be insignificant when no a crack existed prior to testing. However, a major contribution of the dowel action on the shear transfer strength of initially cracked specimens was noted.

It was acknowledged that the shear friction hypothesis ignores the cohesion of the concrete and compensates that with an apparent friction coefficient that is higher than the actual one. Therefore, the shear friction equation (Eq. 2.6**)** was found to be reasonably conservative at low values of the clamping stress and un-conservative for concrete strengths higher than 28 MPa and when the clamping stress exceeds 4.2 MPa (600 psi).

A limit of clamping stress of 4.2 MPa was suggested in addition to Mast's limit of $0.15f_c'$ (Mast, 1968). However, for heavily reinforced cracked joints, the shear friction equation can be used with a friction coefficient of 1.0 and a clamping stress that does not exceed the minimum of $0.3f_c'$ and 10.5 MPa.

A continuation study of the previous research was done by Mattock and Hawkins (1972). Additional series of push-off specimens with cracked and uncracked interfaces were conducted. Additional pull-off and modified push-off specimens, shown in Figure 2.14, were used to investigate the influence of the direct tensile stress and normal stresses on the shear transfer strength, respectively. Similar conclusion with regard the influence of the pre-existing crack was noted. However, initially uncracked push-off specimens exhibited higher strength than the companion uncracked pull-off specimens. The authors believed this to be caused by the reduction of cohesion when tensile stresses parallel to the shear plane were introduced. In contrary, tensile stresses did not influence the strength of initially cracked specimens.

The effect of the stresses normal to the shear plane was studied through the push-off specimens with an oblique shear plane (modified push-off specimens). It was concluded that the external normal compressive stresses σ_n could be added to the reinforcement index ($\rho_v f_y$) in the evaluation of the shear transfer strength.

The shear transfer along a shear plane in monolithic concrete was believed to be developed by the truss action (see Figure 2.8) after diagonal cracks across that plane occurred. The behaviour of heavily reinforced precracked specimens was characterized by the formation of the diagonal cracks across the shear plane similar to initially uncracked specimens.

The authors presented a design expression to predict the ultimate shear stress resistance across a crack in monolithic concrete (cracked interfaces) as a lower bound of their test results, as follows:

$$\boldsymbol{v_u = 1.38 + 0.8(\rho_v f_y + \sigma_n)} \quad \text{(MPa)} \tag{2.8}$$

The ultimate shear strength v_u was limited to the smaller of $0.3f_c'$ and 10.34 MPa (1500 psi), provided that the total clamping stress is not less than 1.38 MPa (200 psi).

The previous expression of Mattock and Hawkins (1972) was formulated as lower bound for the experimental tests used for calibration. Yet, in a subsequent publication Mattock (1974) presented a modified expression that corresponded to the mean values of the test results reported in this publication and the previous work of Mattock and Hawkins (1972) as follows:

$$\boldsymbol{v_u = 2.76 + 0.8(\rho_v f_y + \sigma_n)} \quad \text{(MPa)} \tag{2.9}$$

provided that the total clamping stresses should not be less than 1.38 MPa (200 psi) and the ultimate shear transfer strength v_u is limited to the minimum of $0.3f_c'$ and 10.34 MPa.

These expressions are usually referred to as the modified shear friction equations which correspond to an interface crack model as shown in Figure 2.15. The first term added to account for the cohesion of the interface, which represents the resistance of shearing of the asperities of the local roughness. The second term represents the frictional shear resistance to shear, which is associated with the general roughness, represented by μ.

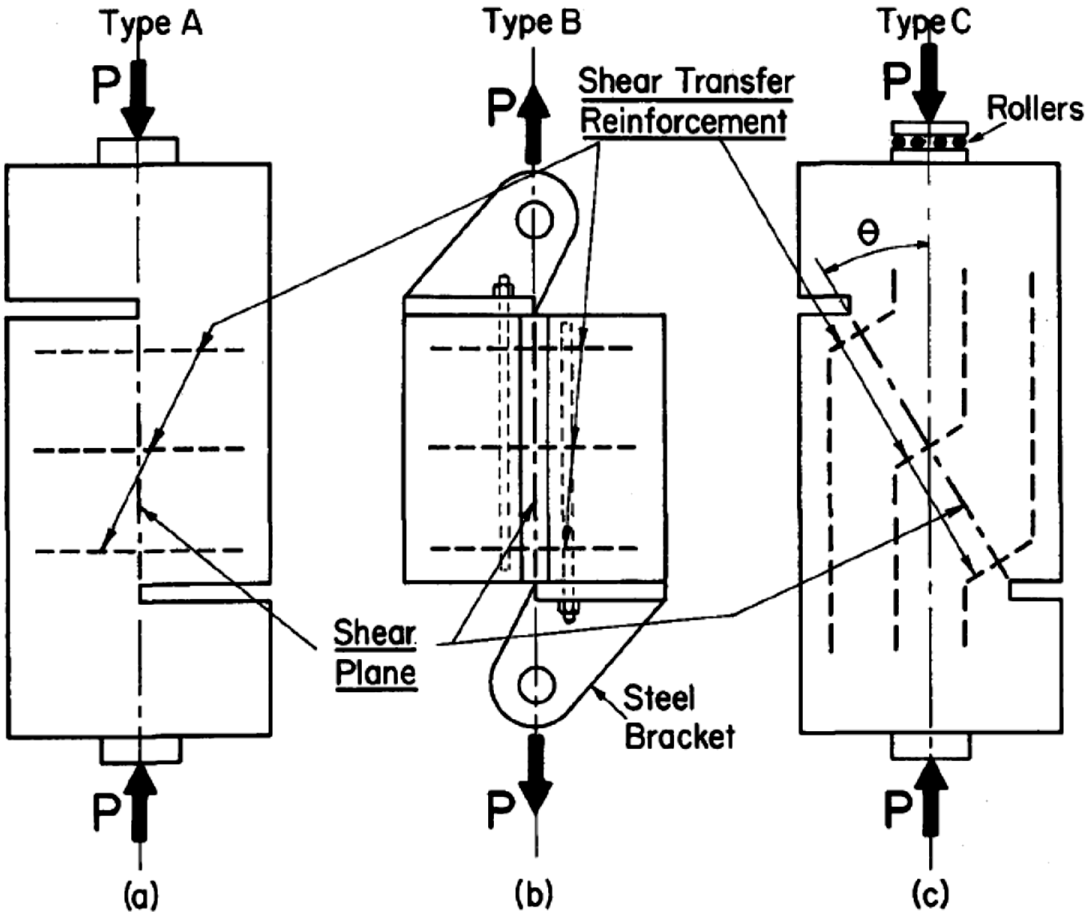

Figure 2.14 Shear transfer test specimens: (a) push-off; (b) pull-off; (c) modified push-off (Mattock and Hawkins, 1972)

Figure 2.15 General and local roughness of a crack face (Walraven et al. 1987)

Mattock (1974) also presented an experimental program involved 23 push-off specimens to study the shear transfer across a plane inclined at an angle to a parallel or orthogonal array of reinforcement (Figure 2.16). For parallel reinforcement crossing an initially cracked concrete interface at an angle θ (Figure 2.17), the following expression was proposed:

$$\boldsymbol{v_u = 2.76\, sin^2\theta + \rho_v f_s(0.8\, sin^2\theta - 0.5\, sin\, 2\theta)} \quad \text{(MPa)} \qquad (2.10)$$

provided that v_u shall not exceed $0.3f_c'$. The term f_s in the above equation was evaluated from the test results for a coefficient of friction μ of 0.8 as follows:

$f_s = 0$ for $0 < \theta < 51.3^o$

$f_s = -1.6f_y\, cos(\theta + 38.7^o)$ for $51.3^o \leq \theta < 90^o$

$f_s = f_y$ for $90^o \leq \theta \leq 180^o$

Mattock et al. (1975) investigated the design considerations of the shear transfer along a shear plane when the direct shear is accompanied by a moment and normal forces acting on that plane. In addition, the effect of the tension force acting transversal to the shear plane on the direct shear that can be transferred across that plane was investigated through series of push-off tests. Specimens were provided with anchorages on opposite sides of the shear plane as illustrated in Figure 2.18.

The most relevant to the present work and important conclusion drawn in this study, is that the variation in the shear stress due to the change of the total clamping stress ($\sigma = \rho_v f_y + \sigma_n$) is the same whether that change was in the reinforcement parameter $\rho_v f_y$ or was in the external normal stress σ_n. Based on this observation, the authors recommended to combine the external clamping stress to the reinforcement index when evaluation the shear transfer strength of an interface.

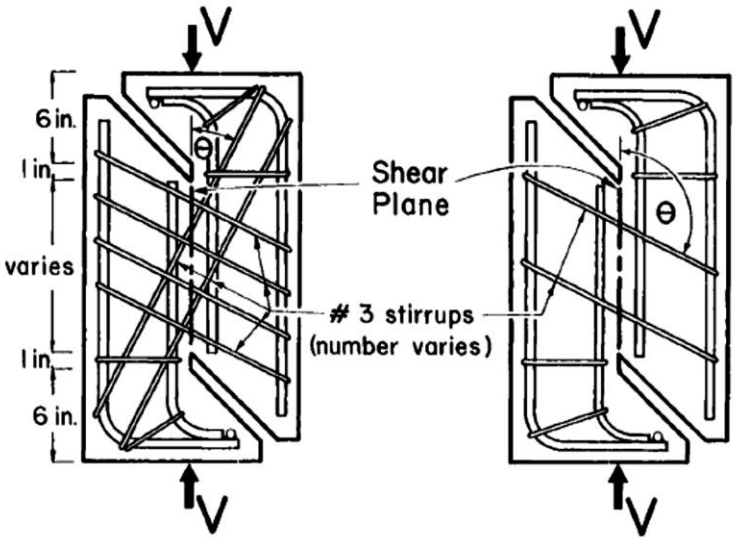

Figure 2.16 Shear transfer test specimens with orthogonal and parallel reinforcement (Mattock, 1974)

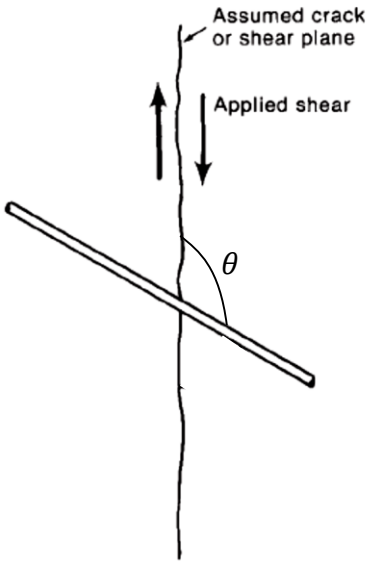

Figure 2.17 Shear-Friction reinforcement at an angle to the shear plane

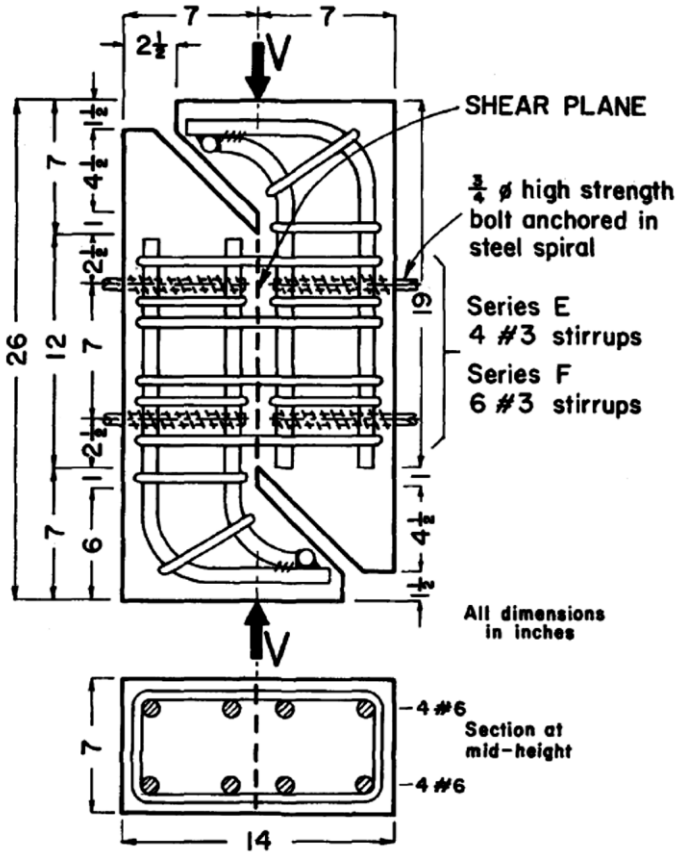

Figure 2.18 Push-off specimen with tension across the shear plane (Mattock et al. 1975)

To study the shear transfer strength of connections in precast structures made of lightweight concrete, Mattock et al. (1976) introduced a testing program involved initially cracked and uncracked push-off specimens made of lightweight concrete (all-lightweight concrete and sanded lightweight concrete).

Diagonal cracks that were observed in the previous tests of Mattock and Hawkins (1972), for heavily reinforced cracked interfaces with normal weight concrete, were not reported when lightweight concrete was used. The shear transfer strength of the initially cracked specimens made of lightweight concrete was less than that of normal weight concrete specimens with the same compressive strength. In the authors' opinion this was

due to the differences in the roughness of the crack faces. When the specimens were cut open at their interfaces, the crack faces in normal weight concrete were rougher than those in lightweight concrete. Two equations for shear transfer strength along pre-cracked interfaces for lightweight concrete were proposed.

For sanded lightweight concrete

$$\boldsymbol{v_u = 1.72 + 0.8\rho_v f_y} \quad \text{(MPa)} \tag{2.11}$$

provided that v_u should not exceed $0.2f_c'$ neither 6.90 MPa (1000 psi), and the clamping stress $\rho_v f_y$ is not less than 1.38 MPa (200 psi).

For all lightweight concrete:

$$\boldsymbol{v_u = 1.38 + 0.8\rho_v f_y} \quad \text{(MPa)} \tag{2.12}$$

provided that v_u is not more than $0.2f_c'$ neither 5.52 MPa (800 psi), and the clamping stress $\rho_v f_y$ is not less than 1.38 MPa (200 psi).

In the discussion of the study of Walraven et a. 1987, Mattock (1988) added the effect of the concrete strength to his previous equation (Eq. 2.9) and represented it as follows:

$$\boldsymbol{v_u = 0.467 f_c'^{\,0.545} + 0.8\left(\rho_v f_y + \sigma_n\right)} \quad \text{(MPa)} \tag{2.13}$$

where the ultimate shear transfer v_u is upper limited to $0.3f_c'$.

Mattock pointed out that the first term in this equation represents the resistance to shearing off the asperities of the interface surface and, hence, this term should include the concrete strength. However, the second term, which denotes the frictional shear resistance, should be independent of the concrete strength.

Mattock (1994), commenting the study of Loov and Patnaik (1994), proposed a design expression of the ultimate shear transfer calibrated as a lower bound of the test results of

Loov and Patnaik (1994) and others. Being the ultimate shear transfer stress for a crack in monolithic normal weight concrete, predicted by:

$$\boldsymbol{v_u = \frac{\sqrt{\rho_v f_y}}{4.536} f_c'^{0.73}} \quad \text{(MPa)} \tag{2.14}$$

where v_u should not exceed $0.3f_c'$.

Mattock (1994) also suggested the following expression for initially cracked and roughened interfaces between concretes cast at different times:

$$\boldsymbol{v_u = \frac{\sqrt{\rho_v f_y}}{4.536} f_c'^{0.73} - 0.02 f_c'} \quad \text{(MPa)} \tag{2.15}$$

where v_u should not exceed $0.3f_c'$.

It was also pointed out that the interface roughness plays a major role in the shear transfer strength of that interface. Therefore, it was recommended that some numerical measure of the roughness should continue to be specified in the design codes.

Mattock (2001) conducted an analytical study on the test results of push-off specimens with initially cracked interfaces of previous studies (Hofbeck et al. 1969; Mattock and Hawkins, 1972; Mattock et al. 1975; Mattock et al. 1976; Mattock, 1976; Walraven et al. 1987; Walraven and Stroband, 1994). It was intended to improve the shear friction provisions of the ACI 318 (1999) in evaluating the shear transfer strength along concrete joints, particularly, when high-strength concrete is used.

The author proposed the following expressions corresponding to various concrete types and strengths and different conditions at the shear interface.

1. For shear transfer along a crack in monolithic concrete, or a crack between concretes cast at different times with its surface intentionally roughened:

a. When the total normal stress ($\sigma = \rho_v f_y + \sigma_n$) is greater than or equal to $K_1/1.45$, or when the longitudinal shear stress is greater than or equal to $1.55K_1$, the ultimate shear transfer stress resistance is given by:

$$\boldsymbol{v_u = K_1 + 0.8(\rho_v f_y + \sigma_n)} \quad (2.16)$$

but not greater than $K_2 f_c'$ neither K_3

b. When the total normal stress ($\sigma = \rho_v f_y + \sigma_n$) is less than or equal to $K_1/1.45$, or when the imposed nominal direct shear stress is less than or equal to $1.55K_1$, the ultimate nominal shear transfer strength is given by:

$$\boldsymbol{v_u = 2.25(\rho_v f_y + \sigma_n)} \quad (2.17)$$

The coefficients, K_1, K_2, and K_3 are defined for the following conditions:

- For monolithic normal-weight concrete, $K_1 = 0.1 f_c'$ but not more than 5.52 MPa (800 psi); $K_2 = 0.3$; and $K_3 = 16.55$ MPa (2400 psi).
- For normal-weight concrete placed against hardened concrete with the interface intentionally roughened, $K_1 = 2.76$ MPa (400 psi); $K_2 = 0.3$; and $K_3 = 16.55$ MPa (2400 psi).
- For Sand-lightweight concrete, $K_1 = 1.72$ MPa (250 psi); $K_2 = 0.2$; and $K_3 = 8.27$ MPa (1200 psi).
- For all lightweight concrete, $K_1 = 1.38$ MPa (200 psi); $K_2 = 0.2$; and $K_3 = 8.27$ MPa (1200 psi).

2. For concrete placed against hardened concrete with the substrate surface not intentionally roughened, the ultimate shear transfer is given by:

$$\boldsymbol{v_u = 0.6\lambda\rho_v f_y} \quad (2.18)$$

provided that v_u does not exceed $0.2f_c'$ neither 5.52 MPa (800 psi)

3. For concrete placed against clean, unpainted, as-rolled steel using headed studs or reinforcing bars, the ultimate shear transfer is predicted by:

$$\boldsymbol{v_u = 0.7\lambda\rho_v f_y} \quad (2.19)$$

provided that v_u does not exceed $0.2f_c'$ neither 5.52 MPa (800 psi).

The concrete density coefficient, λ is taken as 1.00 for normal density concrete; 0.85 for sand-lightweight concrete; and 0.75 for all-lightweight concrete.

2.4.6 Paulay, Park and Phillips (1974)

In this systematic and comprehensive study, 36 push-off specimens with different configurations from the previous research were tested (see Figure 2.19). The investigated parameters were, the roughness of the contact surface, the reinforcement dowel action and the reinforcement ratio. Six specimens were cast monolithically as control specimens. few specimens were subjected to alternating cyclic loading. The bond at the interface was initially destroyed in some specimens to determine the contribution of the dowel action to the shear transfer strength. The authors concluded that the large displacements associated with significant dowel action resistance are not practical and, hence, the dowel action cannot be considered in the design of the construction joints regarding the shear transfer strength. It was observed that the roughness of the joint is a major parameter in the shear transfer along construction joints. Specimens with rough surfaces and the bond destroyed (by spraying three coats of varnish) along their joints exhibited higher slips and lower shear strengths. The bond was pointed out to be most significant in increasing the joint stiffness.

The interface shear strength of construction joints was reported to be maintained during the cycling loading without accumulating of excessive residual slips.

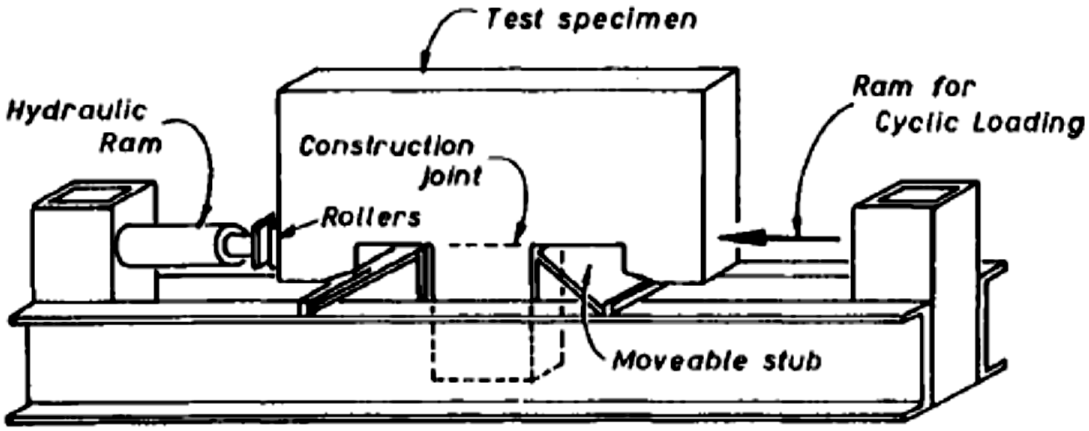

Figure 2.19 Test specimen and setup (Paulay et al. 1974)

2.4.7 Loov (1978, 1994)

Loov (1978) was the first to incorporate the influence of concrete strength in the shear transfer strength of concrete-to-concrete interfaces. His proposed equation was in the following non-dimensional form:

$$\frac{v_u}{f'_c} = k\sqrt{\frac{\sigma}{f'_c}} \tag{2.20}$$

It can also be written as:

$$v_u = k\sqrt{\sigma f'_c} \tag{2.21}$$

The author suggested a value of 0.5 for the constant k for initially uncracked shear interfaces. It should be noted that this equation is identical to Birkeland's equation (Eq. 2.7) when $k = 0.5$, and $f'_c = 30.9$ MPa. If no external normal stresses are applied on a shear plane crossed by a perpendicular reinforcement (i.e. $\sigma_n = 0$), the above equation becomes:

$$v_u = k\sqrt{\rho_v f_y f'_c} \tag{2.22}$$

A research regarding the longitudinal shear transfer strength along the interfaces between precast girders and cast-in-place slabs was done by Loov and Patnaik (1994). A total of 16 composite concrete beams were tested in which the reinforcement ratio and the concrete strength was the primary investigated parameters. Clamping stresses ($\rho_v f_y$) were varied from 0.4 to 7.72 MPa. In this study, the interface surface was left as-cast in all beam specimens and was described as "well compacted having a rough surface, clean and free of laitance, with coarse aggregate protruding but firmly fixed in the matrix".

The ultimate horizontal shear resistance of the studied beam specimens was not obtained until a minimum slip of at least of 0.5 mm was reached. The authors indicated that at a slip of 0.13 mm suggested by Hanson (1960), the stresses in the steel reinforcement were much lower than the yield stress. However, at 0.5 mm slip, the stresses in most of the steel passing the interface were near the yield point.

The evaluation of the horizontal shear at the interface between the web and its flange, at the ultimate load, was based on the elastic shear equation (Eq. 2.1) using the cracked transformed properties of the beam cross section. However, the authors realized that this equation is an approximate and provides only a basis of comparison.

The following expression for the shear strength for interfaces in composite beams without shear ties was proposed.

$$v_u = 0.6\sqrt{0.1 f'_c} \quad \text{(MPa)} \tag{2.23}$$

This equation was combined with Loov's equation (Eq. 2.22) to provide a general expression for the ultimate shear transfer in composite concrete beams as follows:

$$\boldsymbol{v_u = \lambda k\sqrt{(0.1 + \rho_v f_y) f'_c}} \quad \text{(MPa)} \tag{2.24}$$

As a lower bound for all tests data, a value of 0.6 for the constant k was suggested. However, for design purpose and to account for the roughness variation of the interface during construction, a value of 0.5 for k was granted. The constant, k, was kept as 0.6 kept for monolithic construction where the variation of the roughness is not warranted. The maximum value of the longitudinal shear stress is limited to $0.25f'_c$. In the above expression, λ is taken equal to 1.00 for normal weight concrete; 0.85 for sand-lightweight concrete; and 0.75 for all lightweight concrete.

2.4.8 Patnaik (2001)

This study was conducted by Patnaik (2001) to study the behaviour of composite concrete beams with smooth interfaces. The results of 24 test beams tested in this study, in addition to eighteen test beams results of a previous research were used in the analysis of the horizontal shear across smooth interfaces. Some remarkable conclusions were drawn and a design expression for the ultimate shear transfer along smooth interfaces was proposed. It was shown that the concrete strength and the ratio of the effective depth to the shear span (*d/s*) do not influence the horizontal shear strength of smooth interfaces. The most significant factor, in this case, was the reinforcement parameter. Accordingly, the ultimate longitudinal shear stress of smooth interfaces was suggested as follows:

$$\boldsymbol{v_u = 0.6 + \rho_v f_y} \quad \text{(MPa)} \tag{2.25}$$

provided that v_u should not exceed $0.2f'_c$ neither 5.52 MPa (800 psi), and the reinforcement clamping stress $\rho_v f_y$ is not less than 0.35 MPa (50.8 psi). Although it was

mentioned that some longitudinal shear resistance can be delivered from unreinforced smooth interfaces, because of the associated uncertainty, the author suggested that no shear strength (i.e. $v_u = 0$) should be considered in the case when $\rho_v f_y$ is less than 0.35 MPa (50.8 psi).

2.4.9 Kahn and Mitchell (2002)

It was intended, in this study, to examine the applicability of the ACI 318 (1999) shear friction provisions for high-strength concretes. 50 push-off specimens with initially uncracked, cracked and cold-joint interfaces were tested. In specimens with cold-joint condition, the interface surface was left as-cast which provided a rough surface equivalent to an artificially roughened surface to an average amplitude of 6 mm. The failure of specimens with uncracked and cold-joint interfaces was initiated by diagonal cracks to the shear plane and was accompanied by large amount of concrete spalling. This fracture was similar to what was observed by Hofbeck et al. (1969) and Mattock and Hawkins (1972). The authors made an observation that the ultimate strength of uncracked and cold-joint specimens were similar, and the residual capacities of the latter specimens were similar to those of precracked specimens. The precracking procedure, initially proposed by Hofbeck et al. (1969), which was also applied to test specimens of this study, was considered to stimulate an initial fracture of the joint rather than just an accidental crack. In conclusion, the ACI 318 (1999) shear friction provisions were found to be conservative in estimating the interface shear strength for high-strength concrete and the following shear friction equation was proposed for both uncracked and cold-joint rough interfaces:

$$\boldsymbol{v_u = 0.05 f'_c + 1.4 \rho_v f_y} \tag{2.26}$$

where the ultimate shear strength v_u was upper limited to 20% of the concrete compressive strength f_c' (i.e. $v_u \leq 0.2f_c'$).

2.4.10 Mansur, Vinayagam and Tan (2008)

The objective of this research was to look for a more representative model for tests data of precracked interfaces with high strength concrete of 70 to 100 MPa, and to examine the validity of the previously proposed models by different researchers. The experimental part of this study involved 19 precracked push-off specimens with the concrete strength and the reinforcement parameter are the variables among them. The analytical analysis involved 154 data collated from the literature, including the results of this study.

The cohesion of the interface was found to be mainly dependent of the concrete strength. The actual coefficient of friction of precracked interfaces was found independent of the concrete strength and equal to 0.55. A single curve formulation was proposed based on the expression of Mau and Hsu (1988). This expression was given as:

$$\frac{\boldsymbol{v_u}}{\boldsymbol{f_c'}} = \mathbf{0.566}\left(\frac{\boldsymbol{\rho_v f_y}}{\boldsymbol{f_c'}}\right)^{\mathbf{0.5}} \leq \mathbf{0.3} \tag{2.27}$$

In addition, the authors proposed a trilinear correlation, in which the shear transfer strength was given by an expression for each of three different linear branches of the idealized load-defamation curve proposed in this paper. For the first branch corresponding to the normalized clamping stresses ($\rho_v f_y / f_c'$) less than 0.075, the proposed expression was:

$$\frac{\boldsymbol{v_u}}{\boldsymbol{f_c'}} = \mathbf{2.5}\left(\frac{\boldsymbol{\rho_v f_y}}{\boldsymbol{f_c'}}\right) \tag{2.28}$$

For normalized clamping stresses varying in the range of 0.075 to 0.270, corresponding to the middle branch of the trilinear idealization, the normalized with respect to the concrete strength ultimate shear transfer stress is given by:

$$\frac{v_u}{f'_c} = \frac{0.56}{(f'_c)^{0.385}} + 0.55\left(\frac{\rho_v f_y}{f'_c}\right) \quad \text{(MPa)} \qquad (2.29)$$

For higher values of the normalized clamping stresses, the third linear branch represents the maximum upper limit of the longitudinal shear transfer strength. The authors claimed that this limit was necessary to ensure that the steel will yield at failure. Therefore, the last linear branch was defined as:

$$\frac{v_u}{f'_c} = 0.3 \qquad (2.30)$$

In the conclusion of this study, it was stated that the single curve equation (Eq. 2.27), provided better predictions of the shear transfer strength than the trilinear model does, and hence, it was recommended for design purposes.

2.4.11 Harries, Zeno and Shahrooz (2012)

The authors of this paper made an effort to provide an improved understanding of the shear friction hypothesis in describing the behaviour of reinforced concrete-to-concrete interfaces. The primarily focus of this study was to verify what was implied by all the previous shear friction equations that the ultimate shear stress is achieved at the yielding of the steel across the shear plane. Eight typical push-off tests with cold-joint condition at their interfaces were tested. Two types of steel were used, which are intermediate strength steel with an average yield strength of 424 MPa and high strength steel with a yield strength of 896 MPa. No.3 (9.5 mm) and No. 4 (12.7 mm) bars were used for each type of steel.

The authors reported that the ultimate shear transfer strength was not affected by the grade of steel. The most critical finding of this study is that the stresses in the interface steel reinforcement were reported to be significantly lower than the yield stress at the ultimate load. In the light of these observations, it was suggested that the clamping stresses at the ultimate load should be a function of the modulus of elasticity of steel E_s rather than the yield strength f_y. Three different expressions of the ultimate shear transfer stress were proposed as follows:

For interfaces in monolithic concrete

$$\boldsymbol{v_u = 0.075 f'_c + 0.002 E_s \rho_v} \tag{2.31}$$

For rough cold-jointed interfaces

$$\boldsymbol{v_u = 0.040 f'_c + 0.002 E_s \rho_v} \tag{2.32}$$

For cracked interfaces

$$\boldsymbol{v_u = 0.002 E_s \rho_v} \tag{2.33}$$

As implied by these equations, a value of the friction coefficient of 1 was granted. The authors proposed that external clamping stresses contribute in the shear strength prior to the cracking of the interface. Therefore, they should be neglected in shear friction calculations, unless no cracking, along the interface plane, is permitted. The ultimate shear transfer stress v_u is upper limited to $0.2 f'_c$.

2.5 Design Requirements of Shear Transfer in Major Design Codes

In this section, the design requirements for shear transfer strength design requirements in various major design codes are presented. The limitations and conditions associated with each code are also pointed out.

2.5.1 ACI 318 (2014)

The American building code requirements for structural concrete ACI 318 (2014) and commentary ACI 318R (2014) adopted the original expression of the shear friction theory proposed by Birkeland and Birkeland (1966) and Mast (1968). The ultimate nominal shear transfer resistance is governed by friction only as specified in Clause 22.9 of the ACI 318 (2014) as follows:

$$\boldsymbol{v_u = \rho_v f_y(\mu \sin \alpha_f + \cos \alpha_f)} \tag{2.34}$$

The latter equation does not explicitly account for concrete cohesion neither for the dowel action of the reinforcing bars. The coefficient of friction μ is defined in clause 22.9.4.2 of the ACI 318 (2014) according to the condition and preparation of the interface surface as represented in Table 2.1. In this table, λ is a modification factor related to concrete density and is identified as: 1.00 for normal-weight concrete; and 0.75 for all lightweight concrete. For other cases, λ is calculated based on the volumetric proportions of lightweight and normal-weight aggregates but should not exceed 0.85.

Table 2.1 Coefficient of friction, μ proposed by ACI 318 (2014)

Contact surface condition	$\boldsymbol{\mu}$
Concrete placed monolithically	1.4λ
Concrete placed against clean, free of laitance, and hardened concrete that is intentionally roughened to an amplitude of 0.25 in (6.35 mm)	1.0λ
Concrete placed against clean, free of laitance, and hardened concrete that is not intentionally roughened	0.6λ
Concrete placed against as-rolled structural steel that is clean, free of paint, and provided with headed shear studs or welded deformed bars or wires	0.7λ

However, section 16.4 of the ACI 318 (2014) permits the nominal shear transfer resistance of contact surfaces of the interconnected members of composite concrete beams to be taken according to Table 2.2 only if the nominal longitudinal shear stress induced along a shear plane does not exceed 500 psi (3.45 MPa).

The minimum shear transfer reinforcement area $A_{v,min}$ is defined in section 16.4.6 as follows:

$$\boldsymbol{\rho_{v,min}} = \textbf{the greater of } \begin{cases} \boldsymbol{0.75\sqrt{f'_c}/f_y} \textbf{ in psi} & (\boldsymbol{0.06\sqrt{f'_c}/f_y} \text{ in MPa}) \\ \boldsymbol{50/f_y} \textbf{ in psi} & (\boldsymbol{0.34/f_y} \text{ in MPa}) \end{cases} \quad (2.35)$$

A maximum ultimate shear transfer stress, computed by Eq. 2.34**,** was also introduced in the ACI 318 (2014) in the shear friction provisions as follows: (a) for normal weight concrete placed monolithically or against hardened and roughened concrete to an amplitude of at least 0.25 in. (6.35 mm), the value of the shear strength v_u is upper limited to the lesser of $0.2f'_c$, 480+0.08f'_c psi (3.3+0.08f'_c MPa), and 1600 psi (11 MPa). In all other cases, the maximum limit of the shear transfer stress is taken as the minimum of $0.2f'_c$ and 800 psi (5.52 MPa).

Table 2.2 Nominal horizontal shear strength specified by ACI 318 (2014)

Shear transfer reinforcement	Contact surface preparation	Longitudinal shear strength, V_{nh}
$\rho_v \geq \rho_{v,min}$	Concrete placed against hardened concrete intentionally roughened to a full amplitude of approximately 0.25 in (6.35 mm)	lesser of $\begin{cases}\lambda(260 + 0.6\rho_v f_y) \\ 500\end{cases}$ (psi) Or lesser of $\begin{cases}\lambda(1.8 + 0.6\rho_v f_y) \\ 3.45\end{cases}$ (MPa)
	Concrete placed against hardened concrete not intentionally roughened	80 psi (0.55 MPa)
Other cases	Concrete placed against hardened concrete intentionally roughened	80 psi (0.55 MPa)

2.5.2 CAN/CSA A23.3 (2004)

According to the Canadian design code of concrete structures CAN/CSA A23.3 (2004), an existing crack along a shear plane shall be assumed. The relative displacement of the structural components connected at an interface is resisted by cohesion and friction as indicated by the modified shear friction theory (Mattock and Hawkins, 1972; Mattock, 1974; Mattock et al., 1976 and others). Based on these considerations, the nominal (un-factored) ultimate shear transfer stress for an interface is given as:

$$\boldsymbol{v_u = \lambda(c + \mu\sigma) + \rho_v f_y \cos \alpha_f} \tag{2.36}$$

Provided that the term $\lambda(c + \mu\sigma)$ is upper limited to $0.25f_c'$ and where λ is the concrete density modification factor and is taken as: 1.00 for normal density concrete; 0.85 for semi-low-density concrete; and 0.75 for low-density concrete, c is the cohesion stress,

μ is the friction coefficient, $\sigma = \rho_v f_y \sin\alpha_f + N/A_{cv}$ is the effective total normal stress to the shear plane, ρ_v is the ratio of the reinforcement crossing the shear plane, f_y is its yield strength, α_f is the angle of inclination to the shear plane of the shear friction reinforcement, N is the unfactored permanent load perpendicular to the shear plane, and A_{cv} is the area of the concrete section of the shear plane resisting shear transfer. Table 2.3 shows the values of c and μ associated with various conditions of the shear plane according to the CSA A23.3 (2004).

Table 2.3 Values of c and μ proposed by CAN/CSA A23.3 (2004)

Surface condition	c (MPa)	μ
concrete placed against hardened concrete with the surface clean but not intentionally roughened	0.25	0.60
Concrete Placed against hardened concrete with the surface clean and intentionally roughened to a minimum of 5 mm	0.50	1.00
concrete placed monolithically	1.00	1.40
concrete placed against as-rolled structural steel with headed studs or reinforcing bars	0	0.60

As an alternative to the shear friction equation, the Canadian standard CSA A23.3 (2004) introduces an expression for the nominal shear transfer (i.e. $\phi_c = 1$ and $\phi_s = 1$) based on the equation proposed by Loov (1978). The code, however, limits the application of the following expression to interfaces where the concrete is placed monolithically or placed against hardened concrete with the surface intentionally roughened to an amplitude

of at least 5 mm.

$$\boldsymbol{v_u = \lambda k\sqrt{\sigma f_c'} + \rho_v f_y \cos \alpha_f} \quad (2.37)$$

provided that $\lambda k\sqrt{\sigma f_c'}$ should not exceed $0.25 f_c'$. Where $k = 0.5$ for concrete placed against hardened concrete and $k = 0.6$ for monolithic concrete.

The code also specifies particular situations regarding composite concrete beams to be considered prior to the design using either Eq. 2.36 or 2.37. It is stated in section 17 that the maximum nominal longitudinal shear stress (i.e. $\phi_c = 1$) of a clean interface that is intentionally roughened should not be taken as greater than 0.7 MPa if ties are not provided across such an interface. Furthermore, when minimum ties are provided according to Eq. 2.38 across a clean but not intentionally roughened interface the maximum shear transfer resistance of such interface is 0.7 MPa. The minimum reinforcement for the longitudinal shear transfer proposed by this code is similar to transversal shear minimum reinforcement and it can be written in term of the reinforcement ratio as follows:

$$\boldsymbol{\rho_{v,min} = 0.06\sqrt{f_c'}/f_y} \quad (2.38)$$

where f_c' and f_y are in MPa. The maximum spacing of the lesser of 600 mm (24 in) and four times the least dimension of the supported member is also recommended.

2.5.3 CAN/CSA S6 (2014)

The Canadian bridge and highway design code CSA S6 (2014) adopted the same procedure outlined by the CSA A23.3 (2004). The alternative approach of the CSA A23.3 (2004) is not considered in the bridge code. Some slight differences can also be noted. in Eq. 2.36 the concrete density modification factor λ is to be multiplied by the term that

includes the coefficient of friction μ specified according to Table 2.3, instead of being multiplied by the entire first term of the latter equation. Additional to the maximum limit of the shear transfer specified by the CSA A23.3 (2004) of $0.25f_c'$, the Canadian Bridge Code specifies another limit of 6.5 MPa, whichever is less.

2.5.4 CPCI (2007)

The interface shear transfer procedure outlined in section 3.6.4 of the Precast and Prestressed Concrete Institute design manual, CPCI (2007) is based on the interface shear transfer provisions of the CSA A23.3 (2004). However, this manual maintains the maximum nominal shear transfer strength of $0.25f_c'$ recommended by the building code CSA A23.3 (2004) when the concrete compressive strength is equal to or less than 28 MPa, but, for higher concrete strength, the upper limit of the nominal shear transfer strength is specified as 7 MPa.

2.4.5 Eurocode 2 (2004)

The Eurocode 2 (2004): Design of concrete structures selected a design expression for the shear transfer design along interfaces with concretes cast-at-different times similar to the modified shear friction expression proposed by Mattock (1974). This expression incorporates the influence of the surface cohesion and friction.

$$\boldsymbol{v_u = cf_{ctd} + \mu\sigma_n + \rho_v f_y(\mu \sin \alpha_f + \cos \alpha_f) \leq 0.5 v f_{cd}} \qquad (2.39)$$

It also considers four conditions of the interface surface of shear plane in the evaluation of c and μ, namely: (a) very smooth surface, that is the surface resulted when concrete is cast against steel, plastic or specially prepared wooden moulds ($c =$

$0.025\ to\ 0.1$ and $\mu = 0.5)$; (b) smooth surface which is a slipformed or extruded surface, or that left without any further treatment after the vibration ($c = 0.2$ and $\mu = 0.6$); (c) rough surface which has a roughness of an amplitude of 3 mm at a spacing of a minimum of 40 mm, attained by raking, exposing of aggregate or other methods ($c = 0.4$ and $\mu = 0.7$); and (d) indented surface with a longitudinal undulation as shown in Figure 2.20 ($c = 0.5$ and $\mu = 0.9$).

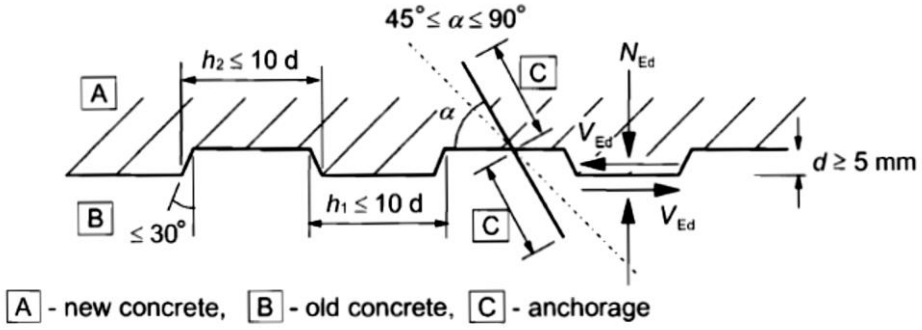

Figure 2.20 Indented interface surface [adpoted from Eurocode 2 (2004)]

2.5.6 AASHTO LFRD Bridge Design Specifications (2012)

The bridge design specifications AASTHO LFRD (2012) specifies several situations where the shear transfer along a definite plane should be considered in section 5.8.4 of this code, they are: (a) an existing or potential crack; (b) an interface between different materials; (c) an interface between two concretes cast at different times; and (d) an interface between different elements of a cross section. The design of such cases is carried according to the modified shear friction equation (Mattock and Hawkins, 1972), which accounts for an interface cohesion provided by the concrete interface. The ultimate nominal shear transfer stress v_u is given by:

$$\boldsymbol{v_u = c + \mu(\rho_v f_y + \sigma_n)} \tag{2.40}$$

where c is the cohesion associated with the concrete plane of an interface, μ is the friction factor, f_y the yield strength of the steel [limited to 60 ksi (414 MPa)], ρ_v is the ratio of the reinforcement crossing, perpendicularly, the interface, and σ_n is the permanent compressive stress normal to the shear plane (zero if tension). The value of the shear resistance calculated according to Eq. 2.54 should not be greater than the lesser of $K_1 f_c'$, and K_2. The fraction of concrete strength available to resist the interface shear K_1, and the factor K_2, c and μ are specified in the code for various conditions of the substrate interface according to Table 2.4.

2.5.7 AASHTO Standard Specifications for Highway Bridges (2002)

Similar to the ACI 318 (2014), the standard specifications or highway bridges AASHTO (2002) granted the original friction theory of Birkeland and Birkeland (1966) and Mast (1968) to predict the shear transfer capacity of an existing or a potential crack in reinforced concrete. Being the ultimate shear transfer stress v_u predicted by:

$$\boldsymbol{v_u = \rho_v f_y(\mu \sin \alpha_f + \cos \alpha_f)} \tag{2.55}$$

The coefficient of friction μ varies according to the interface surface condition as follows: (a) for concrete placed monolithically, $\mu = 1.4\lambda$; (b) for concrete placed against hardened and intentionally roughened concrete to an amplitude of 0.25 in (6.35 mm) surface, $\mu = 1.0\lambda$; (c) for concrete placed against hardened concrete not intentionally roughened, $\mu = 0.6\lambda$; and (d) for concrete anchored to as-rolled, clean and unpainted structural steel by headed studs or reinforcing bars, $\mu = 0.7\lambda$. λ is the concrete density factor: $\lambda = 1.00$ for normal-weight concrete; $\lambda = 0.85$ for sand-lightweight concrete;

and $\lambda = 0.75$ for all lightweight concrete. The shear transfer strength is upper limited so that it should not exceed $0.09f_c'$ neither 360 psi (2.5 MPa).

Table 2.4 Values of c, μ and factors k_1 and k_2 according to AASHTO LFRD (2012)

Interface condition	c	μ	k_1	k_2
cast-in-place concrete slab placed against hardened, clean and roughened to an amplitude of 0.25 in (6.35mm) surface of a concrete girder	0.28 ksi (1.93 MPa)	1.0	0.30	1.8 ksi (12.4 MPa) for normal-weight concrete 1.3 ksi (9.0 MPa) for lightweight concrete
normal-weight concrete placed monolithically	0.4 ksi (2.76 MPa)	1.4	0.25	1.5 ksi (10.3 MPa)
lightweight concrete placed monolithically or non-monolithically against a clean concrete surface intentionally roughened to an amplitude of 0.25 in (6.35 mm)	0.24 ksi (1.66 MPa)	1.0	0.25	1.0 ksi (6.9 MPa)
Normal-weight concrete placed against a clean concrete surface intentionally roughened to an amplitude of 0.25 in (6.35 mm)	0.24 ksi (1.66 MPa)	1.0	0.25	1.5 ksi (10.3 MPa)
Concrete placed against clean concrete surface, but not intentionally roughened	0.075 ksi (0.52 MPa)	0.6	0.20	0.8 ksi (5.5 MPa)
Concrete anchored to as-rolled structural steel by headed studs or reinforcing bars where all steel in contact with the concrete is clean and free of paint	0.025 ksi (0.17 MPa)	0.7	0.20	0.8 ksi (5.5 MPa)

For the horizontal shear along interfaces between interconnected elements in composite concrete beams, AASHTO (2002) specifies some distinct requirements. A minimum reinforcement ratio of $50/f_y$ is defined, however, the spacing of such

reinforcement should not exceed four times the least web width, neither 24 in (610 mm). When the contact surface is initially roughened or not roughened but provided with a minimum reinforcement, the shear transfer strength should not be taken as greater than 36 psi (0.25 MPa). In addition, this code specifies a shear transfer strength of initially roughened interfaces to an amplitude of 0.25 in. (6.35 mm) and crossed by a minimum shear friction reinforcement of 160 psi (1.1 MPa). An additional shear strength of $72f_y/40000$ (psi) to be added to the permissible shear transfer resistance for each one percent increase in the reinforcement ratio crossing the interface in excess of the minimum ratio.

2.6 Summary

Because of their sensitivity in the design, concrete-to-concrete joints, especially, those between precast girders and cast-in-place slabs, have been justifiably and continuously studied over time. The details of the previous research carried out by different researchers prior to the present study have been summarized in this chapter. Various design expressions and hypotheses describing the behaviour of concrete-to-concrete interfaces subjected to direct shear stresses were presented. The design requirements in major codes relative to the shear transfer were emphasized and discussed in detail. The previous research findings can be summarized as follows:

1. The majority of the design expression provided in the previous research were derived based on the analysis of the test results of push-off specimens. These specimens were introduced by Anderson (1960) and Hanson (1960) and reported to exhibit similar behaviour to the interfaces in composite concrete

beams.

2. The shear transfer mechanism between different concrete layers was found to be a complex phenomenon that involves the combination of different sub-transfer mechanisms and depends on several parameters, such as the interface roughness, concrete compressive strength, stresses caused by normal forces at the interface and the amount of reinforcement crossing the interface. Because of this complex nature, it is not possible to explicitly separate all the parameters contributing to the shear transfer behaviour or establish explicit analytical relationships.
3. In earlier practices of composite construction, the longitudinal shear resistance of unreinforced interfaces was assumed to be equal to the allowable shear stress of unreinforced beams (ACI Committee 711, 1953). Therefore, it was suggested that if an interface was properly roughened, it could provide an adequate shear strength when combined with shear keys to prevent the horizontal displacement at the construction joint. However, an extensive research in interface shear transfer has been done since 1960. The shear friction expression was introduced by Birkeland and Birkeland (1966) and Mast (1968). It was investigated extensively, later on, by Mattock and his coworkers through a series of studies as discussed in this chapter.
4. In the majority of the cited studies the ultimate shear transfer strength was directly proportioned to the amount of steel reinforcement across the joint and linear expression were proposed. However, the first non-linear expression was proposed by Birkeland (1968) followed by Raths (1977) and Shaikh (1978).

Loov (1978) was the first researcher to include the influence of the concrete strength f_c' in his nonlinear expression of the shear transfer strength.

5. There were five millstones that can be distinguished in the development of shear transfer design: 1) the first publication of the original shear friction theory by Birkeland and Birkeland (1966); 2) the modified shear friction theory proposed by Mattock and Hawkins (1972), which included the contribution of the cohesion and the external clamping stresses; 3) the first parabolic equation for the shear transfer strength proposed by Birkeland (1968); 4) the explicit incorporation of the concrete strength in the parabolic equation of Loov (1978); and 5) the new approach of the shear friction theory, in which the shear transfer strength was related to the reinforcement stiffness rather than the yield strength of the steel (Harries et al. 2012).
6. Despite the variety of the shear transfer theories corresponding to different conditions of the concrete interfaces (i.e., cracked, uncracked, cold-joint), the shear friction theory was adopted by most researchers and design codes worldwide. According to most advanced version of this theory, the shear is transferred along concrete-to-concrete interfaces by three subsequent mechanisms: 1) Cohesion; 2) friction; and 3) dowel action. The literature review also identified several design expressions proposed by different researchers since 1960. The range of the application of these expressions was very wide, from interfaces in monolithic concrete to composite concrete members with rough, intermediate or smooth contact surfaces. Some of the previous design expressions along with their limitations are presented in Table 2.5.

7. It has to be highlighted that, up to date, concrete-to-concrete interfaces are being designed, constructed and investigated using, only, steel reinforcement. Therefore, this research aims to assess an annotative application of the GFRP as a shear transfer reinforcement.

Table 2.5 Shear transfer models

Research	Expression (SI units)	Limits/Notes
Anderson (1960)	For 20.7 MPa concrete: $v_u = 4.41 + 229\rho_v$ For 51.7 MPa concrete: $v_u = 5.52 + 276\rho_v$	-
Hanson (1960)	For rough bonded interfaces: $v_u = 3.45 + 121\rho_v$	-
Birkeland and Birkeland (1966)	$v_u = \rho_v f_y \mu$	μ = 1.7 for monolithic concrete. $\mu = 1.4$ for artificially roughened joints. μ = 0.8-1 for ordinary construction joints. $\rho_v \leq 1.5\%$; $v_u \leq 5.52$ MPa $f_c' \geq 27.6$ MPa
Mast (1968)	$v_u = \rho_v f_y \mu$	$\mu = 1.4$ for rough interfaces. $\mu = 0.7$ for smooth interfaces. $\rho_v f_y \leq 0.15 f_c'$
Birkeland (1968)	$v_u = 2.78\sqrt{\rho_v f_y}$	-
Mattock and Hawkins (1972)	$v_u = 1.38 + 0.8(\rho_v f_y + \sigma_n)$	$\rho_v f_y + \sigma_n \geq 1.38$ MPa $v_u \leq (0.3 f_c'$ and 10.34 MPa)
Mattock (1974)	$v_u = 2.76 + 0.8\ (\rho_v f_y + \sigma_n)$ For inclined to shear plane reinforcement: $v_u = 2.76\, sin^2\theta + \rho_v f_s (0.8\, sin^2\theta - 0.5\, sin\, 2\theta)$ $f_s = 0$ for $0 < \theta < 51.3^o$ $f_s = -1.6 f_y\, cos(\theta + 38.7^o)$ for $51.3^o \leq \theta < 90^o$ $f_s = f_y$ for $90^o \leq \theta \leq 180^o$	$\rho_v f_y + \sigma_n \geq 1.38$ MPa $v_u \leq (0.3 f_c'$ and 10.34 MPa)

Mattock, Li and Wang (1976)	For sanded lightweight concrete: $v_u = 1.72 + 0.8\rho_v f_y$ For all lightweight concrete: $v_u = 1.38 + 0.8\rho_v f_y$	$\rho_v f_y \geq 1.38$ MPa For sanded lightweight concrete: $v_u \leq (0.2f_c'$ and 6.90 MPa) For all lightweight concrete: $v_u \leq (0.2f_c'$ and 5.52 MPa)
Loov (1978)	$\frac{v_u}{f_c'} = k\sqrt{\frac{\sigma}{f_c'}}$	$k = 0.5$ for initially uncracked interfaces.
Mattock (1988)	$v_u = 0.467{f_c'}^{0.545} + 0.8(\rho_v f_y + \sigma_n)$	$v_u \leq 0.3f_c'$
Loov and Patnaik (1994)	$v_u = \lambda k\sqrt{(0.1 + \rho_v f_y)f_c'}$	$k = 0.5$ for composite construction. $k = 0.6$ for monolithic concrete. λ = 1 for normal weight concrete. λ = 0.85 for sand-lightweight concrete. λ = 0.75 for all lightweight concrete. $v_u \leq 0.25f_c'$
Mattock (1994)	For a crack in monolithic concrete: $v_u = \frac{\sqrt{\rho_v f_y}}{4.536}{f_c'}^{0.73}$ For rough interface between concrete cast at different times: $v_u = \frac{\sqrt{\rho_v f_y}}{4.536}{f_c'}^{0.73} - 0.02f_c'$	$v_u \leq 0.3f_c'$
Mattock (2001)	For a crack in monolithic concrete or a crack between concretes cast at different times with an intentionally roughened interface: $v_u = K_1 + 0.8(\rho_v f_y + \sigma_n)$ $K_1 = 0.1f_c'$ but not more than 5.52 MPa. $K_2 = 0.3$ $K_3 = 16.55$ MPa	$\rho_v f_y + \sigma_n \geq K_1/1.45$ $v_u \geq 1.55K_1$ $v_u \leq (K_2 f_c'$ and $K_3)$
	For a crack in monolithic concrete or a crack between concretes cast at different times with an intentionally roughened interface: $v_u = 2.25(\rho_v f_y + \sigma_n)$ $K_1 = 2.76$ MPa $K_2 = 0.3$ $K_3 = 16.55$ MPa	$\rho_v f_y + \sigma_n \leq K_1/1.45$ $v_u \leq 1.55K_1$ $v_u \leq (K_2 f_c'$ and $K_3)$

	For sand-lightweight concrete: $K_1 = 1.72$ MPa $K_2 = 0.2$ $K_3 = 8.27$ MPa For all lightweight concrete: $K_1 = 1.38$ MPa $K_2 = 0.2$ $K_3 = 8.27$ MPa	
	For concrete placed against hardened concrete not intentionally roughened: $v_u = 0.6\lambda\rho_v f_y$ For concrete placed against clean, unpainted, as-rolled steel using headed studs or reinforcing bars: $v_u = 0.7\lambda\rho_v f_y$	$v_u \leq (0.2f_c' \text{ and } 5.52 \text{ MPa})$ λ = 1.00 for normal weight concrete. λ = 0.85 for sand-lightweight concrete. λ = 0.75 for all lightweight concrete.
Patnaik (2001)	For smooth concrete interfaces: $v_u = 0.6 + \rho_v f_y$	$\rho_v f_y \geq 0.35$ MPa $v_u \leq (0.2f_c' \text{ and } 5.52 \text{ MPa})$
Khan and Mitchell (2002)	$v_u = 0.05f_c' + 1.4\rho_v f_y$	$v_u \leq 0.2f_c'$
Mansur, Vinayagam and Tan (2008)	$\frac{v_u}{f_c'} = 0.566\left(\frac{\rho_v f_y}{f_c'}\right)^{0.5}$	$\frac{v_u}{f_c'} \leq 0.3$
Harries, Zeno and Shahrooz (2012)	For interfaces in monolithic concrete: $v_u = 0.075f_c' + 0.002E_s\rho_v$ For rough cold-joint interfaces: $v_u = 0.040f_c' + 0.002E_s\rho_v$ For cracked interfaces: $v_u = 0.002E_s\rho_v$	$v_u \leq 0.2f_c'$

CHAPTER 3

DETAILS OF THE EXPERIMENTAL PROGRAM

3.1 Introduction

Most of the previous research concerning the shear transfer problem relied on the test results of push-off specimens. These specimens were first introduced by Anderson (1960) and Hanson (1960) and they have been used extensively since then. This type of specimen was shown to be reliable in stimulating similar conditions to actual joints in composite concrete elements. Accordingly, large scale push-off specimens were adopted in the present program to evaluate the shear transfer strength and behaviour of cold-joint concrete interfaces when intersected by GFRP reinforcement. The testing program of the present research program involved casting and testing twenty push-off test specimens to fully investigate the behaviour of concrete joints with GFRP utilized as shear transfer reinforcement. Each specimen consists of two L-shaped concrete blocks cast at different times to achieve a cold-joint condition at their interface, which better stimulates the actual condition between precast girders and cast-in-place slabs of composite concrete beams. No special treatment was applied to the interface surface and was left as-cast. The test specimens were divided into two series according to their concrete strength. This chapter outlines the details of the testing program.

3.2 Details of Test Specimens

All of the test specimens were push-off specimens; each with two L-shaped concrete blocks. In all specimens, one block was cast horizontally first with the appropriate shear

transfer reinforcement projecting from its top surface. The second part was also cast horizontally, on top of the first block, after three days to stimulate the condition of cast-in-place slabs provided on top of precast girders.

Large scale push-off test specimens with GFRP reinforcement provided across their joints were used in the current investigation of the shear transfer of cold-joint concrete connections. The test specimen consists of two L-shaped concrete blocks as shown Figure 3.1. The shear plane, part of the web of the L-shape, is 250 mm wide and 500 mm long. The flange of the L-shape is 250 mm wide, 500 mm long and 250 mm thick. The main purpose of the flange part is to apply a concentric shear load along the shear plane between the two parts. A 19 mm (0.75 in.) gap was provided between the connected parts in the direction of the applied load to allow for free slip between these parts. The total length of the specimen was about 1040 mm. Figure 3.2 shows the typical design and dimensions of the used push-off specimen.

A total of twenty push-off specimens were cast and tested. The test parameters were the GFRP stiffness and geometry, and the concrete strength. Three different shapes of the GFRP reinforcement were provided; (1) stirrup; (2) headed bar; and (3) angle (see Figure 3.3). Also, two different concrete strengths, 30 and 50 MPa were investigated. Accordingly, the twenty test specimens were divided into two series; Series-I includes specimens with a concrete compressive strength of 50 MPa and Series-II represents specimens with a concrete compressive strength of 30 MPa. Some specimens were replicated for the reliability of data.

Figure 3.1 Push-off specimen

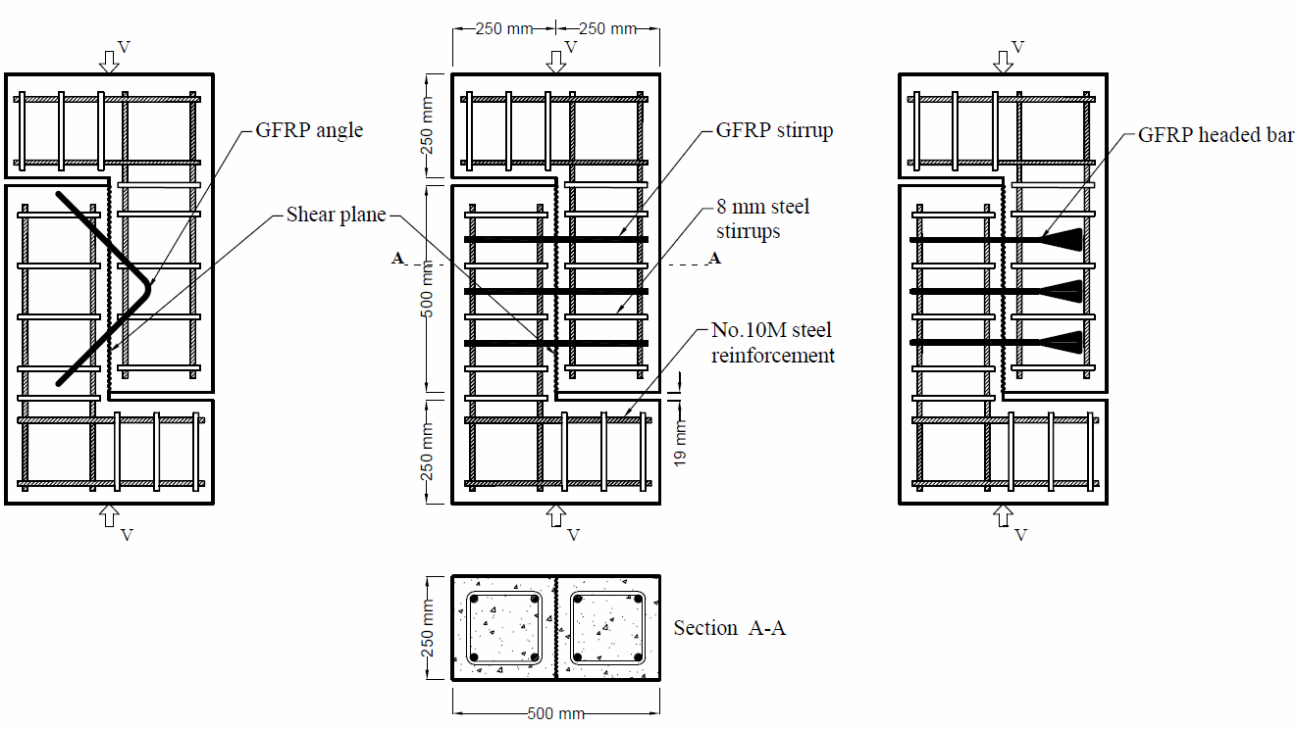

Figure 3.2 Design of push-off specimens

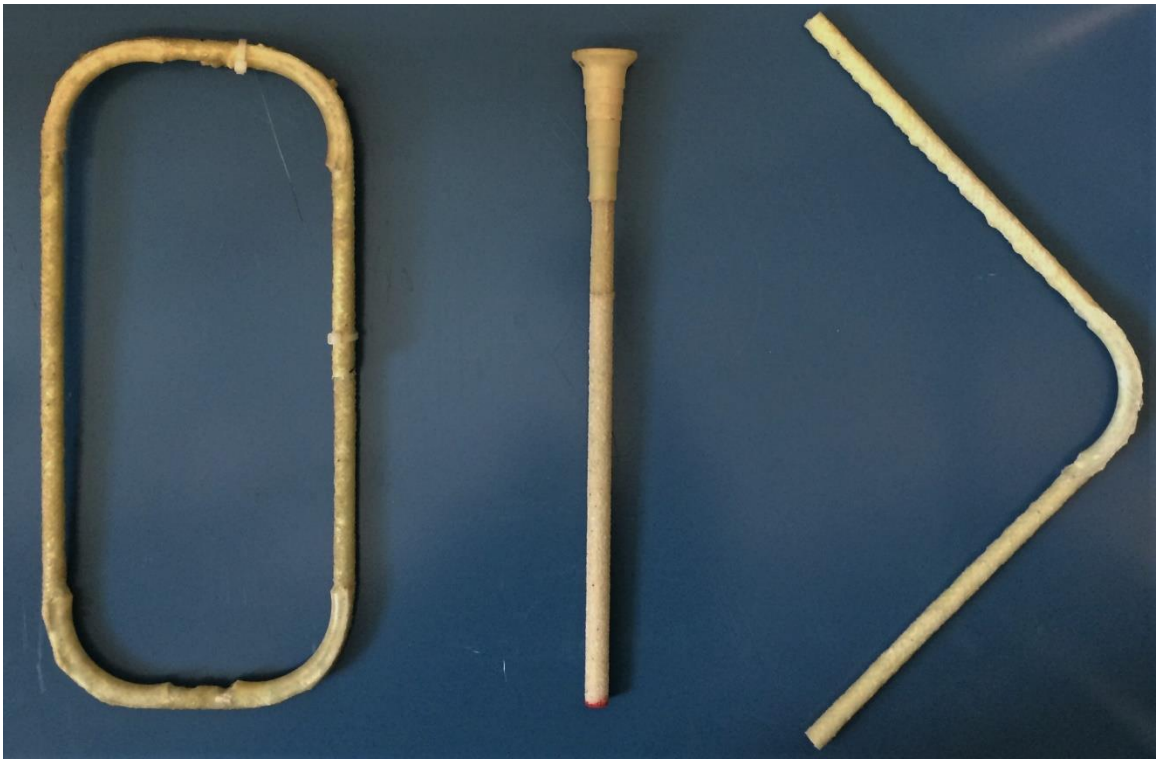

Figure 3.3 Shapes of GFRP reinforcement

The test specimens were designed to have different reinforcement axial stiffness ratios ($E\rho_v$). Specimens were tested with a GFRP reinforcement ratio varying between 0 to 0.61%. In addition, Headed bars had a modulus of elasticity E_F of 60 GPa but stirrups and angles had a modulus of 50 GPa (according to the supplier). Therefore, the axial stiffness ratio of the GFRP reinforcement (i.e. stirrups, headed bars and angles) was the main parameter ($E_F\rho_v$).

Table 3.1 shows the test matrix. In this table, the first character of the specimen's designation represents the reinforcement type; S = steel and F = FRP, the second letter stands for the reinforcement geometry; A = angle, H = headed bar and S = stirrup and the third character indicates the number of the used reinforcement stirrups, headed bars or

angles across the interface. The number after the hyphen indicates the concrete strength of which the specimen is made of.

Moreover, to investigate the behaviour and capacity of plain, as-cast concrete interfaces, one specimen of each series was constructed without any reinforcement across the interface (C0-50 and C0-30). Furthermore, to compare the behaviour of GFRP reinforced interfaces with steel reinforced ones, more control specimens were constructed, in which one and two steel stirrups were used across their shear plane (SS1-50 and SS2-50).

Specimens were loaded as indicated by the arrows in Figure 3.2, so only direct shear without moment is produced along the shear plane. In conformance with the CSA A23.3 (2004) and ACI 318 (2014), only inclined to the shear plane reinforcement that would be placed in tension upon the application of the shear load is considered for specimens with GFRP angles across the shear plane in Table 3.1.

Table 3.1 Test matrix and specimens designation

Series	Specimen ID	f'_c (MPa)	Reinforcement type and shape	A_v (mm^2)	ρ_v (%)	$E\rho_v$ (MPa)
I	C0-50	50	NA	0	0.00	0
	SS1-50		Steel Stirrup	200	0.16	320
	SS2-50			400	0.32	640
	FS1-50		GFRP stirrup	253.4	0.20	101
	FS2-50			506.8	0.41	203
	FS2-50*			506.8	0.41	203
	FS2-50**			506.8	0.41	203
	FS3-50			760.2	0.61	304
	FH2-50		GFRP headed bar	253.4	0.20	122
	FH3-50			380.1	0.30	182
	FH3-50*			380.1	0.30	182
	FH5-50			633.5	0.51	304
	FA2-50		GFRP angle	253.4***	0.20	101
	FA3-50			380.1***	0.30	152
II	C0-30	30	NA	0	0.00	0
	FS2-30		GFRP stirrup	506.8	0.41	203
	FS3-30			760.2	0.61	304
	FH3-30		GFRP headed bar	380.1	0.30	182
	FH5-30			633.5	0.51	304
	FA3-30		GFRP angle	380.1***	0.30	152

** refers to 1st repeated specimen for reliability of data*
*** refers to 2nd repeated specimen for reliability of data.*
**** represents the area of the inclined tensile reinforcement*

3.3 Fabrication of Test Specimens

All test specimens were fabricated in the structural lab at the University of Windsor using a custom formwork to enable the fabrication of the cold-joint along the shear interface. The formwork was deigned such that four specimens were cast at the same time. This formwork consisted of plywood sheets that were used to obtain the required shape of the push-off specimen. The plywood sheets were supported by 4x2 in. wood studs. The

detail of the form work is shown in Figure 3.4(a).

In order to achieve the cold-joint condition, each specimen was cast in two stages. One half of the specimen was cast first, in which the web of the L-shaped block was laying horizontally. Longitudinal and transverse steel bars and stirrups were used to reinforce both of the web and the flange of the L-shape to prevent any flexural cracks during testing. The steel reinforcement was tied together and the resulted steel cages were placed in the formwork with the proper covers. The shear transfer reinforcement was then secured in place as shown in Figure 3.4(b).

The concrete was poured and vibrated well. The top surface was also vibrated so a natural compacted rough interface was achieved [Figure 3.4(c)]. The first parts of the specimens were left in the form work and covered with a wet burlap and a plastic sheet wrapped over the burlap as can be seen in Figure 3.4(d). Figure 3.4(e) shows a typical roughness achieved for the as-cast surface in this study.

After three days of moist curing, the burlap cover was removed. The top surface of the first casted parts was cleaned from any impurities and loose concrete particles, dust, laitance, etc. The steel reinforcement cages, for the second part of each specimen, were then installed with the appropriate cover reinforcement chairs. Also, white polystyrene rigid foam sheets were provided, as shown in Figure 3.4(f), to create a gap between the interconnected blocks at their flanges to allow for a free slip when the shear load is applied. These sheets were removed prior to testing. The white foam sheets were 19 mm thick (0.75in.).

The second half of each specimen was cast in the fourth day after casting the first one using the same concrete admixture used for the first part. The concrete was poured on a dry and clean surface of the interface and was well compacted. The top surface of the second part was troweled smooth. Figure 3.4(g) shows the full four specimens, in the form work, after casting.

After three days, the formwork and the plywood sheets between the specimens were removed as shown in Figure 3.4(h). Afterward, specimens were moist cured under the wet burlap and the plastic sheet, along with the corresponding cylinders, until the desired concrete strength was reached, which was usually at seven days from the casting of the second parts.

Each specimen was also painted with a white paint in order to monitor the development and progress of any cracks that might develop during the test. Figure 3.5 illustrates the shape of the resulting ready-to-test push-off specimen, after removing the foam sheets between the concrete blocks.

(a)

(b)

Figure 3.4 Fabrication of push-off test specimens

(c)

(d)

Figure 3.4 Fabrication of push-off test specimens (*continued*)

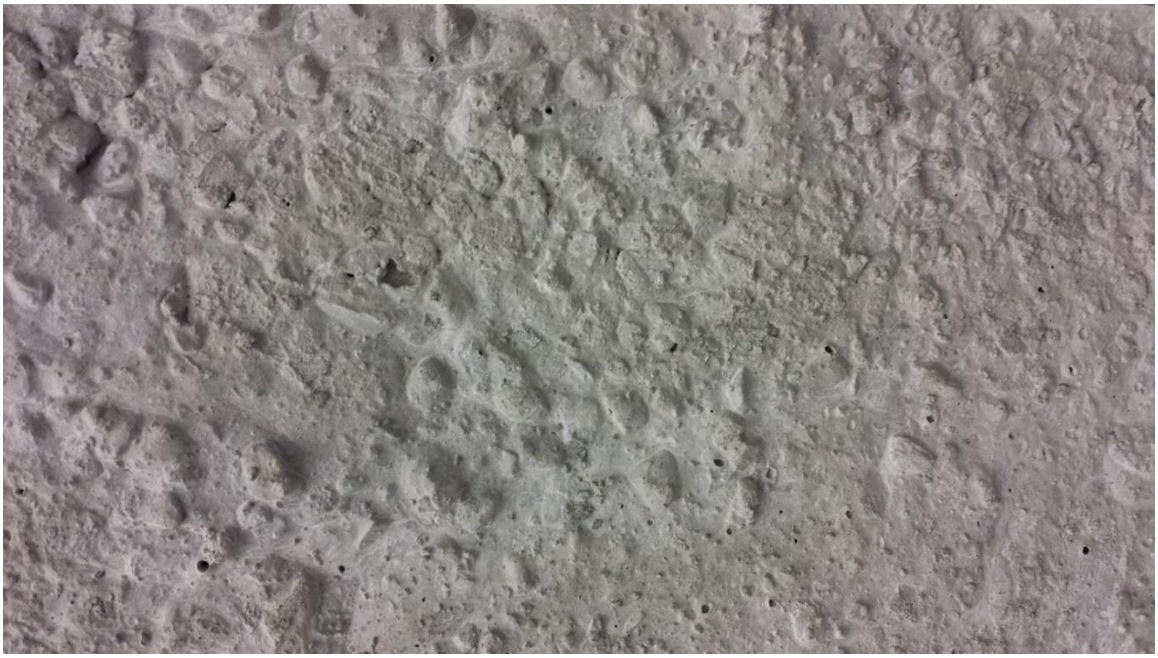

(e)

(f)

Figure 3.4 Fabrication of push-off test specimens (*continued*)

(g)

(h)

Figure 3.4 Fabrication of push-off test specimens (*continued*)

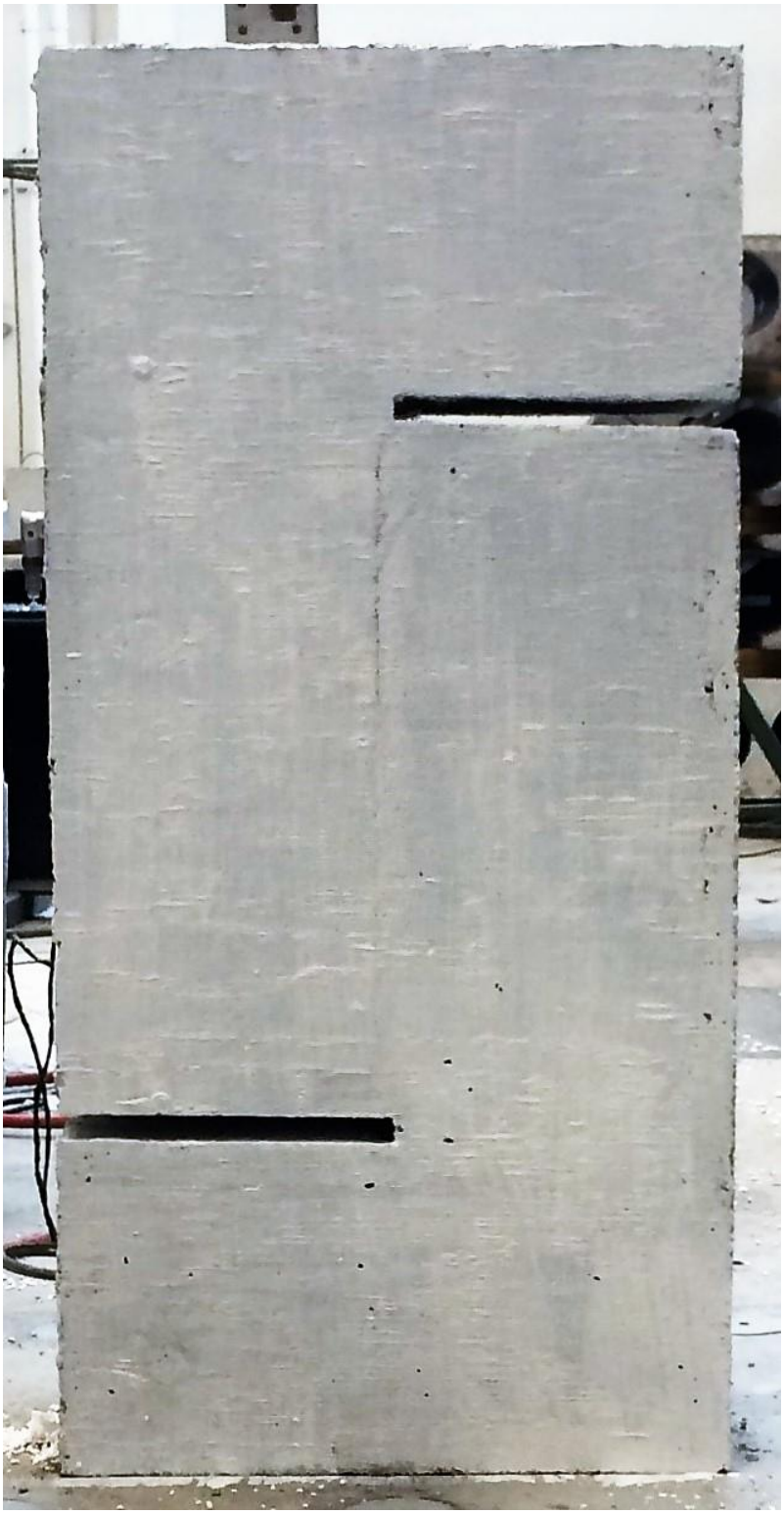

Figure 3.5 Final product of the constituted push-off specimen

3.4 Materials Properties

3.4.1 Concrete

Two different normal weight concretes, 30 and 50 MPa were used. The concrete was mixed in the casting bay of the structural lab using general use (GU) Portland cement. The fine aggregate was washed local river sand and the coarse aggregate was well graded crushed stones with a maximum size of 14 mm. All of these materials were locally supplied. The mix proportions for one cubic meter for two different concrete strengths (30 and 50 MPa) was as shown in Table 3.2. At least twelve 102 x 203 mm (4 x8 in) and three 152 x 305 mm (6 x 12 in) cylinders were prepared for each concrete patch. The cylinders were cured under similar conditions of those of the corresponding test specimens. The average compressive strengths of the cylinders tested on the same day that the corresponding specimens were tested on, were 30.5 and 49.7 MPa for the first and second admixtures, in Table 3.2, respectively. The compressive strength f_c' and the splitting tensile strength f_r of the concrete were evaluated in accordance to ASTM C39 (2015) and ASTM C496 (2011), respectively.

Table 3.2 Mix proportions per one cubic meter of concrete

Target strength (MPa)	**30**	**50**
Cement, kg	380	641
Fine aggregate, kg	788	559
Coarse aggregate, kg	1002	1012
Water, kg	168	177

3.4.2 Steel Reinforcement

Steel shear transfer reinforcement, in form of stirrups, was used in two control specimens of the first series (SS1-50 and SS2-50). This reinforcement consisted of stirrups made of No. 10M metric bars conforming to CSA G30.18 (2009), Grade 400. This steel reinforcement (10M bars) in addition to steel stirrups made of 8 mm imperial bars were used in each specimen away from the shear plane to strengthen the specimen and avoid any local failures except that along the shear plane. The average young modulus of the used steel was about 200 GPa and the yield strength was 400 MPa.

3.4.3 GFRP Reinforcement

Three different configurations of the GFRP reinforcement intersecting the shear planes were used as was presented in Figure 3.3. All of the GFRP reinforcement was supplied by Pultrall Inc. V-ROD stirrups, headed bars and bent bars (angles) were sand coated for the bond purpose and was made of continuous longitudinal fibers. The mechanical and physical properties of the GFRP reinforcement are summarized in Table 3.3 according to the supplier information. 2 grades of V-ROD GFRP products were available and were used; (1) Grade-II GFRP with a medium modulus of elasticity of 50 GPa; and (2) Grade-III GFRP with a high modulus of elasticity of 60 GPa. GFRP stirrups and angles were made of Grade-II, No.4-12M bars with a nominal cross sectional area of 126.7 mm^2. However, headed bars were No.4-12M bars size made of Grade-III.

Table 3.3 Properties of GFRP reinforcement

GFRP Reinforcement	Nominal cross-sectional area (mm^2)	Ultimate tensile strength, f_{Fu} (MPa)	Tensile modulus E_F (GPa)	Average ultimate tensile strain, ε_{Fu} (%)	Poisson's ratio
Stirrup	126.7	1140	50	2.17	0.26
Angle	126.7	1140	50	2.17	0.26
Headed bar	126.7	1312	60	2.00	0.26

3.5 Instrumentations

In addition to the load cell used to monitor the applied shear load, three main types of measurements were used during testing.

3.5.1 Measurement of Slip

The relative slip between the two parts of the push-off specimen along the shear plane was closely monitored for every specimen. A linear variable differential transducer (LVDT) was provided on each side of the push-off specimen. Figure 3.6(a) shows the used LVDT. The first end of the LVDT was attached to one part of the specimen and the other permissible end was resting on an aluminum bracket fixed to the other part of the specimen as can be seen in Figure 3.6(b). The two LVDTs were connected to the data acquisition system to record the measured slips.

3.5.2 Measurement of the Lateral Dilation

The lateral strain across the shear plane (separation) was measured using PI-gauges. The configuration of the used PI-gauge is shown in Figure 3.7(a). Two PI-gauges were used

for each specimen, one attached to each side of the specimen across the shear plane. The PI-gauges were mounted to the specimen's surface perpendicular to the interface as shown in Figure 3.7(b) and were connected to the data acquisition system.

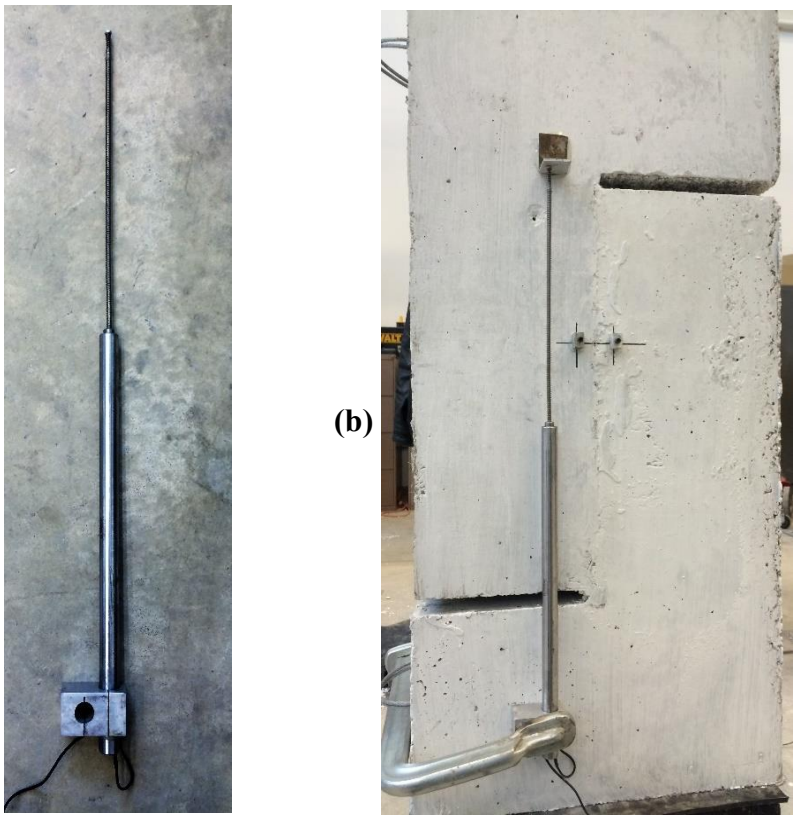

(a) **(b)**

Figure 3.6 Relative slip measurement

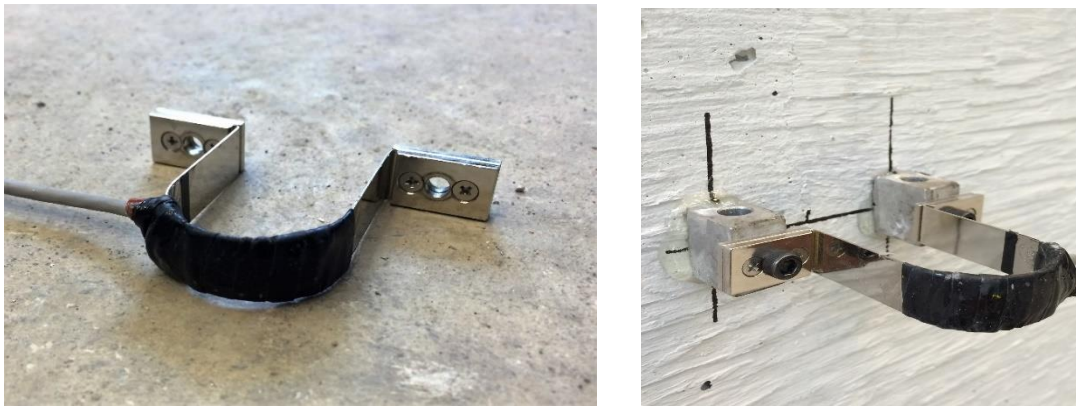

(a) **(b)**

Figure 3.7 Lateral separation measurement using PI-gauges

3.5.3 Measurement of the Reinforcement Strain

In order to evaluate the stress of the shear transfer reinforcement across the shear planes of the test specimens, electronical foil strain gauges were bonded to the reinforcement at the critical location, which is at the level of the interface between the interconnected blocks of the push-off specimen.

The sand coating of the GFRP reinforcement was removed using an air-pressure grinder provided with a sand paper disk (Figure 3.8). The grinding process was done cautiously so that only the coating was removed and not any material from the reinforcing bar. The grinded area was then cleaned with a cloth using ethanol. After the area dried out, it was swabbed with a cloth using a water-based acidic surface cleaner. As a last step of the preparation of the grinded area, it was also cleaned with a water based alkaline surface cleaner (neutralizer). Afterward, the strain gauge was glued to the prepared area using quick setting glue. An appropriate cover of epoxy was applied on top of each strain gauge to provide an extra protection during casting, especially, when vibrating the concrete. The strain gauges were connected to the data acquisition system to continuously record the strains throughout the loading of the specimen. Figure 3.8 shows the prepared area and a strain gauge fixed on a reinforcement bar at this area. Strain gauges were used for all shear transfer reinforcements including steel reinforcement in the control specimens, as illustrated in Figure 3.9.

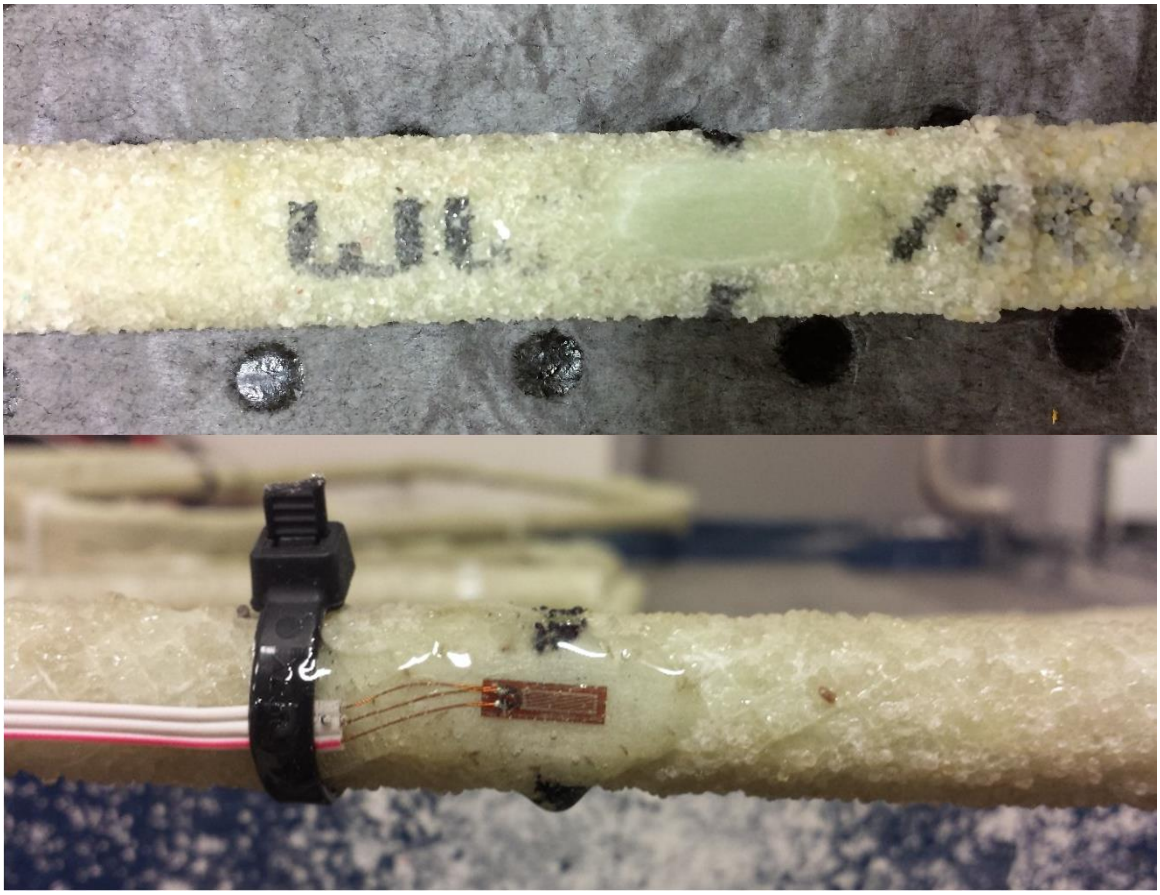

Figure 3.8 Measurement of the reinforcement strain

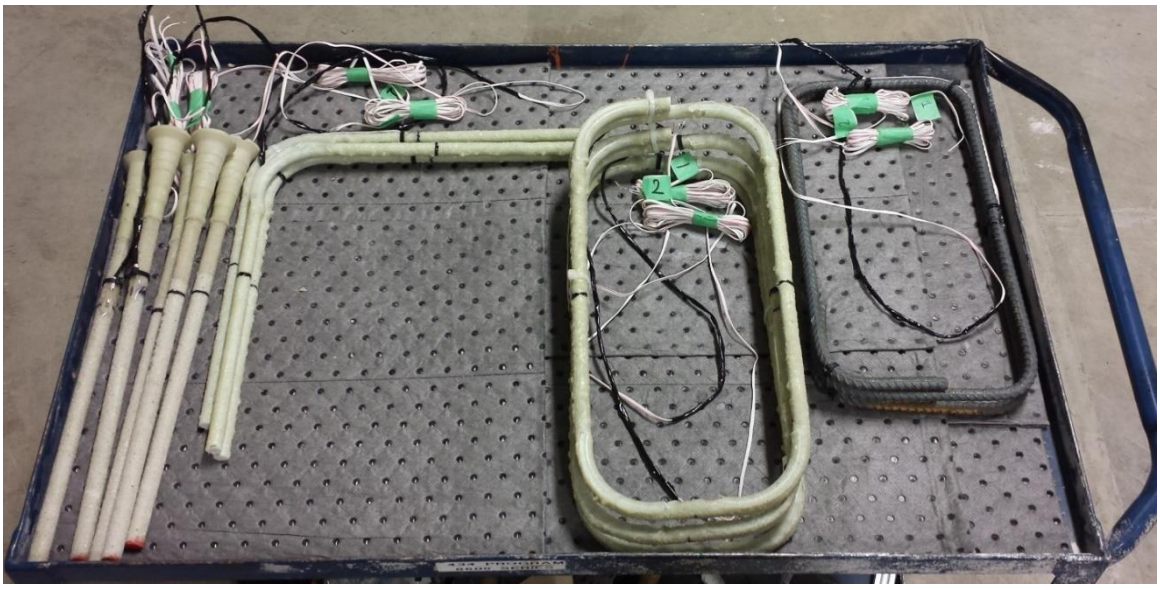

Figure 3.9 Shear transfer reinforcement with strain gauges bonded at the critical section

3.6 Test Setup and Procedure

After curing, the specimens were painted with a white paint as was shown in Figure 3.5, for an easier observation of any cracks that might develop during testing. Afterward, each specimen was put in its vertical position, on a lower stiff steel support, under the hydraulic jack of the testing frame. The specimen was loaded with a monotonic load concentric to the shear plane. A schematic drawing of the test setup and the provided instrumentations is shown in Figure 3.10. With this loading condition, only direct shear was induced onto the shear plane without a bending moment. The specimens were subjected to a monolithic loading at an average rate of 20 kN per minute up to failure. The failure was considered to occur when the slip increased rapidly with a sudden drop of the load.

Figure 3.11 shows photographs of the test setup. Readings of the relative slip measured by the LVDTs of the two blocks of the push-off specimen, lateral separation of the specimen at its interface measured by the PI-gauges, and the strain of the shear transfer reinforcement at the level of the interface measured by the strain gauges, were recorded through the data acquisition system at each loading increment. The loading was halted intermittently to mark any cracks. Each test specimen was closely observed for qualitative behaviour during the entire test. The concrete cylinders were tested on the same day of that of their reference specimen.

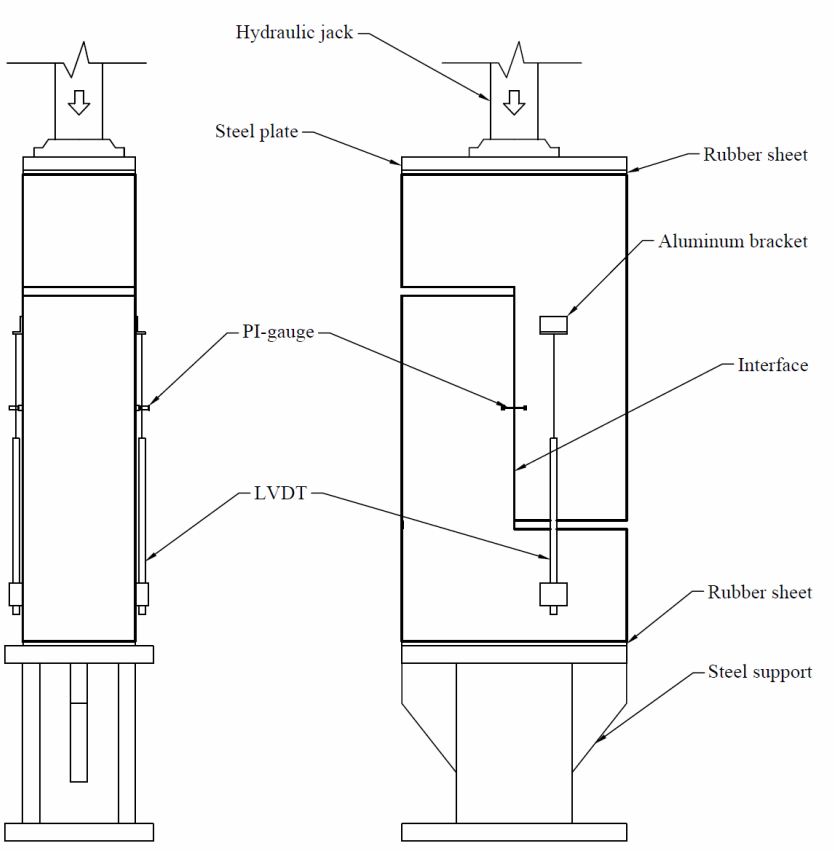

Figure 3.10 Schematic drawing of test instrumentations and setup

Figure 3.11 Test setup

CHAPTER 4

EXPERIMENTAL RESULTS AND DISCUSSION

4.1 Introduction

The results of the push-off tests are discussed in this section. A parametric analysis on the test results is presented according to the variable parameter, whether it is the reinforcement stiffness parameter, $E_F\rho_v$, the concrete strength, f_c' or the reinforcement geometry. Therefore, in each discussion, test specimens are divided into groups so that only one parameter varies among each group. The comparison is carried over within each group, relative to the concerned parameter. The analysis and the discussion of the test results are presented in terms of the relationships between the measured shear loads carried by the specimens and other measurements, which are, the slip, the reinforcement strain and the lateral dilation of the shear plane. The general behaviour and the shear transfer mechanism associated with GFRP shear transfer reinforcement is also addressed in detail.

4.2 General Behavior

The load-slip behavior of the interfaces of the push-off specimens conducted in this study, indicates that the shear transfer mechanism associated with GFRP reinforcement can be divided into three successive phases as shown in Figure 4.1.

Phase-I: Pre-Cracked Behavior

The behavior at loading levels below the cracking load of the interface, which represents the shear resistance capacity of the concrete interface alone, is very similar for all test specimens. It's characterized by a negligible interface dilatation and reinforcement strain at the interface level. This phase involves two stages of shear resistance. In the first stage, the applied shear load is resisted by the concrete shear associated with the strength of the bond between the two surfaces of the connected concrete blocks that form the interface of the push-off specimen. This stage starts at the commencement of the loading and ends at the deponding point, identified as Point-1 in Figure 4.1. At this point the chemical adhesion between the concrete particles of the two faces of the interface (bond) is destroyed.

By increasing the load, the curve starts to indicate softening behavior, after the bond was destroyed, and continues with its slightly reduced stiffness in the second stage of Phase-I. In this stage the shear load is believed to be carried by the interlocking mechanism between the local asperities and protrusions formed by the coarse aggregate and the cement matrix on both faces of the interface plane. Cracking of the shear plane is initiated at the end of Stage-2 at point-2 in Figure 4.1. The cracking is caused due to crushing of these asperities against each other. Up to this point, the relative displacement along the shear plane, the interface dilation and the reinforcement strain are still very small. The slope of the load-slip curve in both stages of Phase-I were shown to be dependent on the concrete strength when a sufficient GFRP reinforcement is provided across the shear plane. The

higher the concrete strength is, the stiffer precracked deformation response will be. The cracking stress of the tested cold-joint interfaces of the specimens of the present research was found to be in the range of 2 to 2.7 MPa, which is consistent with the previous findings in the literature (Hanson 1960; CTA bulletin, 1976; Loov and Patnaik 1994; Harries et al. 2012). This value of the cracking stress was shown to be largely unaffected by the reinforcement crossing the interface. The strain and, therefore, the stress, in the reinforcement at the cracking load is negligible and was varying from 22 to 400 $\mu\varepsilon$, in the GFRP reinforcement. This indicates no practical role of this reinforcement up to this point. Previous studies have also shown that the precracked behaviour is independent of the steel reinforcement (Mattock and Hawkins, 1972; Walraven et al. 1987; Mattock 1988; Harries et al. 2012 and others).

Phase-II: Post-Cracked Behaviour

As it can be seen in Figure 4.1, the post-cracked behaviour of the interfaces from the cracking load to the ultimate load V_u is characterized by softening behaviour, larger and visible cracks widths, higher slips and reinforcement strains than those in the pre-cracked phase (Phase-I). In Phase-II, the reinforcement across the shear plane (when adequately provided) is engaged in the shear resisting mechanism. The resistance to shear of the cracked interface is attributed to the friction that originates from the general roughness and unevenness of both faces of the interface plane and the clamping stresses exerted along these faces by the virtue of the reinforcement crossing that interface. Owing to the general

roughness and irregularities of the interface surface, the slip along the interface is accompanied by widening of the crack along that interface. As a result, the reinforcement crossing the cracked shear plane gets stressed in tension, which in turn provides a clamping stress along the faces of the cracked interface. The shear load is then carried by the resistance provided by the friction between the sliding faces up to the ultimate load at Point-3 (Figure 4.1). The shear displacement values at the ultimate load, V_v of the sufficiently GFRP reinforced interfaces were in the range of 0.37 to 0.94 mm. Comparable slips were reported for the steel reinforced interfaces at their ultimate loads (Hofbeck et al. 1969, Mattock 1974; Valluvan et al. 1999; Harries et al. 2012). The average interface strain of the GFRP reinforcement varied from 3000 to 5000 $\mu\varepsilon$ when adequate reinforcement was provided. However, 98 to 100% of the ultimate load was maintained up to the point corresponding to a reinforcement strain of 5000 $\mu\varepsilon$, whenever the ultimate occurred at reinforcement strain less than 5000 $\mu\varepsilon$. It is important to note here, that not all specimens exhibited a behaviour with Phase-II. Only appropriately reinforced interfaces with a reinforcement content equals to or greater than the suggested in section 4.3.1, of this chapter, exhibited a shear frictional resistance post to cracking, while other specimens failed at the cracking point (Point-2) or very soon after cracking. The reinforcement did not play a major role in the latter case with respect to the ultimate shear resistance. The shear friction resistance in this phase is dependent on the reinforcement stiffness and the general roughness of the interface surface, which is independent of the concrete strength. This conforms with the findings of other researchers such as Mattock (1988) and Mau and Hsu

(1988) and Mansur et al. (2008).

Phase-III: Post-Ultimate Behaviour

The behaviour after reaching the ultimate load is characterized by an increase of the deformations, lateral separations and reinforcement strain without any additional resistance. At the ultimate load (Point-3 in Figure 4.1) the crack width of the cracked interface becomes sufficiently large to prevent the firm contact between the crack faces, which is necessary to ensure a considerable frictional resistance. Any attempt to increase the applied load beyond this point would lead to larger deformations in the reinforcing bars, further widening the interface crack width and causing significant reduction in the friction between the interconnected members. Thus, the shear transfer resistance decreases while the slip increases rapidly up to Point-4 as specified in Figure 4.1.

For interfaces provided with GFRP stirrups and headed bars, the slip at Point-4 becomes large enough to engage the dowel action of the reinforcement intersecting the interface. The post failure dowel action resistance initiated at point-4 was almost maintained up to the total failure of the interface for specimens with GFRP stirrups. However, Specimens with headed bars showed an outstanding post-failure resistance ranged from 91 to 130% of the ultimate load at high slips (see Table 4.1). This behaviour is believed to be attributed to the better bond characteristics of the GFRP headed bars than those of GFRP stirrups. The dowel action associated with GFRP reinforcement was engaged at a slip value in the range of 1 to 2 mm with an average of 1.4 mm. This is

relatively less than the slip associated with dowel action of the steel reinforcement, which was reported to be in the range of 2.5 to 3 mm (Hofbeck et al. 1969; Paulay et al. 1974; Walraven and Reinhardt 1981). This slip associated with a significant contribution of the dowel action is an excess of what can be considered acceptable within the limits of the structural usefulness requirements and, therefore, cannot be considered in the evaluation of the ultimate shear transfer strength (Paulay et al. 1974).

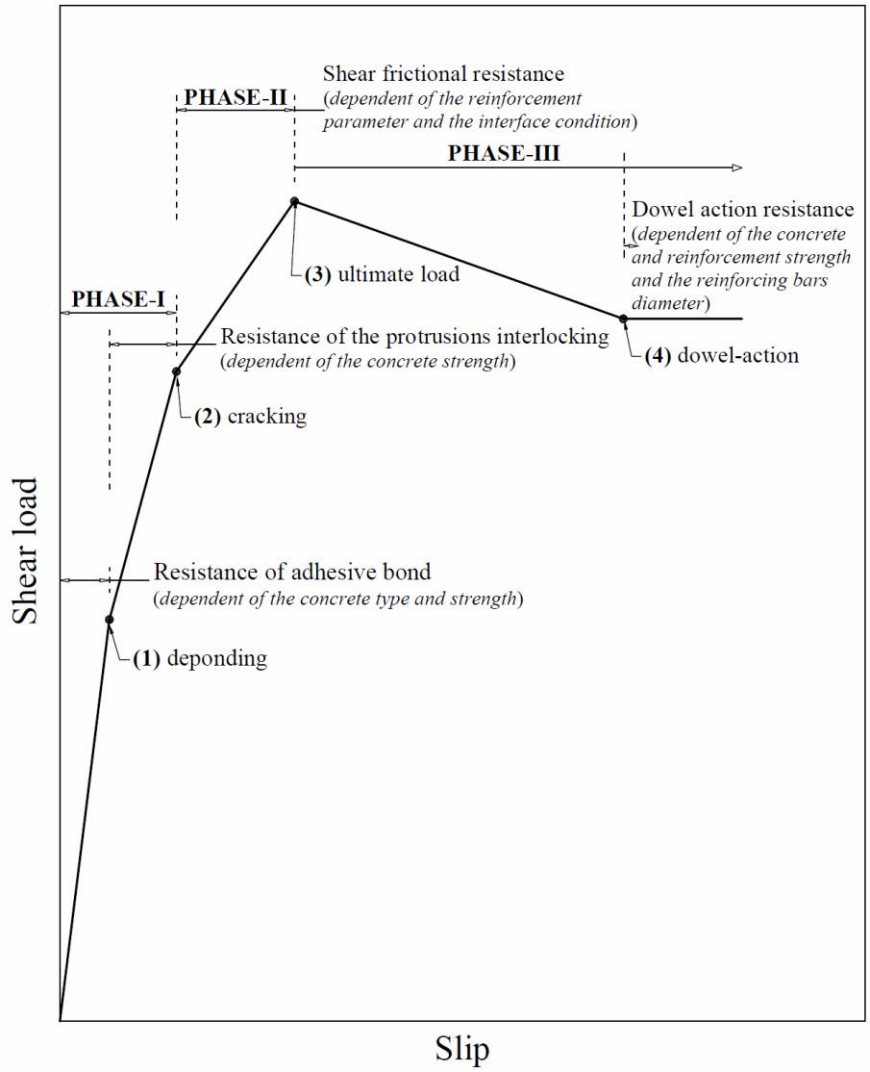

Figure 4.1 Generalized load-slip response of sufficiently GFRP reinforced cold-jointed interfaces

4.3 Analysis of Test Results

A summary of the test results of the push-off specimens of the current study is reported in Table 4.1, which will be referred to frequently in the subsequent sections. The measured ultimate shear transfer capacity and the accompanied slip, reinforcement strain and the lateral dilatation across the shear plane are presented in this table. The percentage of the measured capacity of each specimen relative to the measured one of the reference unreinforced specimen of the same concrete strength is also reported. The maximum post-failure residual shear resistance, for applicable specimens, is included and also described as a percentage of the ultimate load. The residual strengths are only mentioned for specimens that showed a significant load-carrying behaviour in the post-failure loading stage.

Specimen FA2-50 had an earlier premature split failure, which prevented it from developing its full capacity. The measured strength of the later specimen was less than the unreinforced specimen with the similar concrete strength, C0-50. Therefore, it will be excluded in the subsequent discussions of the test results. The failure mode of this specimen will be discussed later in detail.

Each group of replicated specimens (see Table 3.1) showed consistent and similar behaviour. Accordingly, the average values of the measured strength and other measurements are described for each group of the identical specimens, in the following tables of the test data. However, the results of individual specimens of these groups will be reported within the discussions in the following sections whenever it is necessary.

Table 4.1 Summary of test results

Specimen ID	f'_c (MPa)	$E\rho_v$ (N/mm^2)	At ultimate					Residual shear capacity, V_r (kN)	Residual as a percentage of V_u (%)
			V_u (kN)	Strength increase over C0 (%)	Slip (mm)	Lateral dilation (mm)	Reinforcement microstrain		
C0-50	50	0	296	0	0.66	0.021	NA	-	-
SS1-50		320	334	13	0.14	NA	NA	127	38
SS2-50		640	477	61	0.85	0.211	1904	-	-
FS1-50		101	334	13	0.34	0.030	22	-	-
FS2-50$_{(avg)}$		203	402	36	0.48	0.238	3881	345	86
FS3-50		304	617	109	0.37	0.014	402	606	98
FH2-50		122	336	14	0.31	0.028	389	218	65
FH3-50$_{(avg)}$		182	323	9	0.28	0.159	2260	324	100
FH5-50		304	569	92	0.77	0.301	2953	571	100
FA2-50		101	255	-	0.15	NA	NA	-	-
FA3-50		152	540	82	0.66	0.422	4525	-	-
C0-30	30	0	332	0	0.34	0.034	NA	-	-
FS2-30		203	385	16	0.58	0.288	4466	350	91
FS3-30		304	384	16	0.64	0.229	4847	367	96
FH3-30		182	362	9	0.44	0.162	1472	328	91
FH5-30		304	433	30	0.94	0.304	4973	565	130
FA3-30		152	342	3	0.24	0.023	100	-	-

4.3.1 Effect of the Reinforcement Stiffness ($E_F\rho_v$)

As mentioned in the chapter 2, the ultimate limit state of an interface shear failure specified by the yielding of the steel reinforcement across that interface was questioned by Harries et al. (2012). In the latter study, it was shown that this assumption is not always true, especially, when high grade (high strength) steel is used. Therefore, the ultimate shear transfer strength v_u was considered as a function of the stiffness parameter of the reinforcement $E_s\rho_v$, rather than the yield strength of that reinforcement. This appears to be more rational, since the clamping stress maintained by the reinforcement is, in fact, due to the stiffness of this reinforcement at any loading stage. This connotation can be best utilized for GFRP shear transfer reinforcement, since this reinforcement does not yield and remains perfectly elastic up to failure.

The stiffness parameter considered in this analysis is that in the direction perpendicular to the shear plane of the reinforcement, crossing the shear plane, that would be placed in tension under the application of the shear load ($E_F\rho_v \sin\alpha_f$). Such reinforcement would maintain the clamping stresses along the shear plane. The parameter, α_f, is the angle of inclination of the reinforcement relative to interface plane. This is particularly important in the case of GFRP angles, for which the legs have an angle of 45 degrees relative to the shear plane. For specimens with headed bars and stirrups, which are placed normally to the shear plane ($\alpha_f = 90^o$), the reinforcement axial stiffness is in the perpendicular direction to the shear plane.

To study the influence of the stiffness of the GFRP reinforcement on the shear transfer strength, the specimens were grouped so that the specimens of each group share the same reinforcement geometry (i.e. stirrup, headed bar, or angle) and the same concrete

compressive strength f_c'. This allows to clearly and exclusively examine the influence of the reinforcement stiffness on the shear transfer strength. Unreinforced specimens C0-50 and C0-30 are also provided along with the corresponding specimens made of the same concrete strength to allow for comparison. Table 4.2 shows the test results and the specimens sorted in groups for the purpose of the proceeding discussion regarding the reinforcement stiffness.

Figure 4.2 shows the load-slip behaviour of the specimens of Group-I (SS1-50 and SS2-50). The unreinforced specimen of the same concrete strength C0-50 is also incorporated in that figure. It can be seen from Figure 4.2 and the data in Table 4.2 that specimen SS1-50 which had a reinforcement stiffness of 320 N/mm^2 failed just after cracking at an ultimate load 13% higher than that of unreinforced specimen C0-50. However, the specimen with two steel stirrups SS2-50 developed an additional shear resistance after cracking of the shear plane by the mean of friction. Specimen SS2-50 had an ultimate strength 61% higher than that of C0-50. The reinforcement ratio of SS1-50 of 0.16% is close to the minimum ratio of 0.15% suggested by mattock and Kaar (1961). It appears that at this ratio, the stiffness of the reinforcement is not sufficient to resist the progressive separation of the interface faces and, hence, failed to engage the reinforcement in the shear transfer resistance after cracking of the shear plane, therefore, no additional shear frictional resistance was delivered. Whereas, specimens SS2-50 developed extra shear frictional resistance after cracking owing to the adequate clamping stresses provided by the reinforcement. Similar observation was also noted by Mansur et al. (2008) for push-off specimens with low steel reinforcement content. In both specimens SS1-50 and SS2-50 the failure was relatively brittle where the load dropped and the slip increased dramatically.

Table 4.2 Summary of test results (for the discussion of $E_F\rho_v$)

Group	Specimen ID	f'_c (MPa)	$E\rho_v sin\alpha_f$ (N/mm^2)	At ultimate					Residual shear capacity, V_r (kN)	Residual as a percentage of V_u (%)
				V_u (kN)	Strength increase over C0 (%)	Slip (mm)	Lateral dilation (mm)	Reinforcement microstrain		
-	C0-50	50	0	296	-	0.66	0.021	NA	-	-
I	SS1-50		320	334	13	0.14	NA	NA	127	38
	SS2-50		640	477	61	0.85	0.211	1904	-	-
II	FS1-50		101	334	13	0.34	0.030	22	-	-
	FS2-50$_{(avg)}$		203	402	36	0.48	0.238	3881	345	86
	FS3-50		304	617	109	0.37	0.014	402	606	98
III	FH2-50		122	336	14	0.31	0.028	389	218	65
	FH3-50$_{(avg)}$		182	323	9	0.28	0.159	2260	324	100
	FH5-50		304	569	92	0.77	0.301	2953	571	100
IV	FA3-50		108	540	82	0.66	0.422	4525	-	-
-	C0-30	30	0	332	-	0.34	0.034	NA	-	-
V	FS2-30		203	385	16	0.58	0.288	4466	350	91
	FS3-30		304	384	16	0.64	0.229	4847	367	96
VI	FH3-30		182	362	9	0.44	0.162	1472	328	91
	FH5-30		304	433	30	0.94	0.304	4973	565	130

The dowel action of the steel bars across a concrete interface was shown to deliver a considerable shear resistance only at higher slips in the range of 2.5 to 3 mm (Hanson 1960; Hofbeck et al. 1969; Paulay et al. 1974; Walraven and Reinhardt 1981). This situation can be also noted from Figure 4.2 where a post failure resistance of specimen SS1-50 was developed at a slip of 3 mm.

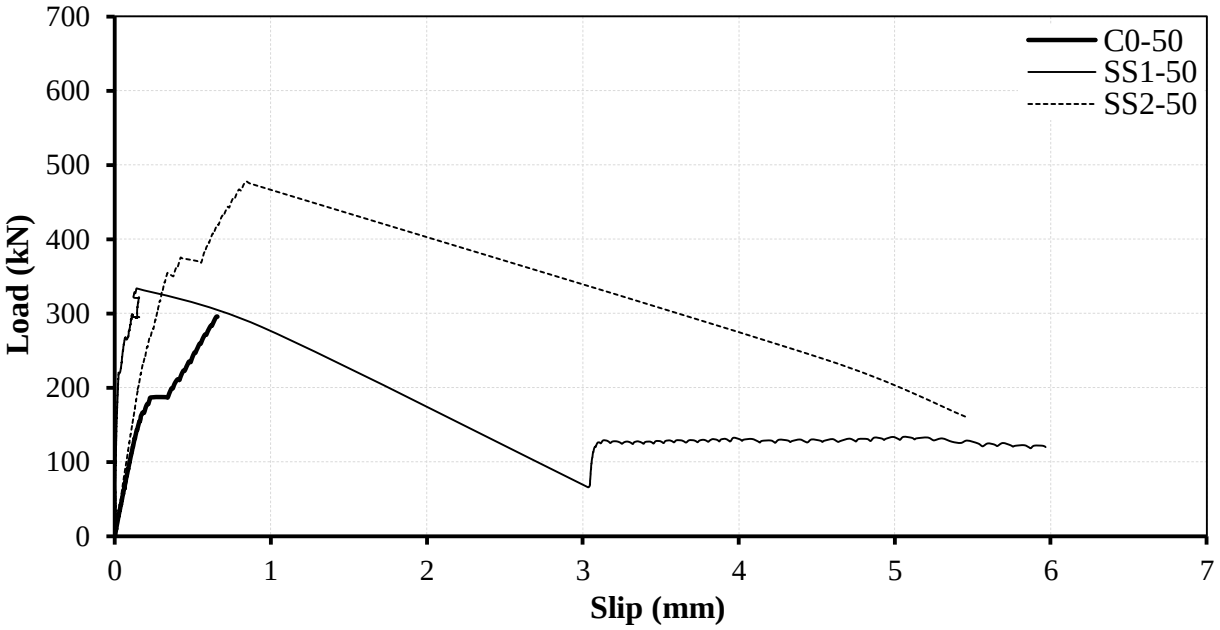

Figure 4.2 Load-slip curves of specimens of Group-

The load-reinforcement strain curve of the specimen SS2-50 of Group-I is illustrated in Figure 4.3. It can be seen that the reinforcement was not really stressed until the crack was initiated along the shear plane at which the strain was around 237 $\mu\varepsilon$. Subsequently, the strain increased with the augmented load up to an approximately the yield strain (1904 $\mu\varepsilon$) at the ultimate load. This is similar to the behavior noted by Loov and Patnaik (1994) in their study of the interfaces of composite concrete beams.

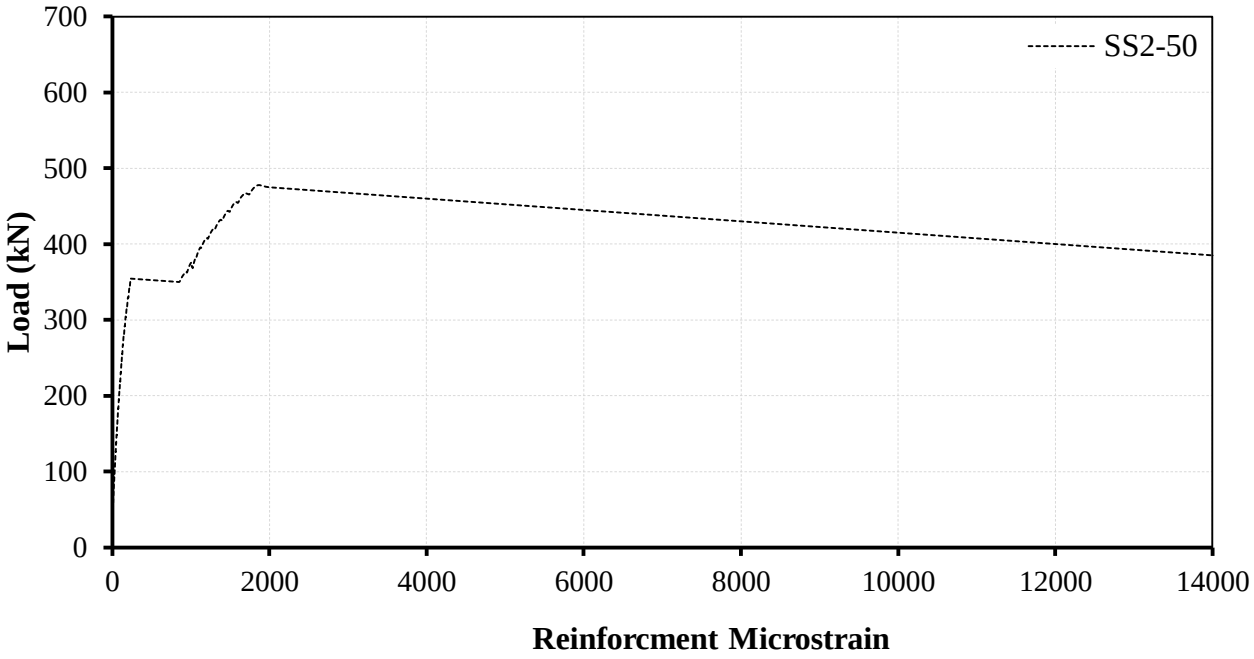

Figure 4.3 Load-reinforcement strain curve of specimen SS2-50

The load-slip relationships of specimens with GFRP stirrups across their interfaces and a concrete strength of 50 MPa, classified as Group-II in Table 4.2 are shown in Figure 4.4. FS2-50 and its second replicated specimen showed a consistent load-deformation response as shown in Figure 4.4. It can be seen from this figure that the specimen with one GFRP stirrup, FS1-50, failed in the similar manner to SS1-50. This specimen also developed only 13% extra strength over that of C0-50 and failed at cracking of the shear plane with no additional shear frictional resistance was provided. The load dropped and the slip increased rapidly after failure. However, specimens with two GFRP stirrups, with a reinforcement stiffness $E_F\rho_v$ equals to 203 N/mm^2, developed an additional frictional shear resistance after cracking of the interface in the similar fashion to SS2-50. This specimen developed an average strength 36% higher than the strength of C0-50.

Although SS2-50 and FS2-50 both delivered a frictional shear resistance, FS2-50

showed a remarkable ductility over specimen with two steel stirrups (see Figures 4.2 and 4.4). Specimens with two GFRP stirrups showed a maximum average residual strength of 86% of the ultimate load. Specimen FS3-50, also shown in Figure 4.4, has a strength 109% higher than C0-50. During the testing of this specimen, the load reached a high level near the capacity of the testing frame (600 kN) so the test had to be stopped, however, the specimen showed cracks along the shear plane but did not totally fail. Comparing the general load-slip patterns of specimens with two and three GFRP stirrups indicates a similar behaviour. The data in Table 4.2 shows that increasing the reinforcement stiffness by 50%, from 203 N/mm^2 for FS2-50 to 304 N/mm^2 for FS3-50, increased the shear transfer strength by about 53%. These observations indicate a major role of the GFRP reinforcement stiffness in the shear transfer strength of a concrete interface when it is sufficiently provided across that interface.

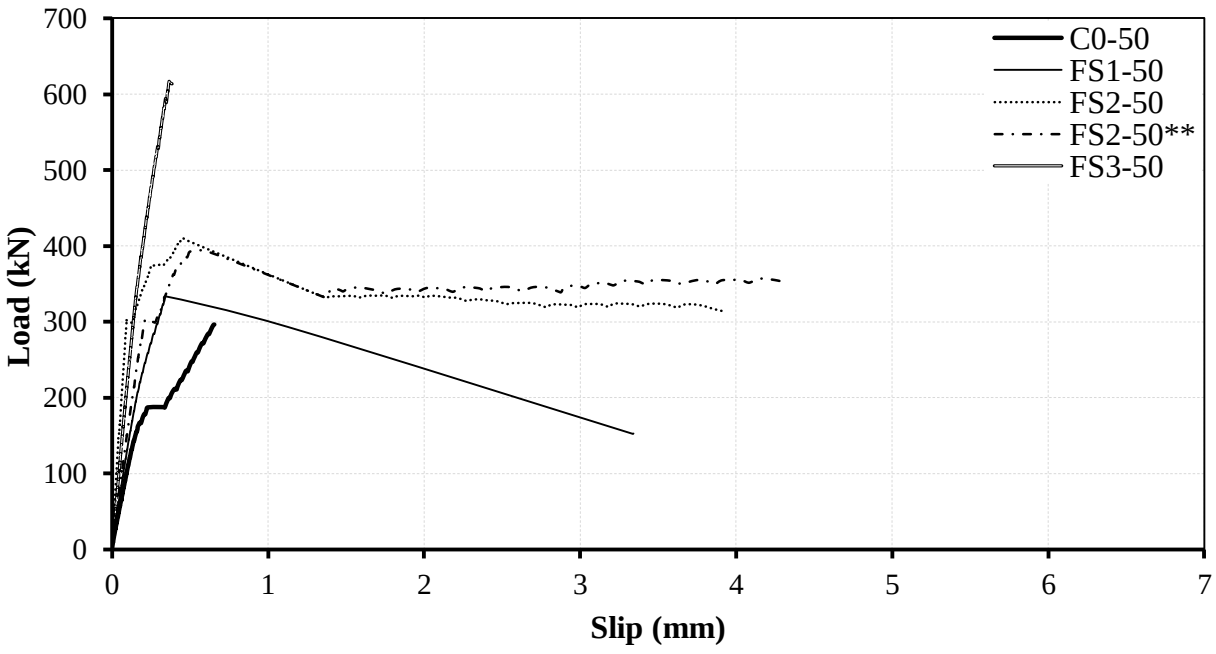

Figure 4.4 Load-slip curves of specimens of Group-II

Figure 4.5 presents the load-reinforcement strain behaviour of Group-II specimens. The reinforcement strain at the ultimate load in the specimen with low reinforcement content, FS1-50, which failed at cracking, was about 22 $\mu\varepsilon$ indicating no practical contribution of the reinforcement, at this stiffness, into the shear transfer strength. However, the average strain of the stirrups of the specimen with two GFRP stirrups, which developed an additional post cracking resistance, increased after cracking with the increasing load and reached about 4000 $\mu\varepsilon$ at the ultimate load. Specimens with two GFRP stirrups sustained a significant load after the failure and it was about 98.5% of the ultimate load at a reinforcement strain of 5000 $\mu\varepsilon$.

From the above discussion, it is evident that similar to the case of steel reinforcement, there is a minimum requirement of the stiffness of GFRP shear transfer reinforcement that has to be met in order to activate the reinforcement in the shear transfer resisting mechanism. Meaning, the shear friction theory can only be utilized and additional shear frictional shear resistance can be delivered if a sufficient GFRP reinforcement is provided across a concrete plane. This limit, based on the proceeding analysis, appears to correspond to a reinforcement ratio of 0.405% of GFRP stirrups which is equivalent to a stiffness parameter $E_F\rho_v$ equals to 203 N/mm^2.

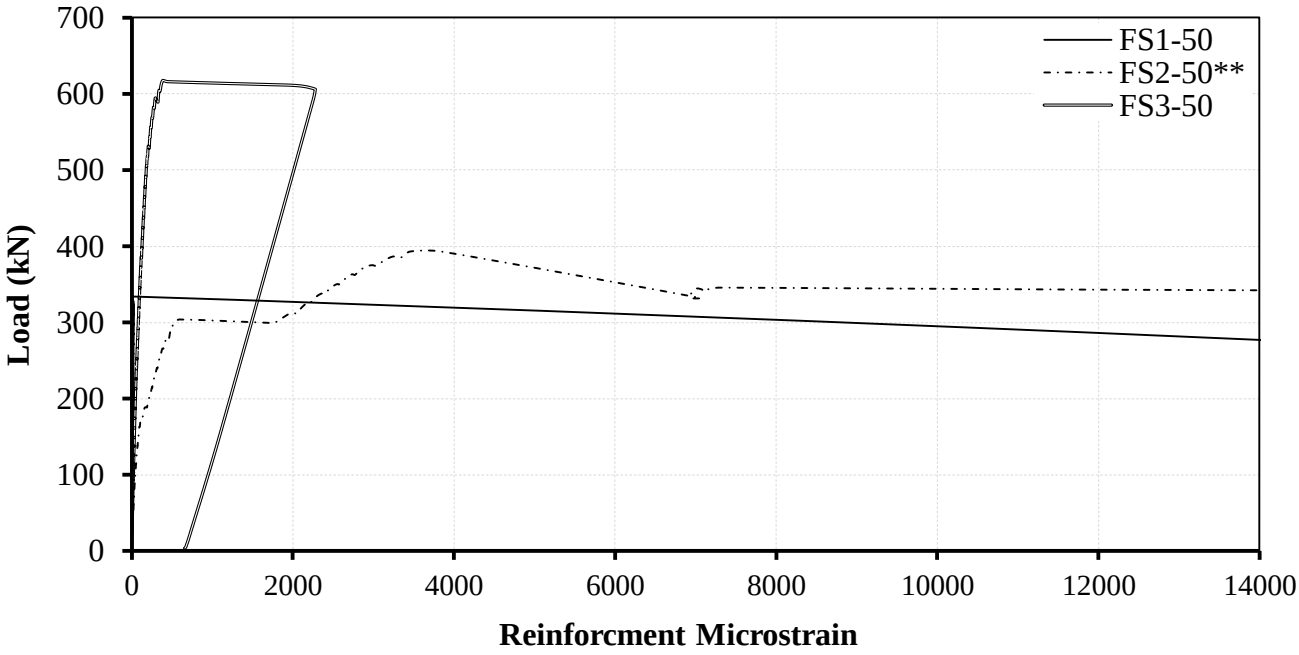

Figure 4.5 Load-reinforcement strain curves of specimens of Group-II

The third group of specimens in this analysis, is the group of specimens with headed bars made of a concrete strength of 50 MPa (see Table 4.2). Figure 4.6 shows the load-slip response of Group-III specimens. Figure 4.6 indicates that specimens with two headed bars and three headed bars failed at the cracking of the interface and developed strengths only 14% and 9% higher than the unreinforced specimen of the same concrete strength, respectively. This is similar to the behavior of the low reinforced specimens of Groups I and II (i.e. SS1-50 and FS1-50). All of these specimens have a GFRP reinforcement stiffness less than the minimum recommended in the previous paragraph of 203 N/mm^2.

However, specimen with five headed bars having a stiffness parameter of 304 N/mm^2 showed an additional resistance to the shear load after cracking of the interface as it can be revealed from Figure 4.6. Specimen FH5-50 developed a strength of about 92% higher than what the corresponding unreinforced specimen C0-50 did. This behaviour is similar to the appropriately reinforced specimens from the earlier discussed groups (i.e. SS2-50, FS2-50

and FS3-50). Again, this performance is attributed to the sufficient clamping stresses provided by the reinforcement after cracking, which in return resists the lateral separation of the interface faces, and hence, higher load and larger slip became necessary to override the roughness and asperities of the interface surface. When the reinforcement stiffness $E_F\rho_v$ was raised from 182 N/mm^2 for three headed bars to 304 N/mm^2 for five headed bars (i.e. 67% increase), the ultimate strength was increased by 76% (see Table 4.2).

It is also important to mention that specimens with headed bars performed very well as at post failure they continued to show load-carrying capacity that is more significant that what was reported for GFRP stirrups. A post failure resistance in the range of 93% to 107% of the ultimate load was shown at higher slips (see Figure 4.6). This behaviour is believed to be attributed to the better bond characteristics associated with headed bars. Similar situation was reported in the literature for two different steels with different bond characteristics (Zeno, 2009; Harries et al. 2012).

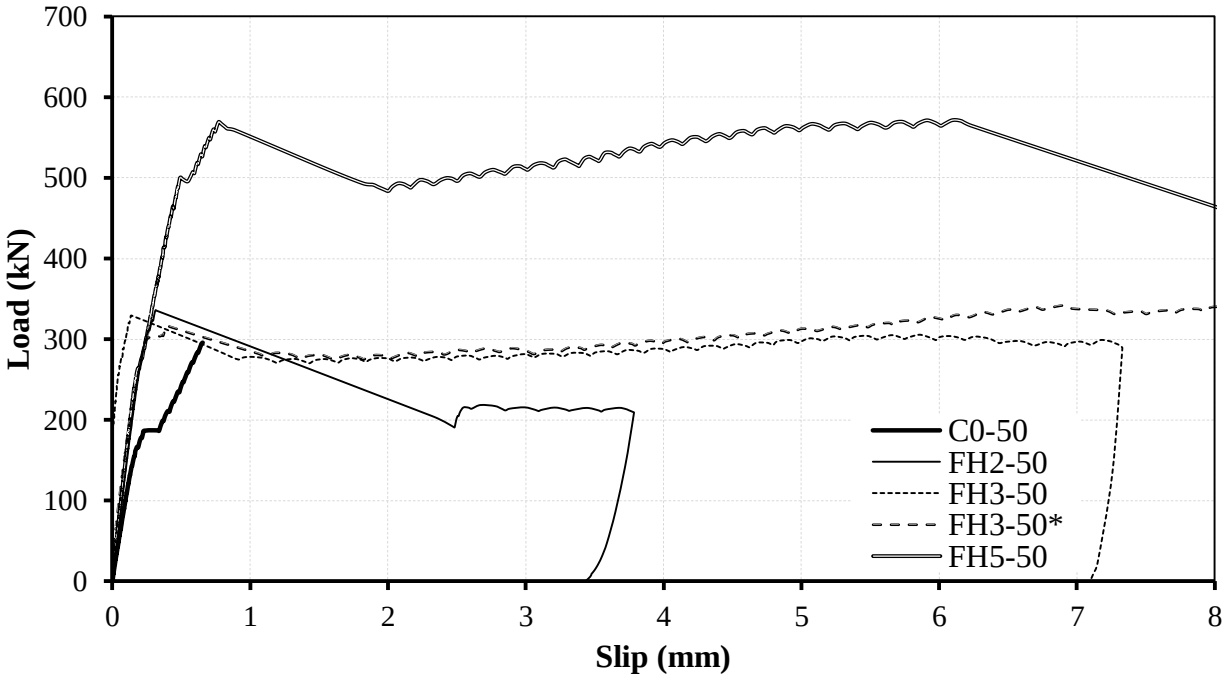

Figure 4.6 Load-slip curves of specimens of Group-III

Observations, from the load-reinforcement strain curves of the specimens of Group-III shown in Figure 4.7, similar to those noted earlier for specimens with GFRP stirrups can be taken. The ultimate load of FH2-50 and FH3-50 occurred immediately after cracking. In fact, as seen in Table 4.2, the strain of the reinforcement in specimen FH2-50 was as low as 389 $\mu\varepsilon$. However, the reinforcement strain increased after cracking of the interface of FH5-50 with the increasing load and reached a value close to 3000 $\mu\varepsilon$ at the ultimate load. Figure 4.8 shows a close-up look into the load-strain behaviour of the headed bars specimens up to 5000 microstrain. It indicates that the load at 5000 $\mu\varepsilon$ of specimen FH5-50 was about 99% of its ultimate load.

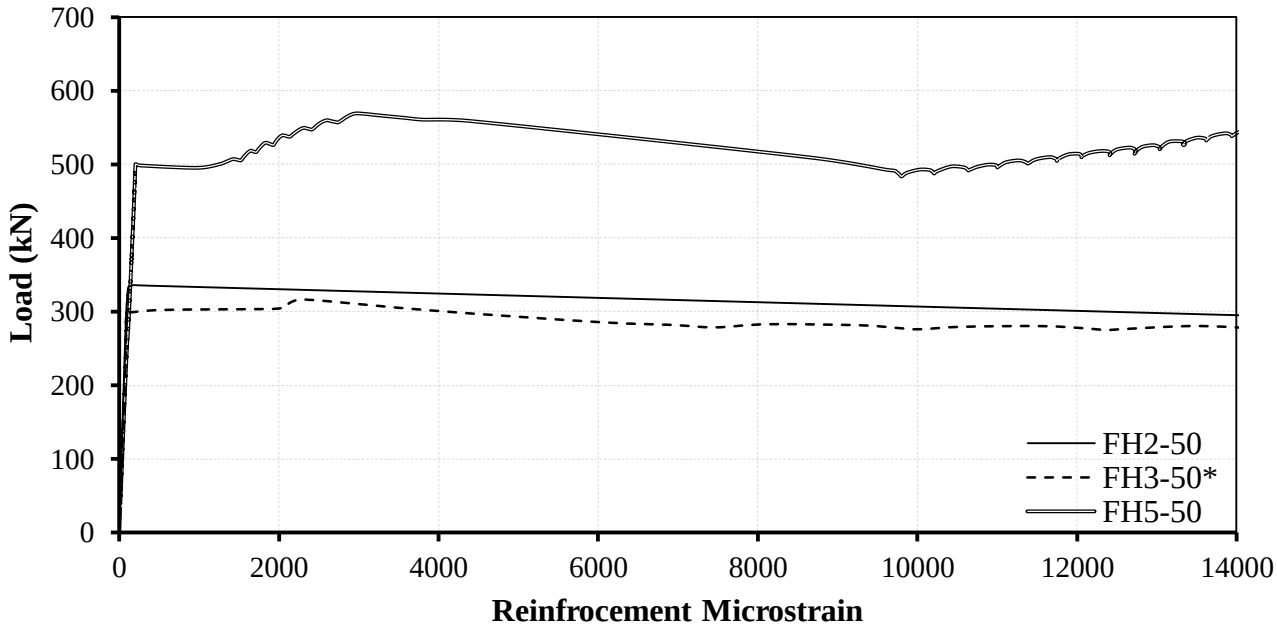

Figure 4.7 Load-reinforcement strain curves of specimens of Group-III

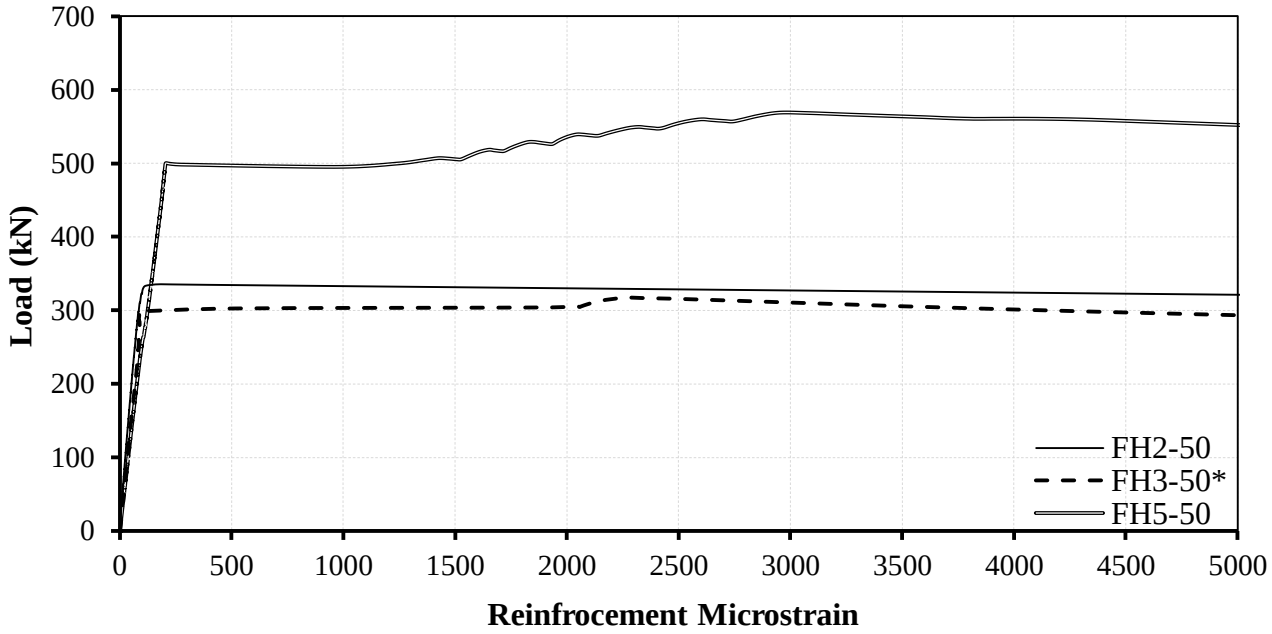

Figure 4.8 Load-reinforcement strain curves of specimens of Group-III (*up to 5000* $\mu\varepsilon$)

Group-IV includes the specimen with three GFRP angles across its interface plane made of concrete with strength of 50 MPa as presented in Table 4.2. Figure 4.9 displays the load-slip behaviour of this specimen. According to concrete design codes such as, CSA A23.3 (2004) and ACI 318 (2014), only reinforcement inclined to the shear plane that would be placed in tension during the shear loading is to be considered in the evaluation of the shear transfer strength. If this condition is applied to specimen FA3-50 only three tensile legs should be considered. According to this assumption, the stiffness of only the three legs perpendicular to the shear plane, $E\rho_v \sin\alpha_f$ $(\alpha_f = 45^o)$ is shown in Table 4.2 as of 108 N/mm^2, which is a little higher than that of one GFRP stirrup (101 N/mm^2) in specimen FS1-50. Giving this relatively low stiffness, the ultimate strength of FA3-50 was 62% higher than that of FS1-50 and 82% higher than the strength of C0-50. This indicates the important parameters additional to the stiffness of the tensile reinforcement, such as the

dowel action and the interlocking mechanism provided by the compressed legs in the opposite side of the shear plane. The strain in the tensile legs of the GFRP angles of the specimen FA3-50 at the interface level was 4525 $\mu\varepsilon$ as seen in Table 4.2 and Figure 4.10.

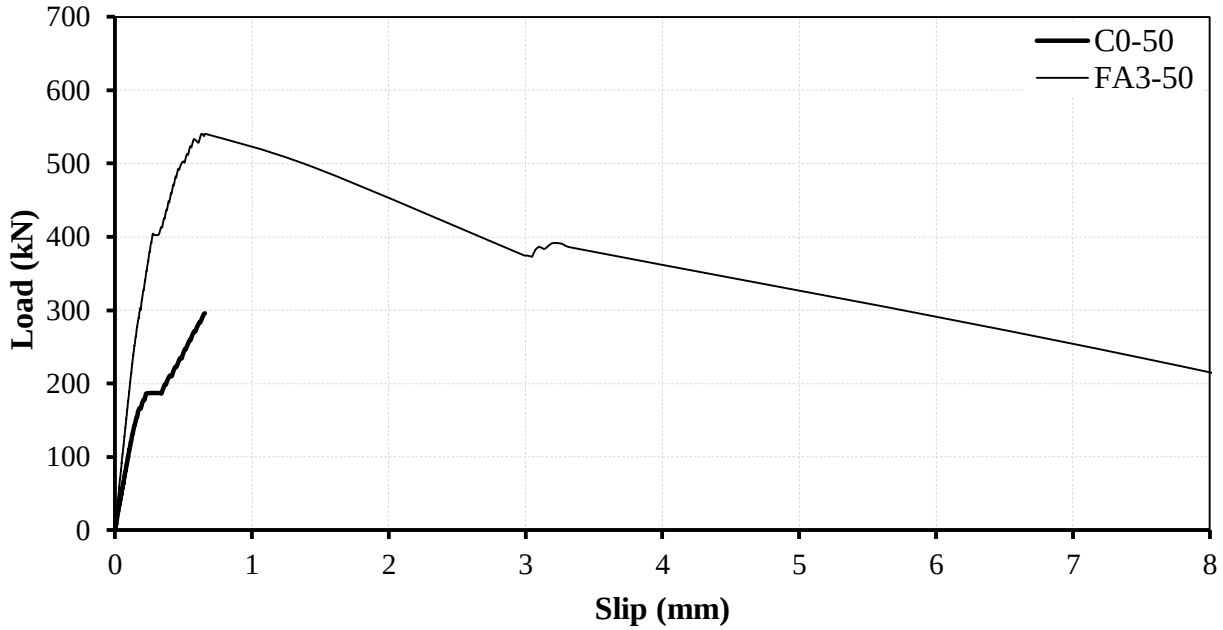

Figure 4.9 Load-slip curves of specimens of Group-IV

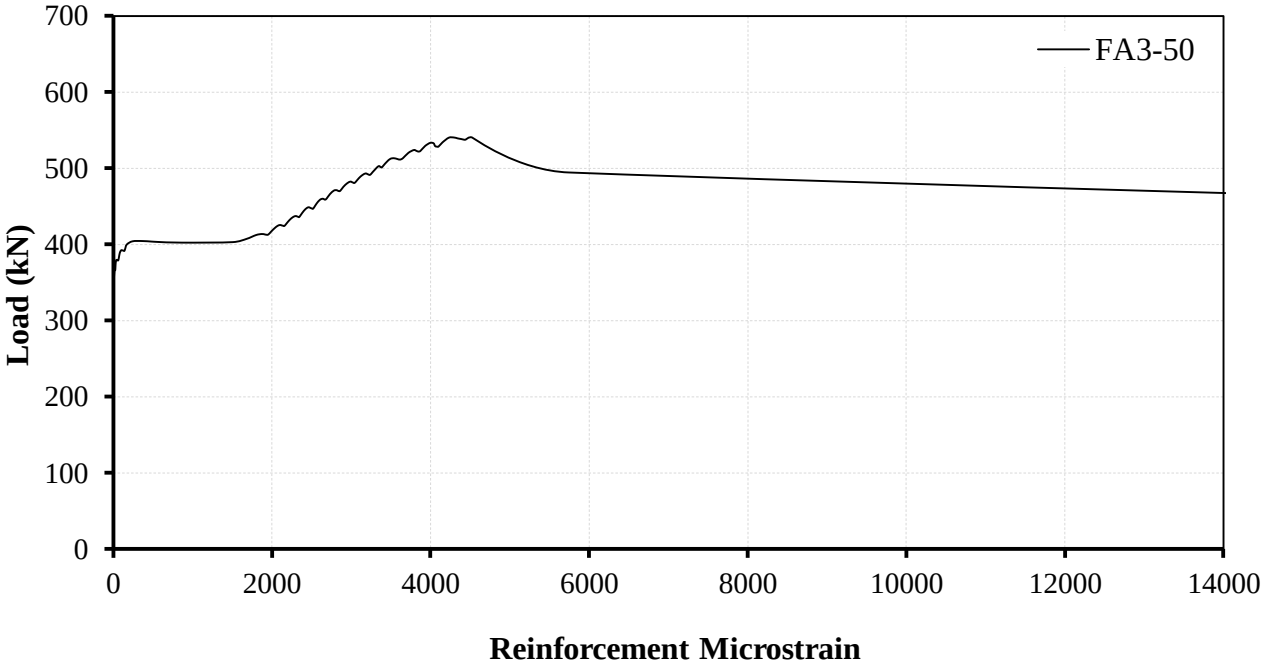

Figure 4.10 Load-reinforcement strain curve of specimen FA3-50

The load-slip curves of specimens of Group-V and VI, with 30 MPa concrete strength, are shown in Figures 4.11 and 4.13, respectively. In both figures the deformation response of the unreinforced specimen made of the same concrete strength is included. As it can be noticed from Figure 4.11 and Table 4.2, specimens FS2-30 and FS3-30 had a similar measured capacity. By carefully examining Figure 4.11, it appears that the crack was initiated at earlier loading stage in specimen FS3-30 than it was in FS2-30. This is reasonable since higher reinforcement content decreases the net concrete interface area which in return would reduce the cracking load, which is mainly attributed to the concrete interface. This observation can be better visualized from the load-reinforcement strain curves of FS2-30 and FS3-30 in Figure 4.12. From this figure, it can be noted that the reinforcement in FS3-30 was engaged in the shear load carrying mechanism at a lower level than it was in FS2-30. However, both of these specimens, FS2-30 and FS3-30 developed additional shear resistance and reached their ultimate load at a reinforcement strain equals to 4466 and 4847 $\mu\varepsilon$. Both of FS2-30 and FS3-30 developed a strength higher than the strength of C0-30 by 16%.

Similar observation is also noted from the load-reinforcement strain curves in Figure 4.14 of the specimens of group VI, with headed bars with a concrete strength of 30 MPa. The reinforcement in the specimen FH5-30 catches the load at an earlier stage than the reinforcement in FH3-30. The under-reinforced specimens FH3-30 failed soon after the cracking point (Figure 4.13), at which the reinforcement strain was 1472 $\mu\varepsilon$. However, FH5-30 developed extra strength after the interface cracking and the ultimate load was attained at a reinforcement strain of 4973 $\mu\varepsilon$ (see Figure 4.14). FH3-30 and FH5-30 showed a load capacity of 9% and 30.4% higher than C0-30, respectively.

When the reinforcement stiffness was increased by 67%, from 182 N/mm^2 for FH3 to 304 N/mm^2 in FH5, it resulted in an increase in the load by about 79% when the concrete strength was 50 MPa. Yet, the same increase in the stiffness lead to a 20% increase in the capacity when the concrete strength was 30 MPa (see Figure 4.6 and 4.13).

In conclusion,

1. In order to achieve a higher strength that exceeds the capacity of an unreinforced concrete interface, a sufficient amount of GFRP reinforcement must be provided across such an interface. The minimum GFRP reinforcement content was shown, in the proceeding discussion, to correspond to a reinforcement having a stiffness parameter $E_F\rho_v sin\alpha_f$ equals to 203 N/mm^2. When, at least, this amount of GFRP reinforcement is provided, the reinforcement will be engaged in the shear transfer process after the cracking along the shear plane takes place, and additional frictional shear resistance will be developed.
2. The strain in the reinforcement, when it is properly provided, at the ultimate, was shown to be in the range of 3000 to 5000 $\mu\varepsilon$. However, whenever the ultimate load was attained at a reinforcement strain below 5000 $\mu\varepsilon$, 98% to 100% of the ultimate load was maintained up to a reinforcement strain of 5000 $\mu\varepsilon$. If inadequate amount of GFRP reinforcement is provided across a concrete joint, it would fail immediately at the cracking load and no noticeable increase in the capacity over that of unreinforced joints would be gained. In the latter case, the strain and, hence, the stress in the reinforcement crossing the joint would be very small at the failure indicating

a little to no influence of this reinforcement in the shear load carrying mechanism.

3. The cracking load represents the shear resistance of the concrete interface alone, which the test results, of this study, indicated to be in the range of 2 to 2.7 MPa. This range conforms with the finding of the previous studies when rough interfaces were used (Hanson, 1960; Mattock, 1974; CTA Bulletin, 1976; Mansur, 2008; Harries et al. 2012). In addition, the shear transfer strength increases more with the reinforcement stiffness for a higher concrete strength. This is similar to what was observed in the study of Mansur et al. (2008).

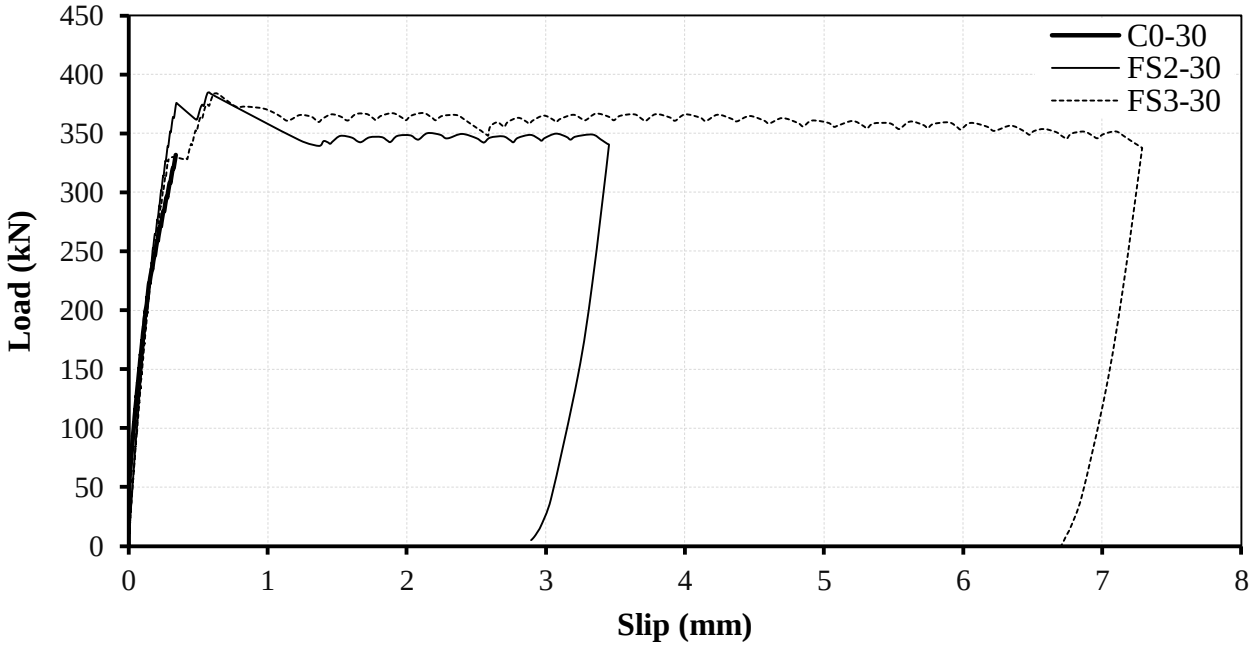

Figure 4.11 Load-slip curves of specimens of Group-V

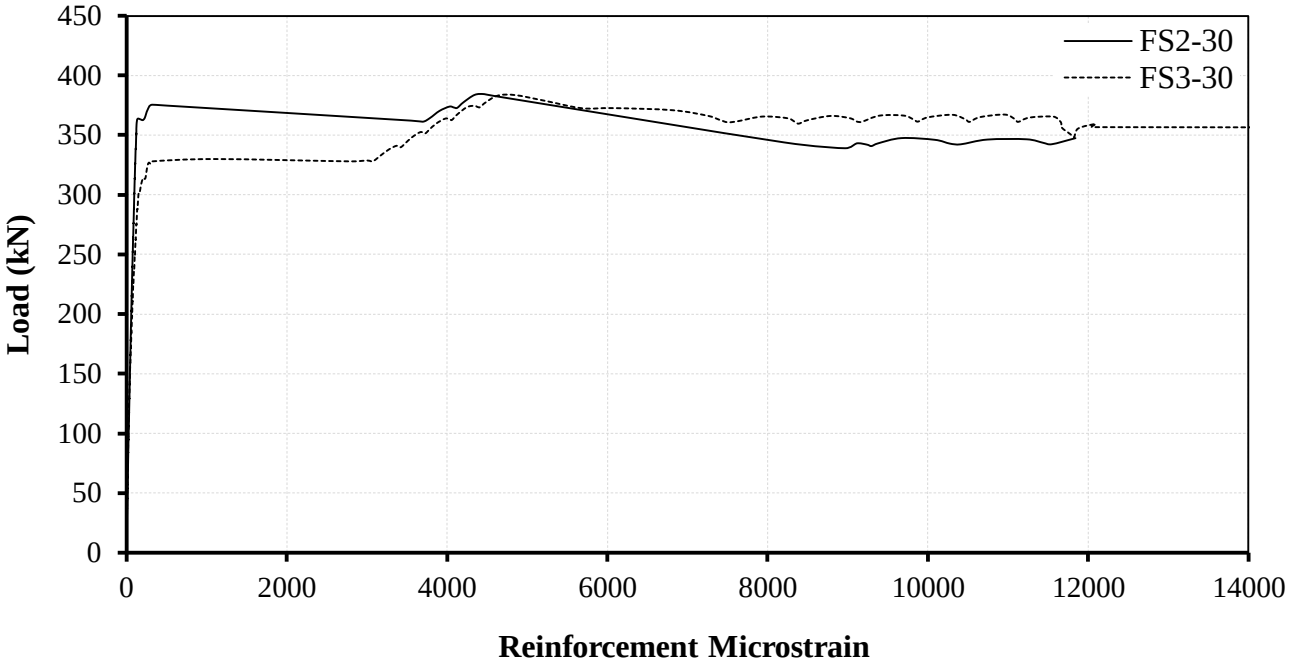

Figure 4.12 Load-reinforcement strain curves of specimens of Group-V

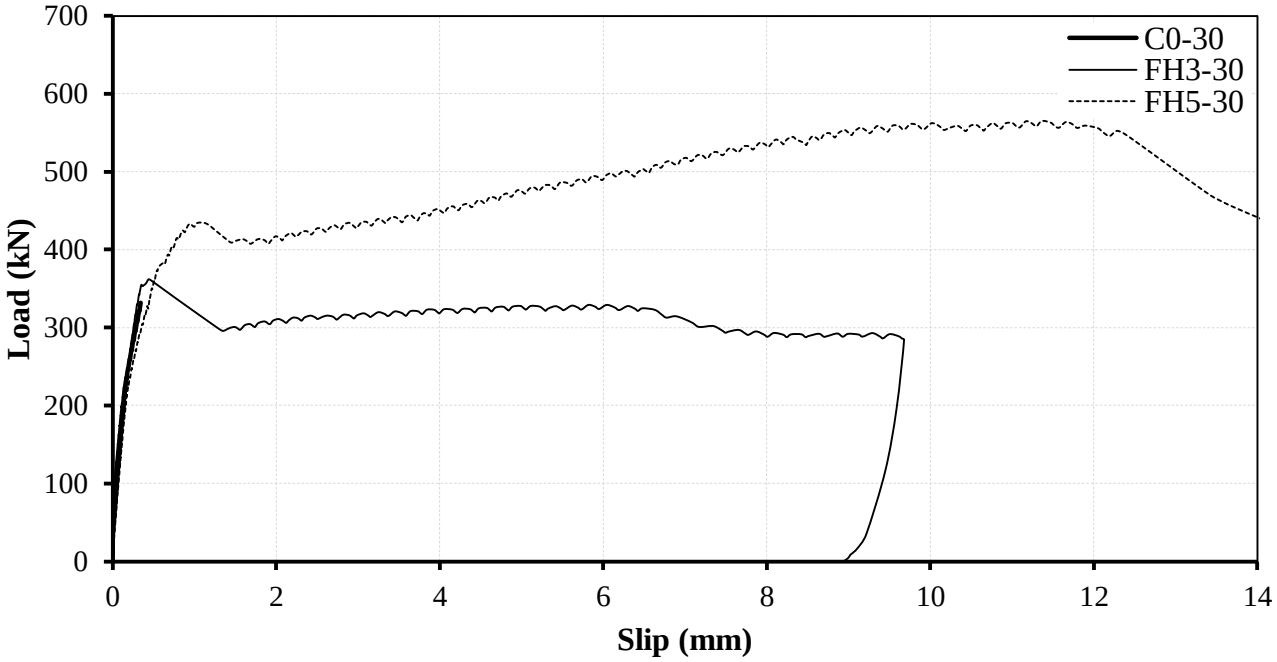

Figure 4.13 Load-slip curves of specimens of Group-VI

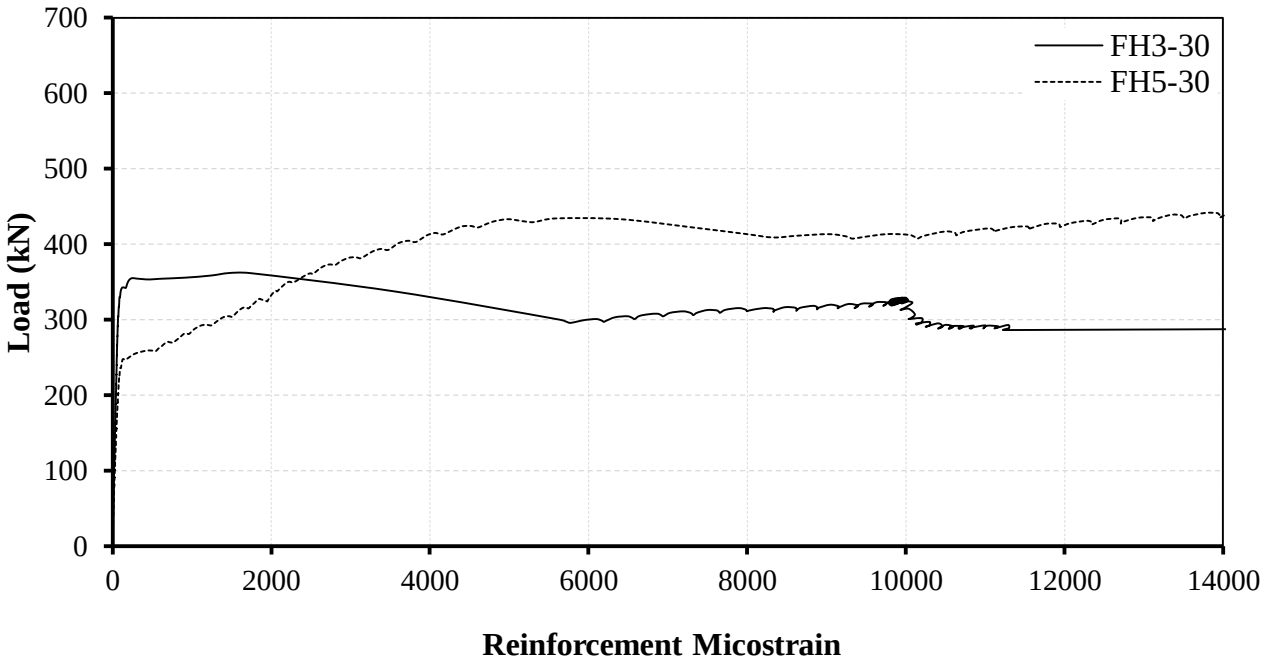

Figure 4.14 Load-reinforcement strain curves of specimens of Group-VI

As expected, lateral dilatations across the interface crack of the push-off specimens were consistent with the strains of the reinforcement intersecting the interface plane. Figure 4.15 shows the load-lateral dilatation relationships of the test specimens that were sufficiently reinforced. The lateral dilatation of the GFRP specimens in Figure 4.15 ranged from 0.23 to 0.3 mm with an average value of 0.27 mm and it was about 0.21 mm for the specimen SS2-50. Harries et al. (2012) reported an ultimate lateral dilation of 0.25 mm, at the ultimate, for steel reinforced interfaces with a reinforcement ratio of 0.41% and 0.75%. This small value of lateral separation corresponded to the ultimate load of sufficiently GFRP reinforced interfaces in which the reinforcement strain was in the range of 3000 to 5000 $\mu\varepsilon$. Lateral separations at earlier loading stages prior to the ultimate were even smaller. Therefore, there will be no serviceability issue with respect to the interface crack width.

It should be noted here that specimens which failed at/or soon after cracking exhibited a negligible dilation across the shear plane in the range of 0.023 to 0.16 mm which is compatible to the lateral dilatations of the unreinforced specimens C0-30 and C0-50 at their ultimate (see Table 4.2).

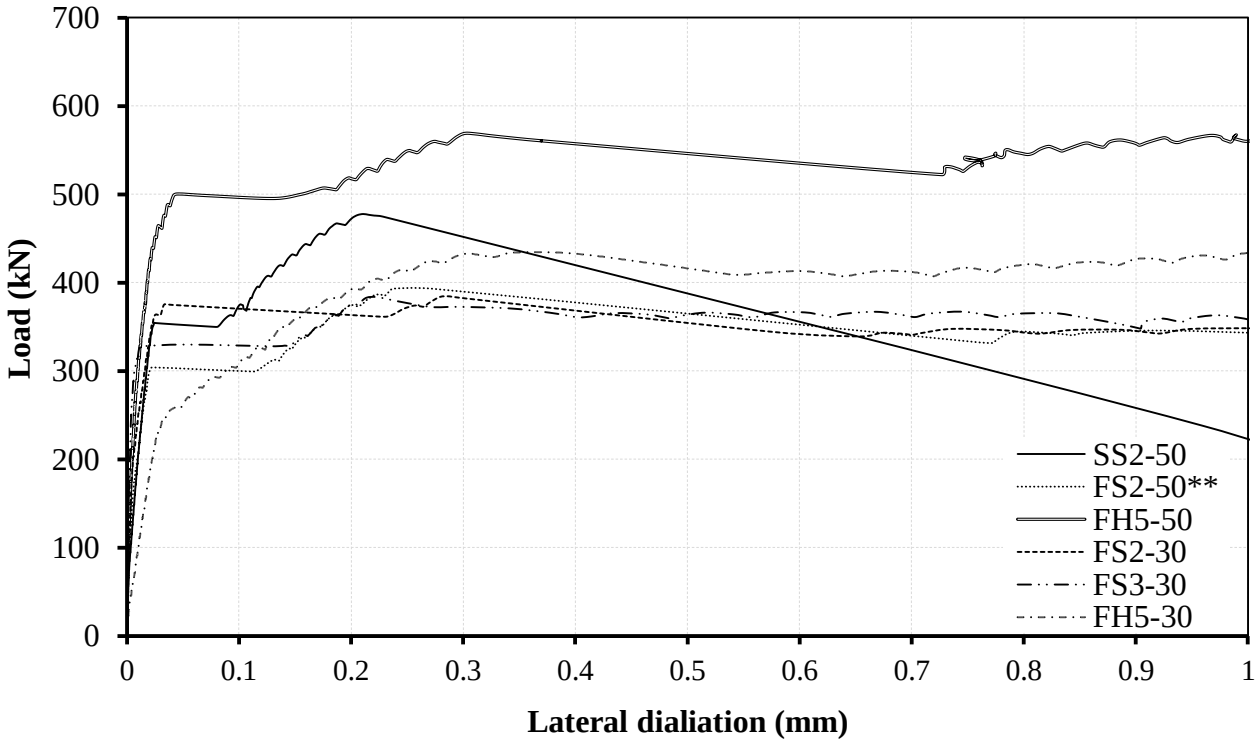

Figure 4.15 Load-lateral dilation curves of test specimens

4.3.2 Effect of the Reinforcement Shape

As mentioned in the previous chapter, three different shapes of the GFRP reinforcement were used, namely: (1) stirrup; (2) headed bar; and (3) angle. Stirrup is the most common shape of the shear transfer reinforcement that is being used along the concrete joints, especially, at the junctions of precast girders and cast-in-place slabs. However, it was decided to examine the use of GFRP headed bars since they are easy to install, particularly, in cases where the replacement of the deteriorated steel reinforcement is required in the rehabilitation work. Also, to examine the assumption of the shear friction theory stipulating, that only reinforcement inclined to the shear plane would be in tension when a direct shear load is applied along that shear plane, should be considered in the evaluation of the shear transfer strength, GFRP bent bars (angles) were also used (see Figure 3.2).

Table 4.3 shows test specimens sorted into groups from 1 to 4 to allow for comparison relative to the reinforcement shape. Group-1 in Table 4.3 includes specimens made of 50 MPa concrete with a reinforcement stiffness less than the minimum suggested in the previous discussion (203 N/mm^2). The load-slip curves of specimens of this group are illustrated in Figure 4.16. It can be seen from this figure that all specimens except FA3-50 failed immediately at the cracking load. These specimens developed a strength in the range of 9 to 14% higher than the corresponding unreinforced specimen C0-50. This confirms that regardless of the shape of a normally to the interface plane shear transfer reinforcement, a minimum stiffness must be provided in order properly engage the reinforcement in the shear carrying mechanism post to cracking. Otherwise, the failure, as in this case, occurs at the cracking load of the interface.

Table 4.3 Summary of test results (for the discussion of the reinforcement shape)

Group	Specimen ID	f'_c (MPa)	$E\rho_v \sin\alpha_f$ (N/mm^2)	At ultimate					Residual shear capacity, V_r (kN)	Residual as a percentage of V_u (%)
				V_u (kN)	Strength increase over C0 (%)	Slip (mm)	Lateral dilation (mm)	Reinforcement microstrain		
-	C0-50	50	0	296	0	0.66	0.021	NA	-	-
1	FS1-50		101	334	13	0.34	0.030	22	-	-
	FA3-50		108	540	82	0.66	0.422	4525	-	-
	FH2-50		122	336	14	0.31	0.028	389	218	65
	FH3-50$_{(avg)}$		182	323	9	0.28	0.159	2260	324	100
2	FS3-50		304	617	109	0.37	0.014	402	606	98
	FH5-50		304	569	92	0.77	0.301	2953	571	100
-	C0-30	30	0	332	0	0.34	0.034	NA	-	-
3	FS3-30		304	384	16	0.64	0.229	4847	367	96
	FH5-30		304	433	30	0.94	0.304	4973	565	130

It has to be mentioned here that both specimens with three headed bars showed a significant load carrying mechanism after the failure. The maximum residual strength was as high as 107% post to ultimate (Figure 4.16).

However, FA3-50 exhibited a shear strength 82% higher than C0-50. This points to an involvement in the shear resistance of the compressed legs of the GFRP angles in the bottom side of the specimen. It is true that these legs do not contribute in providing the clamping stress required to develop an additional shear resistance by the mean of friction, however, they may provide a shear resistance by the dowel action. Additionally, the compressed legs provide a significant interlocking mechanism that resists the slip and the direct shear along the shear plane. It is also noted from Table 4.3 that specimen FA3-50 showed larger slip and dilatation at the interface, at the ultimate load, than the rest of the specimens of its group. In short, disregarding the inclined compressed reinforcement across a concrete joint is a simplification of the problem and a conservative approach.

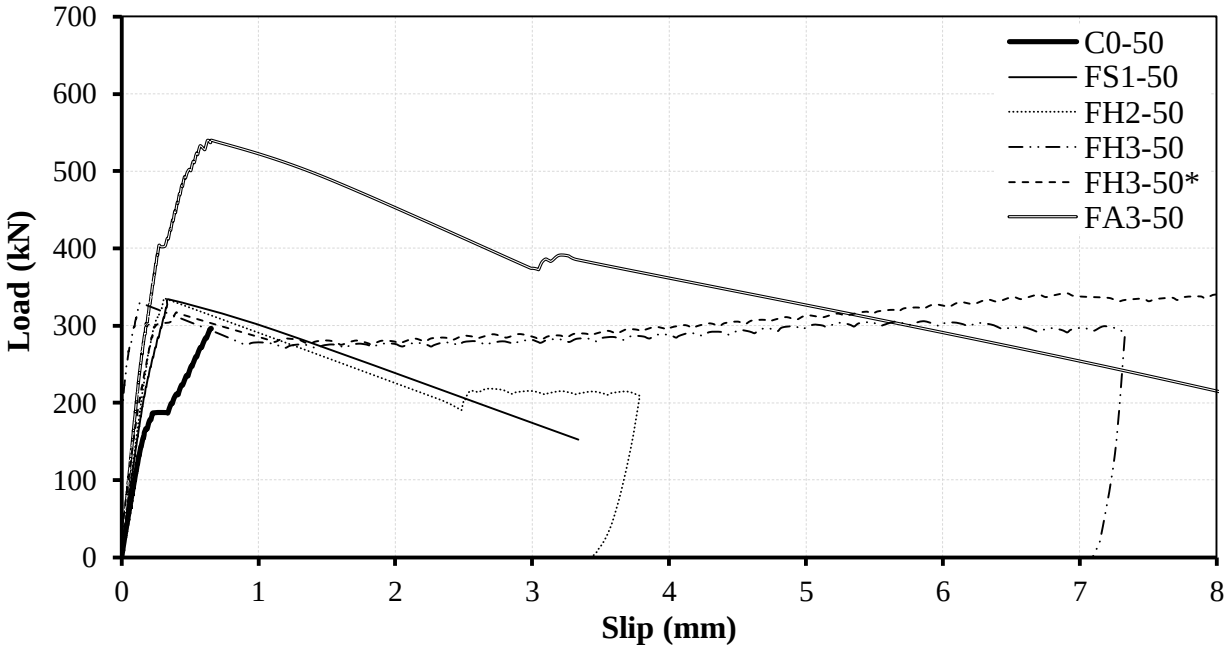

Figure 4.16 Load-slip curves of specimens of Group-1

Plots of the load-slip curves of specimens FS3-50 and FH5-50 (Group-2) are shown in Figure 4.17. The reinforcement stiffness across the interfaces of these two specimens are equal (304 N/mm^2). Specimen FS3-50 developed a shear capacity about only 8% higher than FH5-50. The sufficiently reinforced specimen FH5-50 developed substantial resistance after cracking and exhibited an outstanding ductile failure mode. A significant level of load resisting was maintained at considerably higher slips. The post failure behaviour reported for specimen FH5-50 and earlier for FH3-50 is to be attributed to excellent bond characteristics of the headed bars, which could prevent any slippage of the reinforcement relative to confining concrete. This will keep the two faces on the interface plane as close to each other as possible making it possible for higher dowel action and shear resistance to be delivered. Similar situation was pointed out by Harries et al. (2012) and Zeno (2009) when two types of steel with different bond characteristics were used.

Group-3 in Table 4.3, includes the test specimens FS3-30 and FH5-30. These two specimens have an identical reinforcement stiffness and similar concrete strength (30 MPa). The measured ultimate shear strength of FH5-30 is 12.7% higher than FS3-30. The load-slip behaviour of each of these specimens is plotted in Figure 4.18, along with the behaviour of C0-30. This figure indicates a similar behaviour of the two specimens prior to ultimate. However, the post failure resistance of the specimen with the headed bars is extraordinary.

In conclusion, the influence of the GFRP reinforcement shape whether it is a stirrup or a headed bar on the ultimate strength is not significant. However, headed bars were found to provide a remarkable load-carrying capacity (ductility) after the ultimate load was achieved. This might not be a concern since the design of the concrete joints according to

the ultimate limit state is more interested about the interface stress conditions at the ultimate point.

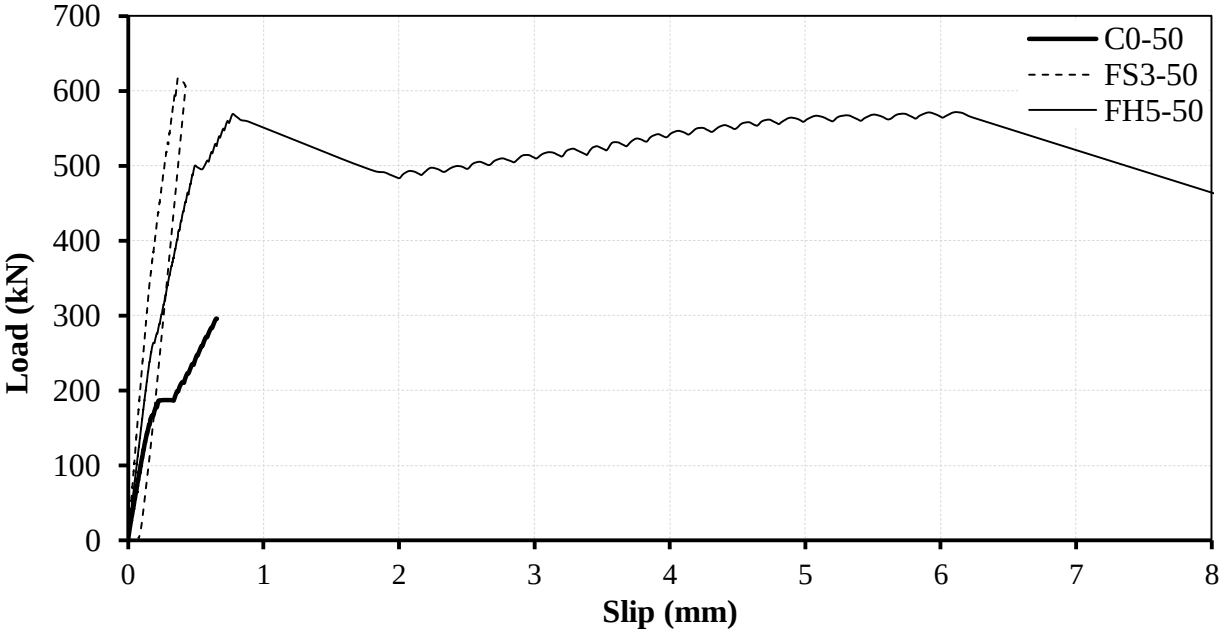

Figure 4.17 Load-slip curves of specimens of Group-2

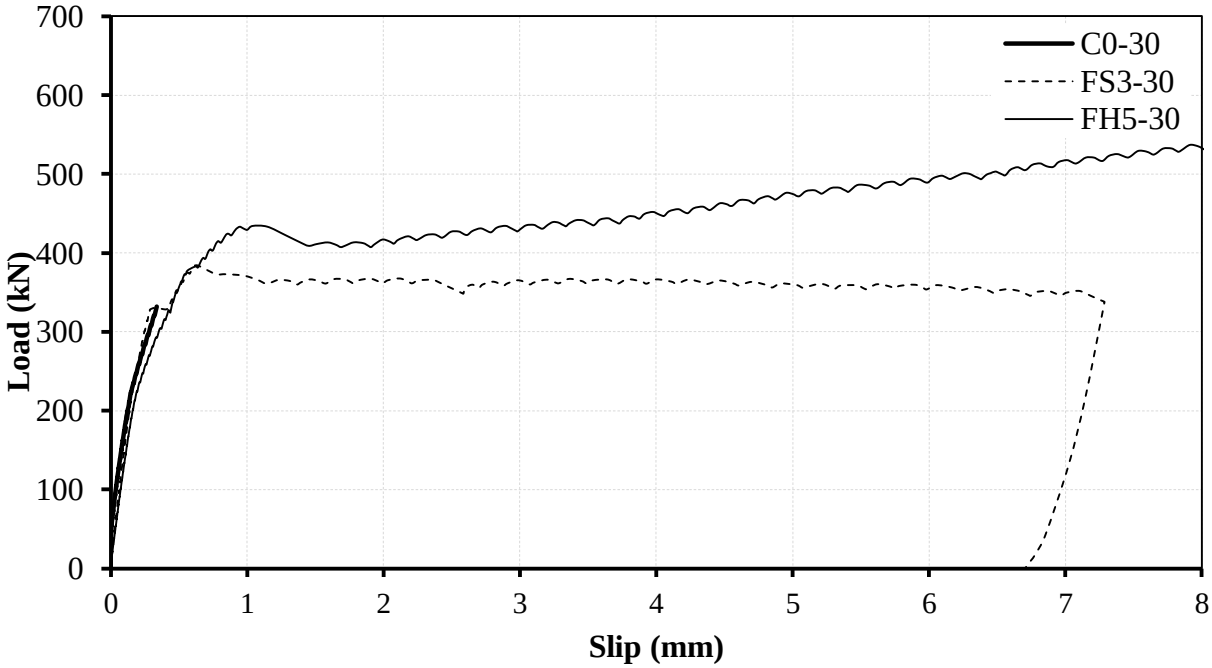

Figure 4.18 Load-slip curves of specimens of Group-3

The compressed legs of the GFRP angles provide an additional resistance to shear by the dowel action and the slippage interlocking mechanism. Ignoring such legs, as recommended by the design codes, is a conservative approach and a simplification for the sake of satisfying the main assumption of the shear friction theory that only frictional shear resistance is delivered after cracking by the virtue of clamping stresses, which are maintained by the tensile reinforcement across the shear plane.

Interfaces with GFRP stirrups suffered from an extensive spalling of the concrete covering the stirrups. This spalling was observed to start at higher values of the shear displacement (slip) and became more widespread as the slip increased. Figure 4.19(a) shows this type of failure mode. This suggests that extra concrete cover than what was provided (25 mm) might be needed to avoid this phenomenon at an advanced loading stages. Specimens with steel stirrups suffered also from concrete cover spalling as illustrated in Figure 4.19(b). Mattock (1972), Khan and Mitchel (2002) and Harries et al. (2012) reported similar behaviour when steel stirrups were used.

When GFRP headed bars were utilized, the previous behaviour was not noticed since more cover was provided. The crack maintained the shape of a clean cut up to the end of the test as can be seen in Figure 4.20(a). This could be also a reason for the remarkable post failure resistance and ductility associated with interface reinforced with GFRP headed bars. Specimen FH5-30 which showed the most load carrying capacity after failure was loaded to a much further stage. Three GFRP headed bars ruptured at the end of the test at a slip of 12 mm. Figure 4.20(b and c) shows the failure mode of this specimen along with the ruptured bars.

It was stated earlier that specimen with two GFRP angles, FA2-50 failed prematurley which resulted in a low measured strength. This failure was charactized by a concrete split developed as a crack on of the specimen faces. This crack had approximately the shape of the emobided angle and prolonged from the angle to the external surface of the specimen as shown in Figure 4.21(a). The face of the specimen on which this crack developed was verified to be the side where less concrete cover was provided, after the specimen was cut open at its interface [Figure 4.21(b)]. This crack developed prior to the ultimate load and is believed to be the reason of the low strength that this specimen showed.

(a) FS2-50 (left) and FS2-50* (right)

(b) SS1-50 (left) and SS2-50 (right)

Figure 4.19 Spalling of concrete cover in test specimens with stirrups

(a) FH3-30 (left) and FH3-50 (right)

(b) FH5-30 (both faces)

Figure 4.20 Failure mode of specimens with GFRP headed bars

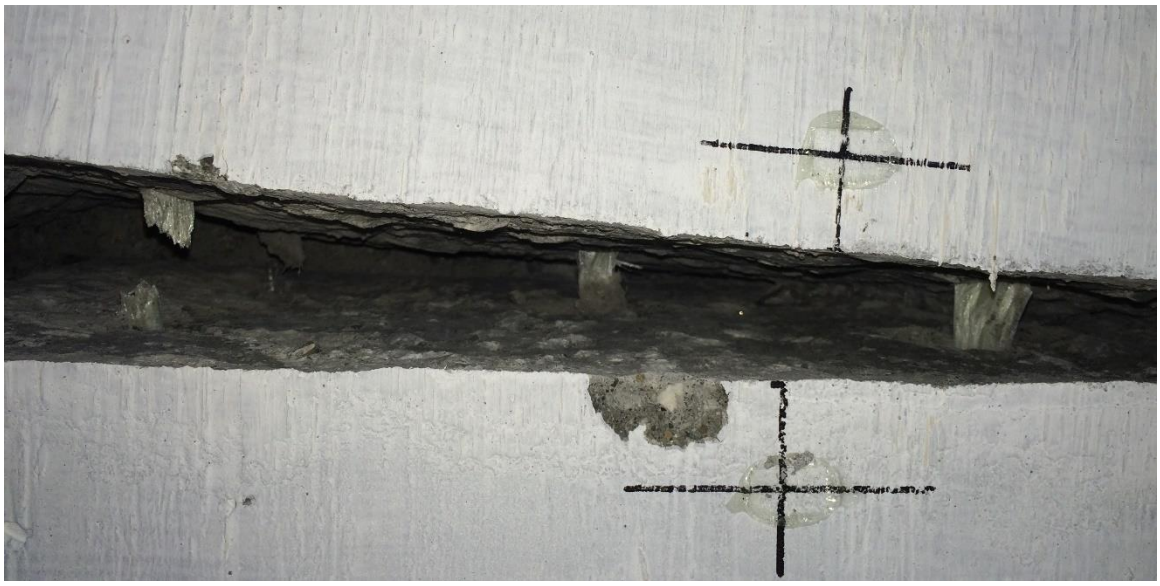

(c) Rupture of headed bars in FH5-30

Figure 4.20 Failure mode of specimens with GFRP headed bars (*continued*)

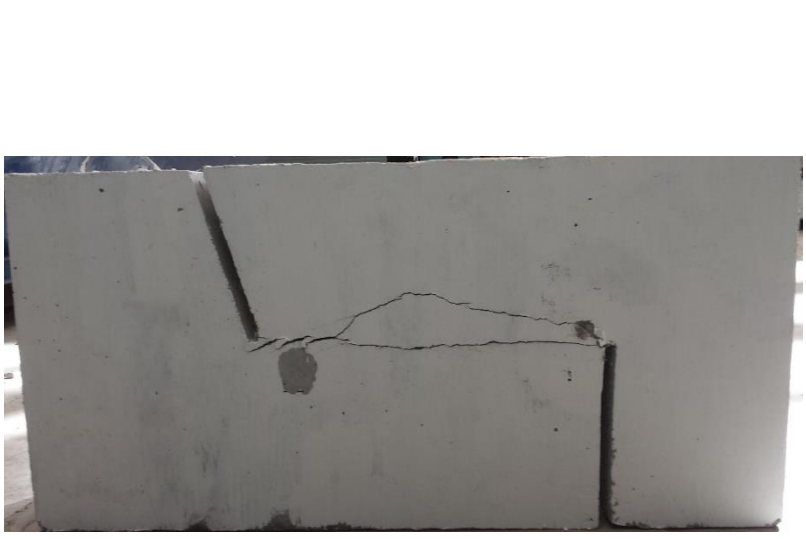

(a)

(b)

Figure 4.21 Failure mode of specimen FA2-50

Despite that specimen FA3-50 had a stiffness close to the stiffness of specimen FS1-50 (calculated based on design codes), it exhibited 1.6 times the strength of the later. Figure 4.22 shows specimen FA3-50 after testing. From closely examination of this figure, one can note a rotational movement of one part of the push-off specimen relative to the other, around the junction of the compressed leg with the shear plane [Figure 4.22(b)]. Also, a diagonal crack on the top corner of the shear plane parallel to the tensile leg of the GFRP angle can be observed. These observations suggest that despite the fact that the compressed legs would not provide clamping stresses along the shear plane, they provide a significant interlocking against slip and, hence, contributed in the shear transfer strength. There is no reasonable doubt that the compressed legs resist the slip along the shear plane and push the two faces of the interface apart on opposite directions. As a result, the stress in the tensile leg increases rapidly which led to the pull out of these legs along with the surrounding concrete on the top part of the specimen causing the reported rotational movement. This also explains the higher separation and reinforcement strain recorded for this specimens than the companion specimens of Group-1 (Table 4.3). Kinking and dowel action of the compressed legs can also be additives to the shear resisting mechanism.

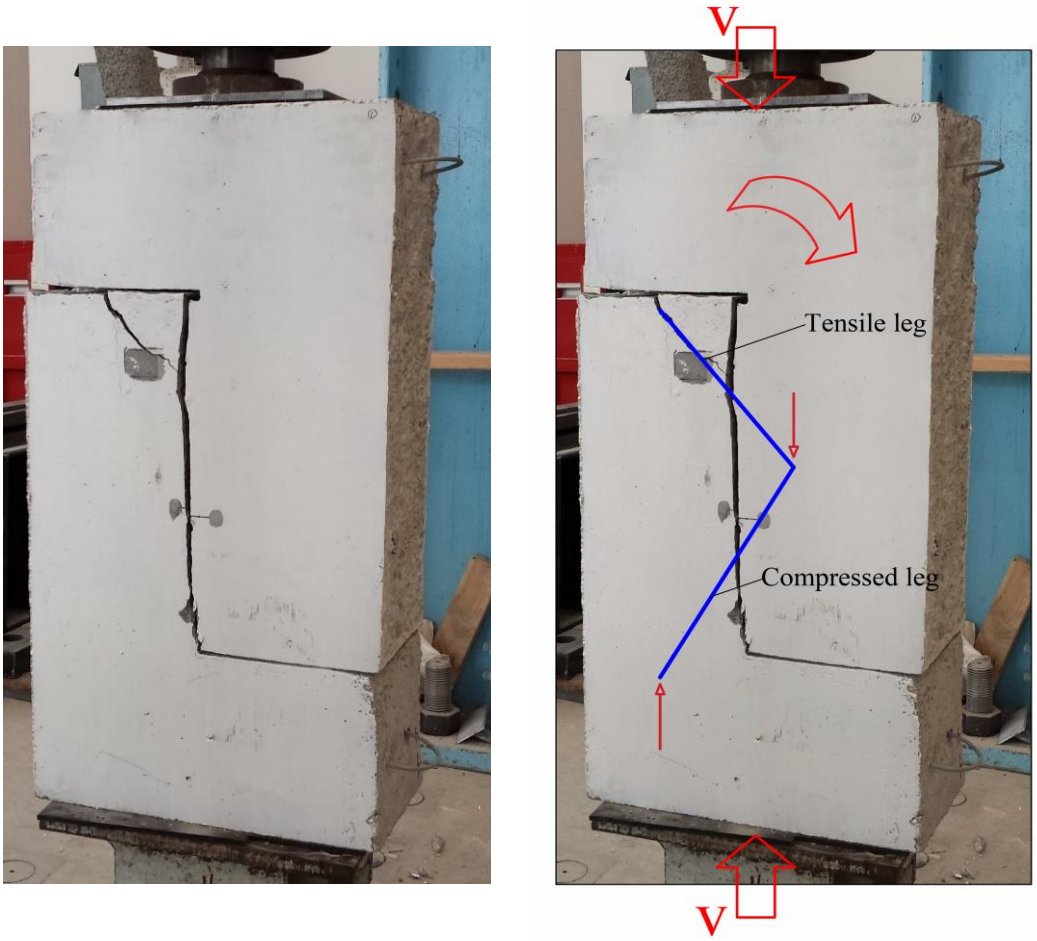

(a) **(b)**

Figure 4.22 Failure mode of specimen FA3-50

4.3.3 Effect of the Concrete Strength, f'_c

The influence that the concrete strength might has on the shear transfer strength or behaviour of the concrete-to-concrete interfaces was an argumentative point as was shown in the literature detailed in Chapter 2. While some researchers believed that it has no influence on the shear transfer capacity as imposed by the original shear friction theory (Anderson, 1960; Birkeland and Birkeland, 1966; Mast 1968;), others were convinced on its effect and included, empirically, the influence of the concrete strength in their models of the ultimate shear transfer strength (Walraven et al. 1987; Loov and Patnaik 1994; Khan and Mitchell 2002 and others).

To exclusively investigate the influence of the concrete strength, specimens in Table 4.4 arranged into groups, I to V. Each group includes specimens with the same reinforcement content and shape.

Group-I includes the test specimens with two GFRP stirrups made of a concrete of 30 and 50 MPa. The load-slip curves of these specimens along with the unreinforced ones C0-30 and C0-50 are shown in Figure 4.23(a). It can be noted from this figure that the strength of FS2-50 was higher by 6.5% than the capacity of FS2-30. Yet, the general deformation behaviour of these specimens is similar and consistent with the findings discussed in the previous sections. A closer look on the load-slip curves of FS2-50 and FS2-30 is shown in Figure 4.23(b). It reveals that the prior to failure stiffness of the specimen made of 50 MPa was higher than that of the one made of 30 MPa.

Table 4.4 Summary of test results (for the discussion of the concrete strength)

Group	Specimen ID	f'_c (MPa)	$E\rho_v \sin\alpha_f$ (N/mm^2)	At ultimate					Residual shear capacity, V_r (kN)	Residual as a percentage of V_u (%)
				V_u (kN)	Strength increase over C0 (%)	Slip (mm)	Lateral dilation (mm)	Reinforcement microstrain		
-	C0-50	50	0	296	0	0.66	0.021	NA	-	-
I	FS2-50$_{(avg)}$	50	203	402	36	0.48	0.238	3881	345	86
	FS2-30	30	203	385	16	0.58	0.288	4466	350	91
II	FS3-50	50	304	617	109	0.37	0.014	402	606	98
	FS3-30	30	304	384	16	0.64	0.229	4847	367	96
III	FH3-50$_{(avg)}$	50	182	323	9	0.28	0.159	2260	324	100
	FH3-30	30	182	362	9	0.44	0.162	1472	328	91
IV	FH5-50	50	304	569	92	0.77	0.301	2953	571	100
	FH5-30	30	304	433	30	0.94	0.304	4973	565	130
V	FA3-50	50	108	540	82	0.66	0.422	4525	-	-
	FA3-30	30	108	342	3	0.24	0.023	100	-	-
-	C0-30	30	0	332	0	0.34	0.034	NA	-	-

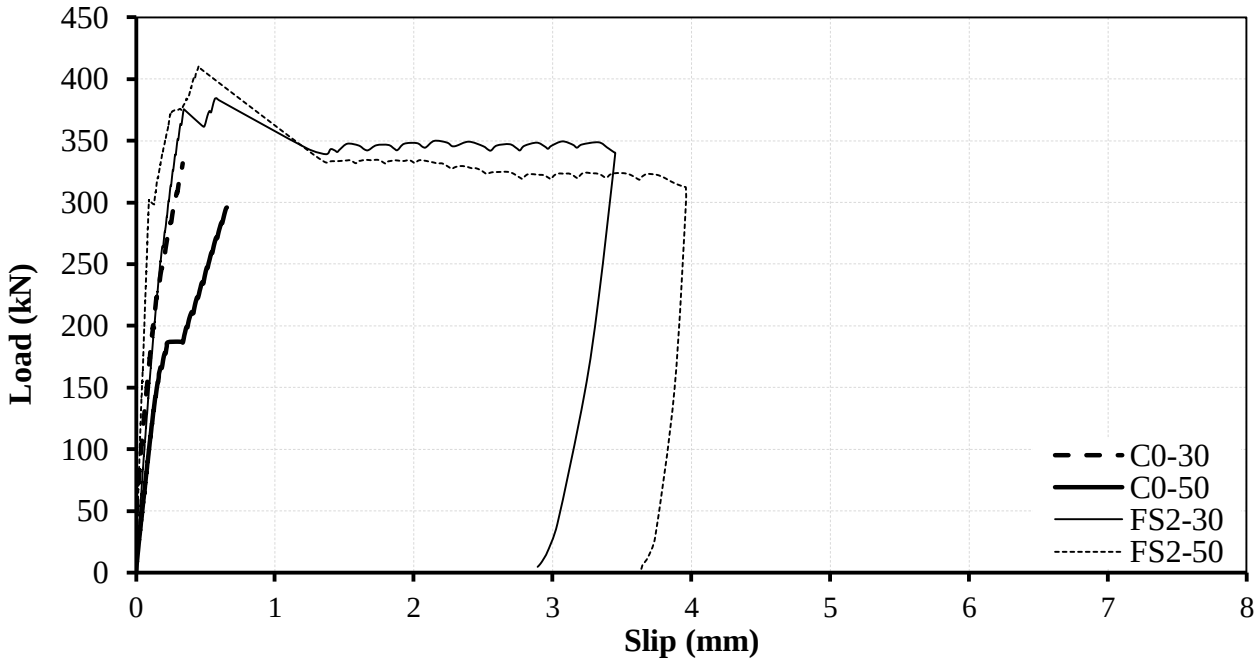

(a)

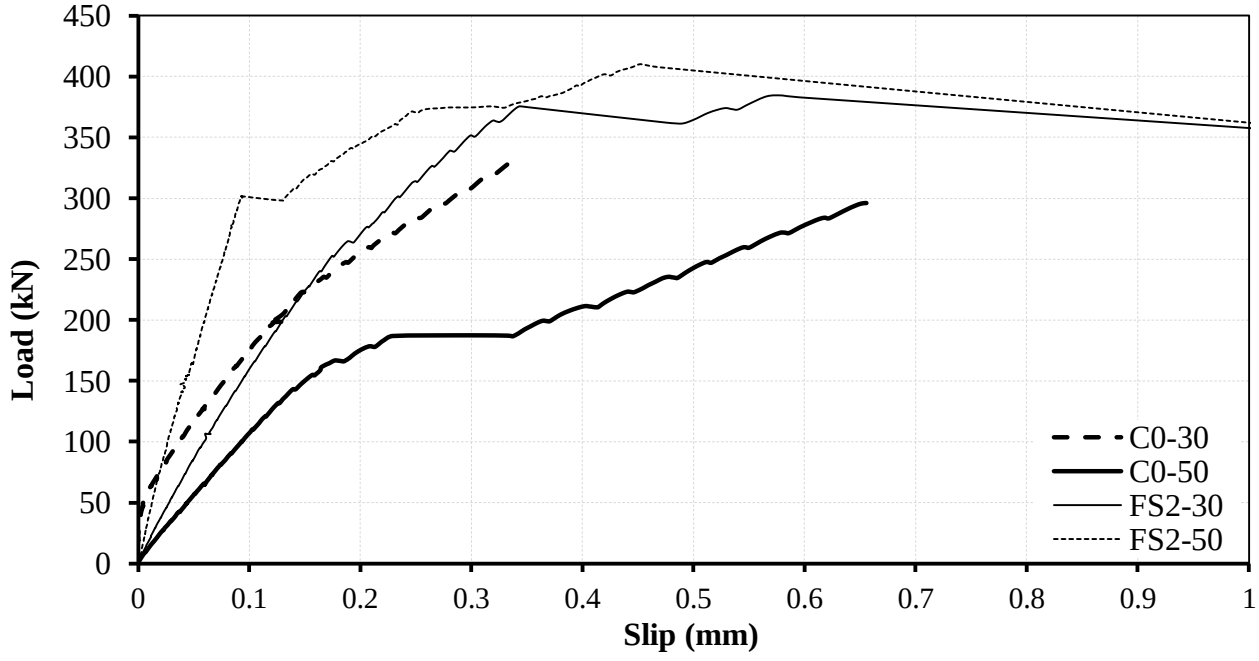

(b)

Figure 4.23 Load-slip curves of specimens of Group-I

The influence of the concrete strength on the shear transfer capacity appears to be more significant when higher reinforcement stiffness was used. Each of the specimens of Group-II had three GFRP stirrups across its interface and they had a similar reinforcement stiffness. The specimen made of 50 MPa concrete, FS3-50, exhibited a measured capacity exceeded the capacity of FS3-30 by 61% [Figure 4.24(a)], which is a considerable increase as compared to the previous case (2 GFRP stirrups). The load-deformation responses of these specimens up to a slip of 1 mm are shown in Figure 4.24(b). As it can be seen, the specimen with higher concrete strength exhibited much higher stiffness in the stage prior to the cracking load.

Illustrated in Figure 4.25(a) are the load-slip responses of the specimens of three headed bars sorted as Group-III with identical reinforcement stiffness. From this figure, it can be seen that there is no evidence of the effect of the concrete strength. In contrary, specimen made of 30 MPa concrete, FH3-30, developed 12% extra strength over the average strength of the specimens with three headed bars made of 50 MPa concrete (Table 4.4). In fact, this confirms the importance of the reinforcement stiffness in controlling the behaviour of the concrete interfaces and making it more predictable. If the reinforcement stiffness across a concrete joint is inadequately provided, the concrete interface dominates the behaviour and controls the strength of this interface in resisting the direct shear (Harries et al. 2012). This gives the shear transfer problem a high level of unpredictability associated with the, well established, uncertainty of the shear resistance and behaviour of unreinforced concrete sections.

Figure 4.25(b) shows that specimens of Group-II had almost similar stiffness prior to ultimate indicating no effect of the concrete strength relative to stiffness in this case.

The influence of the concrete strength appears again in the well reinforced specimens of Group-IV, which are provided with five GFRP headed bars across their interfaces (Table 4.4). Specimens with a higher concrete strength FH5-50 displayed a strength exceeded the strength of FH5-30 by 31.4%. The general load-deformation behaviour of these specimens are very close as shown in Figure 4.26(a). The narrow range of the deformation behaviour of these specimens is shown in Figure 4.26(b). As can be seen, the prior to failure branch of the load-slip curve of FH5-50 is stiffer than the corresponding one of specimen FH5-30.

The last group in this discussion is Group-V. It includes the specimens with three GFRP angles and made of 50 and 30 MPa concretes. The shear transfer strength of FA3-50 is reported, in Table 4.4, as of 58% higher than FA3-30. The general load-slip behaviour of both specimens is pretty much the same as it can be noticed from Figure 4.27(a). Additionally, the stiffness of both specimens prior to cracking of the interface was not significantly influenced by the concrete strength [Figure 4.27(b)]. This observation is consistent with what have been reported for low reinforced specimens so far in this section. The capacity that the specimens with GFRP angles have shown is attributed to both the tensile reinforcement stiffness (which is below the suggested minimum in section 4.3.1) and to the compressed legs in the opposite side, which do not add any clamping stresses along the interface. This means, that the actual stiffness that clamps the two faces of the interface together is, in fact, low, and therefore, the stiffness of the load-slip curves did not

change for the specimens of Group-V similar to the scenario of the specimens with three headed bars mentioned earlier in the proceeding section.

The examination of the load-slip curves of the specimens in the assigned groups for this section, revealed that raising the concrete strength would result in a higher shear transfer strength and stiffer pre-cracking part of these curves only if the reinforcement stiffness is higher than the minimum amount indicated section (4.3.1). Otherwise, there would be limited to no influence of the concrete strength on the shear transfer strength. In other words, the benefits of a stronger concrete are better utilized in a combination with higher reinforcement stiffness parameter. Similar conclusions were pointed out by Mansur et al. (2008) based on their push-off tests using steel reinforcement across their shear planes.

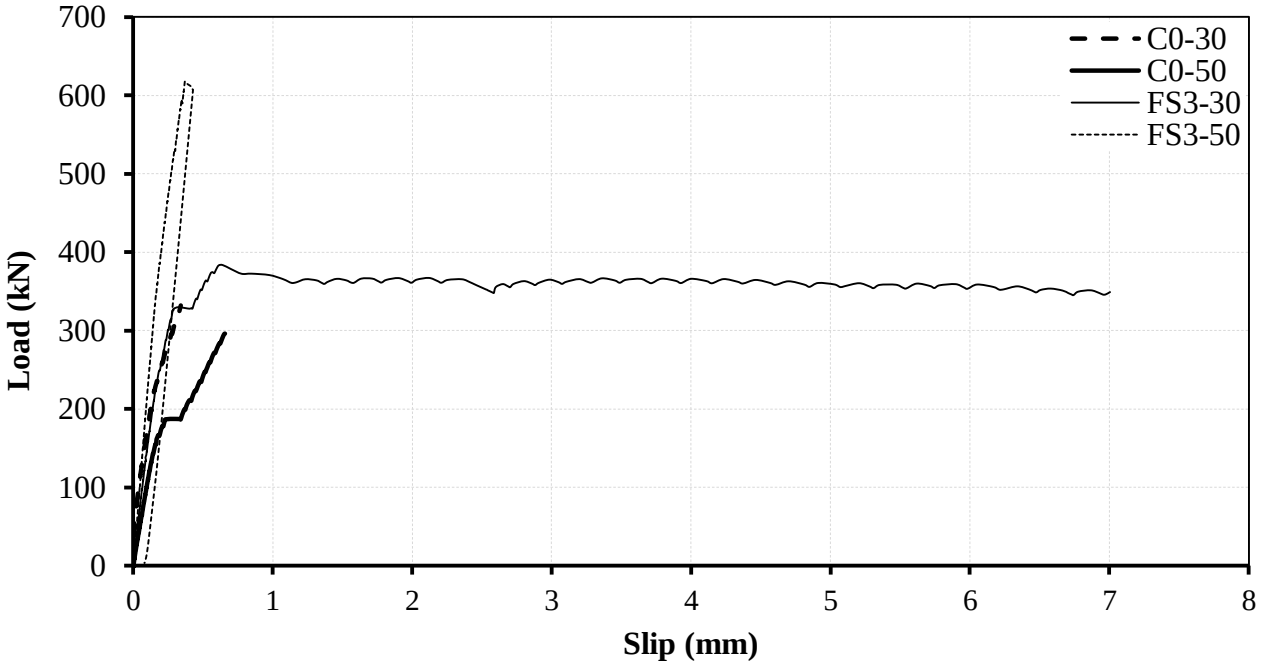

(a)

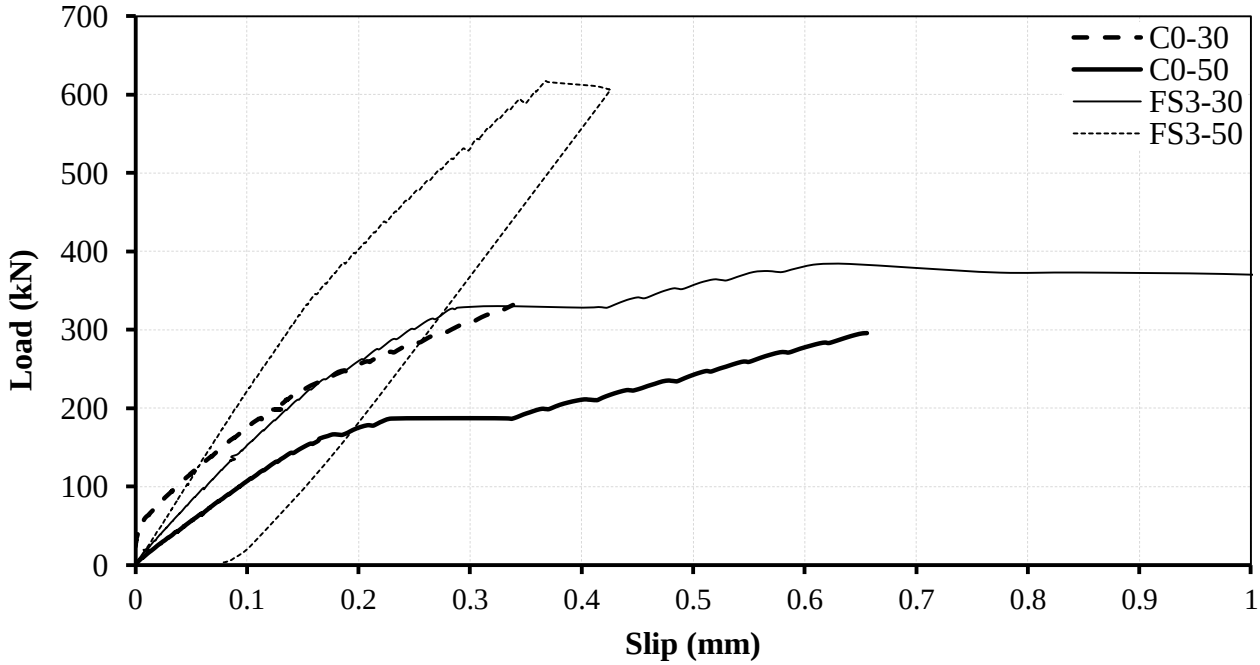

(b)

Figure 4.24 Load-slip curves of specimens of Group-II

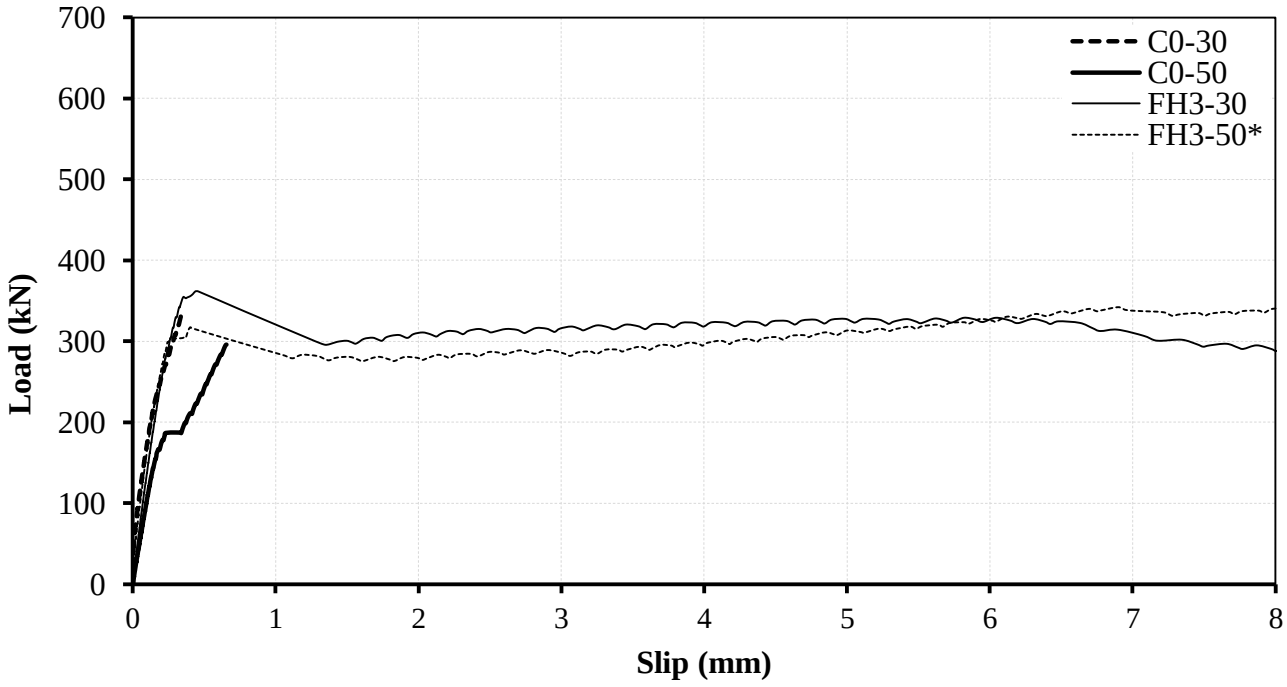

(a)

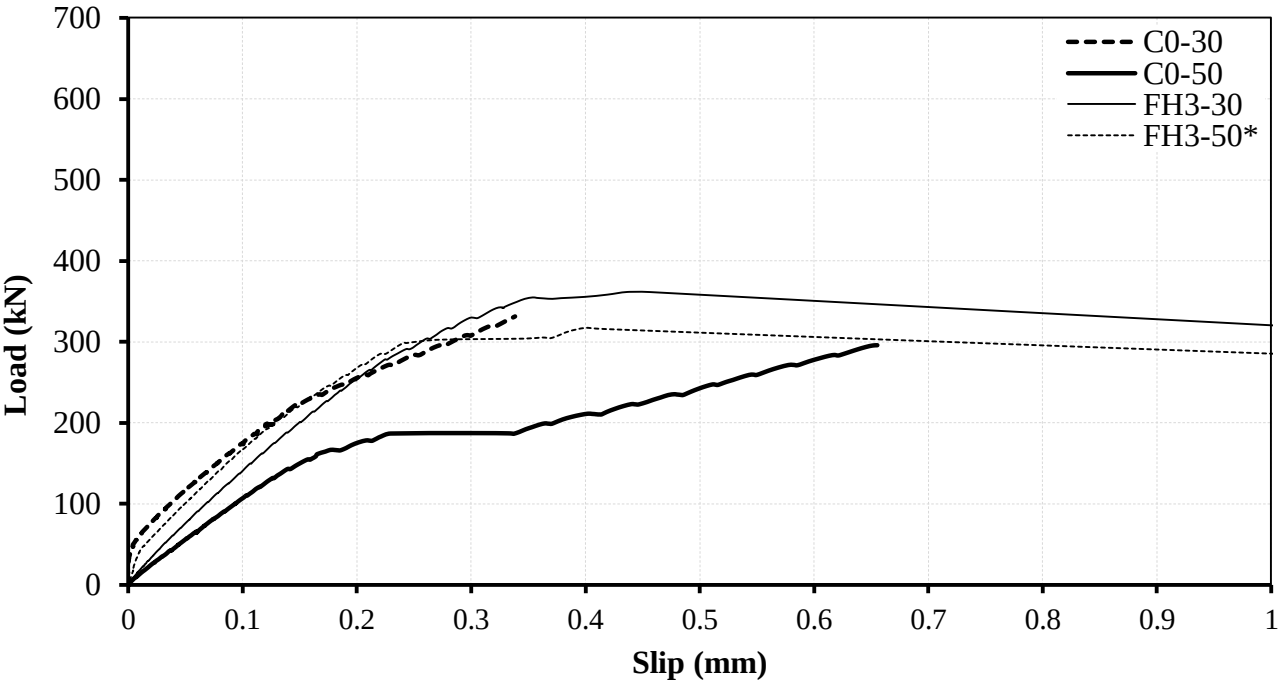

(b)

Figure 4.25 Load-slip curves of specimens of Group-III

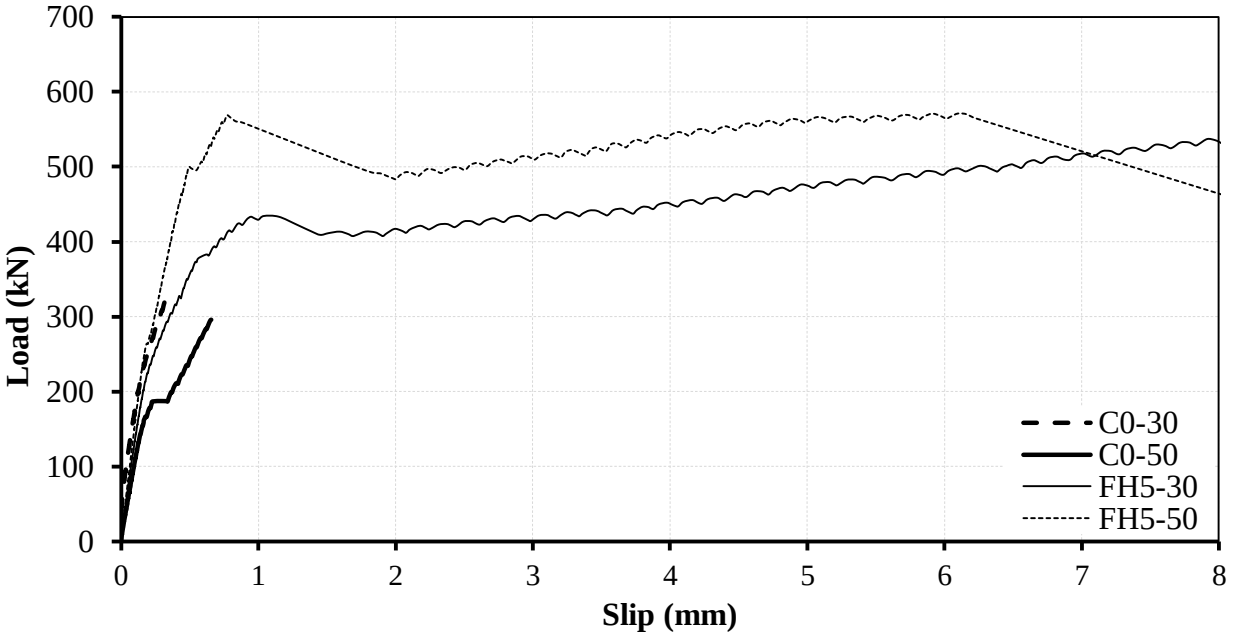

(a)

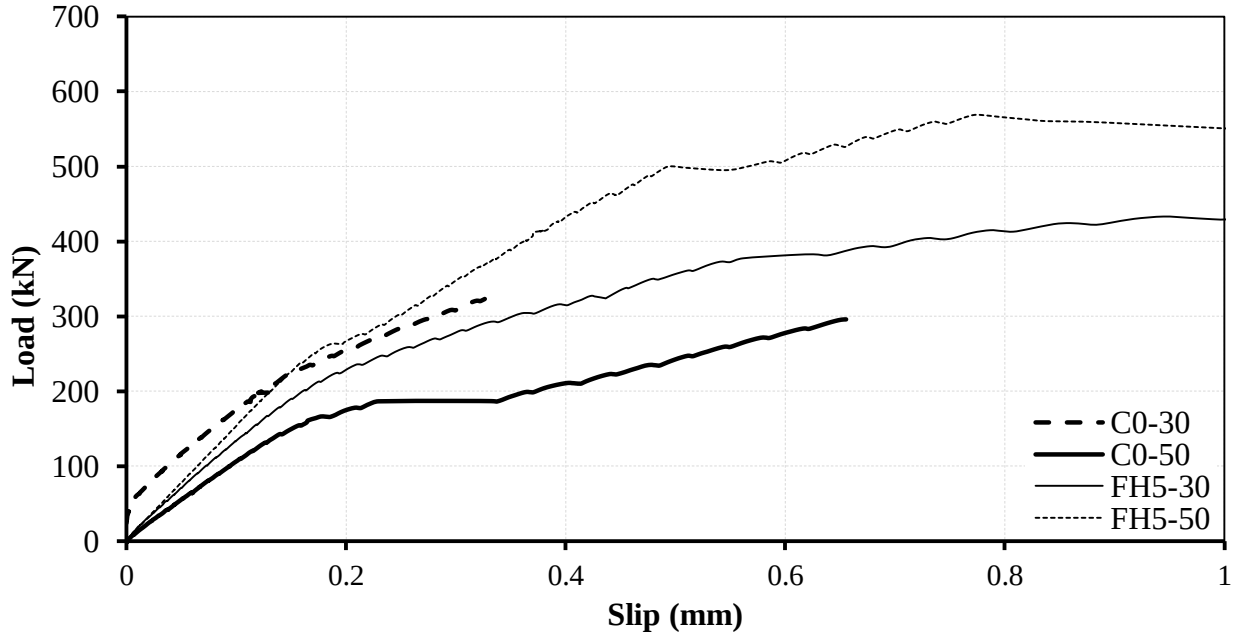

(b)

Figure 4.26 Load-slip curves of specimens of Group-IV

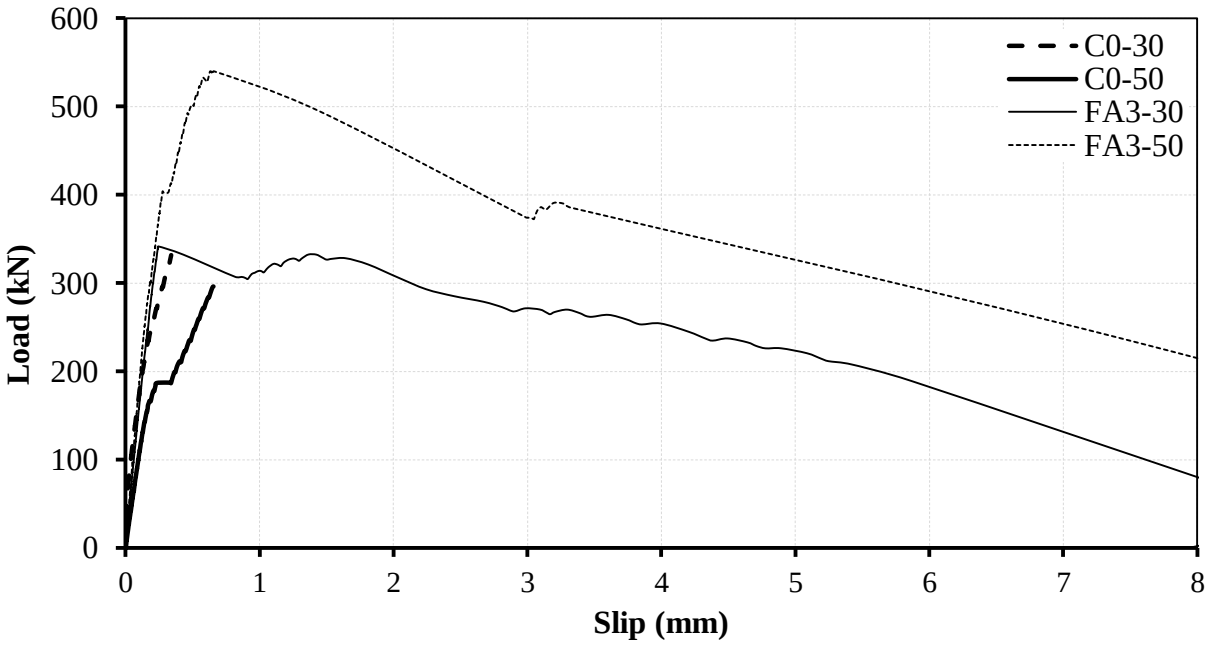

(a)

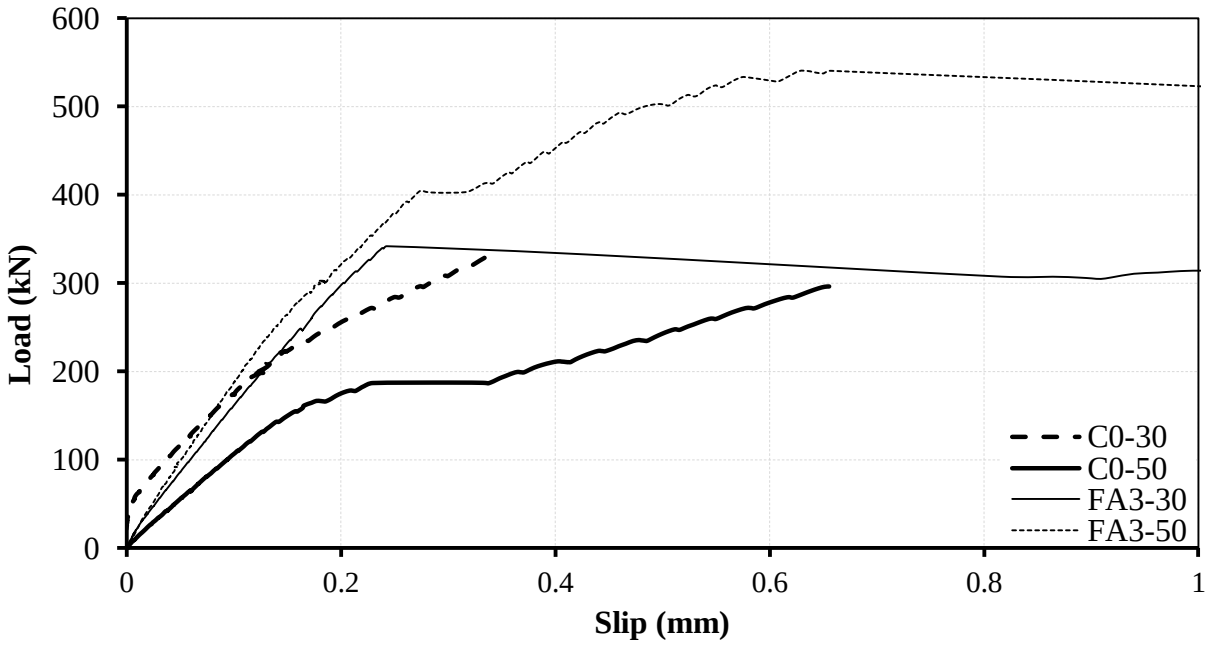

(b)

Figure 4.27 Load-slip curves of specimens of Group-V

4.4 Proposed Shear Friction Equation

The shear friction hypothesis postulates that the interface crack width, at the ultimate, is large enough to stress the steel reinforcement intersecting the shear plane to its yield stress. The clamping force, which is attributed to the steel reinforcement, is engaged once the interface crack starts to open. However, in the case of the GFRP reinforcement where no yielding occurs, another ultimate limit state must be introduced. In the following discussion, an attempt has been made to identify this ultimate limit state and to investigate the relationship between the nominal ultimate shear transfer strength, reinforcement stiffness and the concrete strength.

The ultimate frictional shear resistance is mainly related to the following interdependent parameters: (a) apparent coefficient of friction, μ; (b) crack width; and (c) clamping stress. In fact, these parameters are not constants but they vary from the cracking instant to the ultimate load. Increasing the crack width would, indeed, increase the stress in the reinforcement leading to a higher clamping stress, but it would also decrease the friction coefficient. However, determining the actual variation of the coefficient of friction can be a very complex matter, therefore, the coefficient of friction was considered to be independent of the crack with and the clamping stress level during the loading history, in all of the previous studies. This assumption will be considered true herein as well. The so-called "coefficient of friction" μ is a measure of the general surface roughness of the interface. Different values of the friction coefficient were specified for different conditions of the interface roughness, as was discussed in detail in Chapter 2. CSA A23.3 (2004)

granted a value of 1 of the shear friction coefficient for an interface surface formed by placing concrete against hardened surface that is clean and intentionally roughened to a full amplitude of 5 mm (ACI 318-14 specifies 0.25 in. roughness). To simplify the construction of composite members, many researchers conducted their experimental programs on the basis of as-cast interfaces (Loov and Patnaik 1994; Khan and Mitchell, 2002; Khan and Slapkus, 2004). This type of an interface was found compatible to the intentionally roughened interface describe by the design codes (Khan and Slapkus, 2004; Khan and Mitchell, 2002).

The clamping stress is directly related to the stiffness of the reinforcement intersecting the shear plane which is characterized by the modulus of elasticity of this reinforcement (i.e. E_F for GFRP reinforcement). At the ultimate load, the crack width becomes considerably large reducing, significantly, the friction between the interconnected members. Any attempt to increase the load would only result in further widening of the crack increasing the strain and, hence, the stress in the reinforcement but without any increase in the applied loading as discussed the in previous sections.

In the following development of an equation to evaluate the ultimate shear transfer strength, the stress in the GFRP reinforcement at the ultimate load, which are equal to the exerted clamping stress, is correlated to the stress condition along the concrete joint. It should be stated that since the construction of concrete-to-concrete joints are necessarily associated to fabrication and erection variations, it is almost impossible to have two identical connections, and the nature of stresses would never be the same from a connection

to another (Mast, 1968).

As was illustrated in the discussion regarding the influence of the reinforcement stiffness in section 4.3.1, the interface strain of the GFRP reinforcement, at the ultimate load, was near 5000 $\mu\varepsilon$. The later situation corresponds to the case where the GFRP reinforcement is sufficiently provided across the interface. By this debate, the clamping force introduced to the faces of the interface, at the ultimate, by the GFRP reinforcement (see Figure 4.28), can be given as, $\varepsilon_F E_F A_{vf} sin\alpha_f$. Therefore, the induced clamping stress will be:

$$\boldsymbol{\sigma = \varepsilon_F E_F \rho_v sin\alpha_f} \tag{4.1}$$

The resisting force component in the direction parallel to the interface, as shown in Figure 2.28, is $\varepsilon_F E_F A_{vf} cos\alpha_f$. In terms of stresses, the latter force may be expressed as follows:

$$\boldsymbol{v_l = \varepsilon_F E_F \rho_v cos\alpha_f} \tag{4.2}$$

where ε_F is the strain in the GFRP reinforcement at the ultimate load and it equals to 5000 $\mu\varepsilon$, E_F is the modulus of elasticity of the GFRP reinforcement (50 GPa for stirrups and angles and 60 GPa for headed bars used in this study), and $\rho_v = A_{vf}/A_{cv}$ is the GFRP reinforcement ratio; A_{vf} is the area of the GFRP reinforcement (mm^2); A_{cv} is the area of the shear plane (mm^2).

Plotted in Figure 4.29 are the normalized, with respect to the concrete strength, clamping stress ($0.005E_F\rho_v sin\alpha_f/f_c'$) on the horizontal axis and the normalized net direct shear stress [$(v_u - 0.005E_F\rho_v cos\alpha_f)/f_c'$] of the test specimens, at the ultimate load. The

mean line through the data (dotted line in Figure 4.29) is given by the following equation:

$$v_u = 0.05f'_c + \varepsilon_F E_F \rho_v sin\alpha_f + \varepsilon_F E_F \rho_v cos\alpha_f \quad (4.3)$$

This equation yields to a test/calculated strength ratio of 1.06, with a standard deviation of 0.019.

Following the general philosophy of the shear design, where a lower bound formulation is preferred, Eq. 4.4, represented by straight solid line in Figure 4.29, is proposed. It is developed to give conservative, simple and rational predictions of the shear capacity of cold-joint interfaces intersected by a sufficient GFRP shear reinforcement that meets the requirements proposed in section 4.3.1. This equation has a component in the form of the original shear friction equation proposed by Birkeland and Birkeland (1966) and Mast (1968). However, it also conforms with the basis of Mattock and Hawkins (1972), Mattock (1974), Basler and Witta (1966) and Khan and Mitchell (2002), Harries et al. (2012) and others. This equation incorporates a frictional resistance component with a friction coefficient of μ equals to 1, identical to the slop of the mean line (Eq. 4.3). This is similar to the value suggested by the design codes (CSA A23.3-04; ACI 318-14; AASHTO, 2002; AASHTO LFRD, 2012) for intentionally roughened interfaces. It includes a component for adhesion bond and protrusions shear of the concrete interface ($0.04f'_c$). It provides the designer with visual and physical impact of the shear transfer mechanism. As discussed previously the concrete strength has an insignificant influence on the frictional shear resistance post to cracking of the interface. After cracking, the dominate factors are the clamping stress σ, maintained by the reinforcement, and the general roughness of the

interface, presented by μ. This concept was also emphasized by many researchers, such as Mattock (1988), Khan and Mitchell (2002) and Mansur (2008).

Being the ultimate nominal shear transfer stress resistance of as-cast rough cold-joint concrete joint intersected by GFRP reinforced predicted by:

$$\boldsymbol{v_u = 0.04 f'_c + \varepsilon_F E_F \rho_v sin\alpha_f + \varepsilon_F E_F \rho_v cos\alpha_f} \quad (4.4)$$

where

$$\boldsymbol{0.04 f'_c + \varepsilon_F E_F \rho_v \sin \alpha_f \leq 0.25 f'_c} \quad (4.5)$$

Despite the soundness of Eq. 4.4 in predicting the shear transfer strength at a low value of the clamping stress of the GFRP reinforcement, it is recommended that the minimum value of the clamping stress to be used. Using a minimum amount of GFRP reinforcement across a concrete interface raises the predictability of the shear transfer behaviour and strength of such and allows to avoid immediate failure modes after cracking for under reinforced interfaces or brutal and sudden failures associated with unreinforced interfaces. It will also allow to utilize the GFRP reinforcement after cracking of the shear plane. The minimum reinforcement requirement was shown to correspond to a reinforcement stiffness perpendicular to the shear plane of 203 N/mm^2. Using Eq**.** 4.1 would result in a clamping stress σ of 1.02 MPa, which can be defined as the minimum required clamping stress that needs to be delivered by the GFRP reinforcement in order to raise the strength of the interface beyond the cracking load and to develop an additional shear frictional resistance post to cracking. In fact, the necessity of a minimum requirement of the shear transfer was discussed in the literature, especially by Mattock (1974) and Mattock et al. (1976). In these

studies, a minimum clamping stress of the steel shear transfer reinforcement of 1.38 MPa was suggested to ensure the legitimacy of the shear friction hypothesis.

An upper limit specified by the Canadian Code CSA A23.3 (2004) as suggested by Eq. 4.5 is maintained. This limit appears to be in an agreement with the test results. Although it is possible to achieve a higher strength when higher GFRP content is used, this limit seems desirable until further tests with higher clamping stresses of GFRP reinforcement are carried out to determine whether this is merely a detailing problem.

If the design criteria implied by the design codes that an existing crack along the interface has to be assumed prior to application of the shear load, only the second term of Eqs. 4.4 shall be used in the evaluation of the shear transfer strength. It has to be noted that only perpendicular or inclined to the shear plane reinforcement such that the shear force produces tension in that reinforcement shall be included in the evaluation of the shear transfer strength using Eq. 4.4.

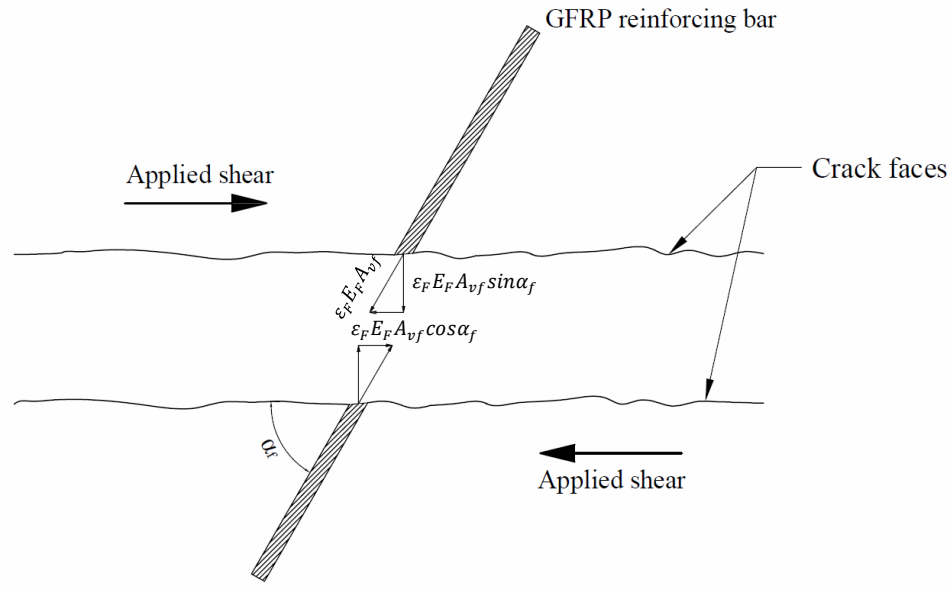

Figure 4.28 Inclined GFRP shear transfer reinforcement

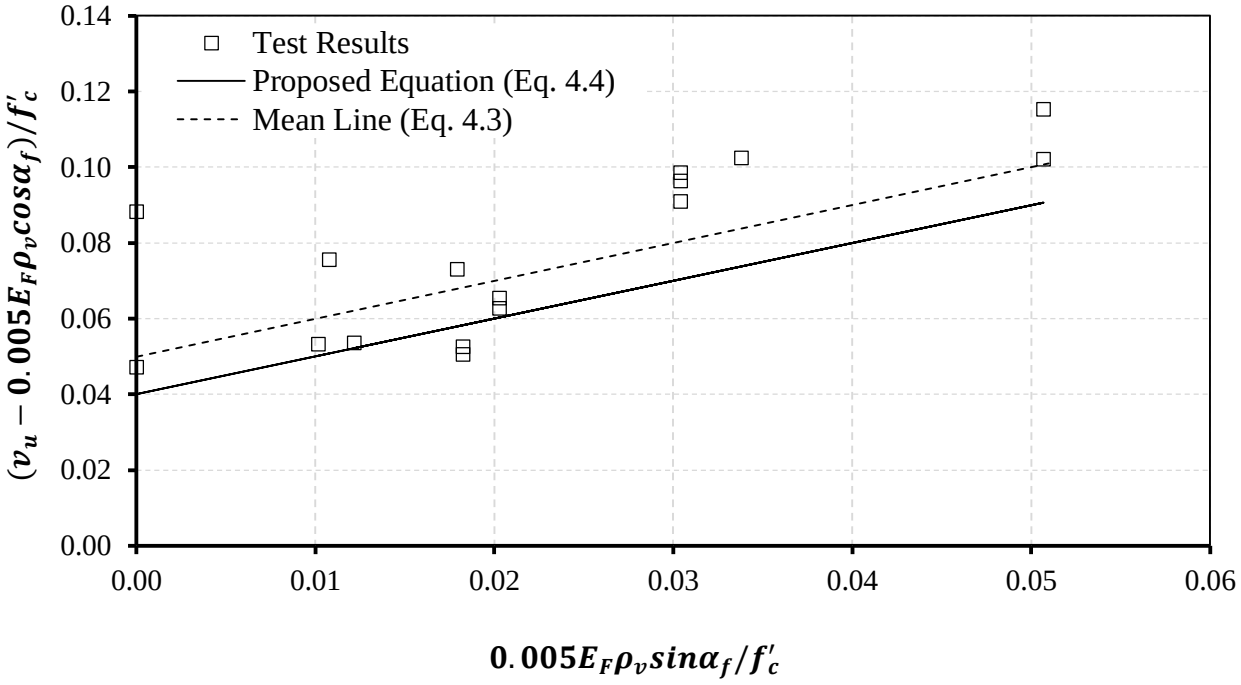

Figure 4.29 Comparison of Eq. 4.3 and Eq. 4.4 with the test data

4.5 Summary

The results of the push-off tests conducted in this research were presented in this chapter. The influence of each of the studied parameters, which are the reinforcement stiffness, reinforcement shape and concrete strength was discussed in details. The general behaviour of an adequately reinforced interfaces with GFRP reinforcement was described. A minimum requirement of the GFRP shear transfer reinforcement was also specified. The ultimate limit state for the cold-joint joints intersected by a sufficient GFRP reinforcement, on which the formulation of a shear friction equation was based, was introduced. An upper limit of the shear transfer strength in agreement with the test results and design codes was suggested.

CHAPTER 5

CONCLUSIONS AND RECOMMENDATIONS

5.1 Overview

This study proposed a new application of the GFRP reinforcement as a shear transfer reinforcement at the cold-joint concrete joints with as-cast rough interfaces. To explore the feasibility and effectiveness of this innovative application, this study focused on the experimental testing on the conducted push-off test specimens.

Twenty large scale double L-shaped push-off specimens with cold-joint conditions at their interfaces were constructed and tested. The test specimens were divided into two series; Series-I included fourteen specimens made of a concrete strength of 50 MPa and series-II involved six specimens with a concrete strength of 30 MPa. The test variables among the specimens of each series were: (1) the reinforcement stiffness; and (2) the reinforcement shape. The substrate interface surface between the interconnected blocks of the push-off specimen was left as-cast

5.2 Conclusions

Based on the detailed and parametric analysis of the test results of the push-off specimens of the present study, the following conclusions can be drawn:

- There is a minimum requirement of the reinforcement stiffness perpendicular to the

interface plane of 203 N/mm^2 that has to be met in order to activate the role of the GFRP shear transfer reinforcement in providing additional shear frictional resistance post to the cracking of the interface.

- Specimens with low GFRP reinforcement content fail immediately at cracking load which is dominated by the concrete interface resistance. Practically, the reinforcement did not play any role in the resistance. However, the presence of the reinforcement reduced the violent brittle failure mode associate with unreinforced concrete interfaces.
- The strain in the GFRP reinforcement at the ultimate, when the minimum reinforcement requirement is satisfied, was in the range of 3000 to 5000 $\mu\varepsilon$.
- The reinforcement stiffness was found to be the dominant parameter in the shear transfer mechanism. Interfaces with GFRP headed bars and stirrups having similar stiffness were found to exhibit similar behaviour and strength.
- GFRP reinforced interfaces with headed bars and stirrups showed a remarkable ductility and post-ultimate load carrying capacity, particularly, when GFRP headed bars were used.
- For appropriately reinforced interfaces with GFRP reinforcement, the shear transfer strength increases more with the reinforcement stiffness for higher concrete strength.
- Higher concrete compressive strength would result in higher shear transfer strength and a stiffer precracked part of the load-deformation response, if the reinforcement stiffness is higher than the minimum specified above.

- For appropriately reinforced interfaces, the slip at the ultimate load was in the range of 0.37 to 0.94 mm and the average lateral separation of the faces of the interface was about 0.27 mm. Because of these limited values of deformations associated with GFRP reinforced interfaces at the ultimate, there is no concern regarding the serviceability requirements which are usually the most warranted in FRP reinforced concrete elements.

5.3 Future Work

The following recommendations are suggested for future work on this topic:

- The influence of high strength or/and lightweight concrete on the shear transfer strength and behaviour requires further study.
- The shear transfer mechanism and strength of concrete joints with smooth and intentionally roughened interfaces need to be investigated.
- The behaviour of the GFRP reinforced joints under fatigue and sustained loads is recommended to be explored.

REFERENCES

AASHTO LFRD Bridge Design Specefications (6 ed.). (2012). American Association of State Highway and Transportation Officials, ISBN 978-1-56051-523-4.

AASHTO Standard Specefications for Highway Bridges (17 ed.). (2002). American Association of State Highway and Transportation Officials, ISBN 156051-171-0.

ACI Committee 318. (1963). *Building requirements for Reinforced Concrete (ACI 318-63).* Detroit, Michigan, USA: American Concrete Institute.

ACI Committee 318. (1995). *Building requirements for Reinforced Concrete (ACI 318-95) and Commentary (ACI 318R-95).* Farmington Hills, MI, USA: American Concrete Institute.

ACI Committee 318. (1999). *Building requirements for Reinforced Concrete (ACI 318-99) and Commentary (ACI 318R-99).* Farmington Hills, MI, USA: American Concrete Institute.

ACI Committee 318. (2014). *Building Code Requirements for Structural Concrete (ACI 318-14) and Commentary (ACI 318R-14).* Farmington Hills, MI, USA: American Concrete Institute.

ACI Committee 440. (2015). *Guide for the Design and Construction of Structural Concrete Reinforced with FRP bars ACI 440.1R-2015.* Farmington Hills, MI, USA: American Concrete Institute.

ACI Committee 711. (1953). Minimum Standard Requirements for Precast Concrete Floor Units (ACI 711-53). *ACI Journal Proceedings, 50*(9), 1-15.

ACI Committee 711. (1953). Minimum Standard Requirments for Precast Concrete Floor Units (ACI 711-53). *Journal of the American Concrete Institute* , 7-8.

ACI-ASCE Committee 333. (1960, December). Tentative Recommendations for Designof Composite Beams and Girders for Building. *ACI Journal*, 609-628.

Ali, M. A., & White, R. N. (1999). Enhanced Contact Model for Shear Friction of Normal and High-Strength Concrete. *ACI Structural Journal, 96*(3), 348-361.

Anderson, A. R. (1960, September). Composite Deisgns in Precast and Cast-in-Place

Concrete. *Progressive Architecture, 41*(9), 172-179.

ASTM A615. (2015). *Standard Specification for Deformed and Plain Carbon-Steel Bars for Concrete Reinforcement.* West Conshohocken, PA: ASTM International.

ASTM C39. (2015). *Standard Test Method for Compressive Strength of Cylindrical Concrete Specimens.* West Conshohocken, PA: ASTM International.

ASTM C496. (2011). *Standard Test Method for Splitting Tensile Strength of Cylindrical Concrete Specimens.* West Conshohocken, PA: ASTM International.

Badoux, J. C., & Husbos, C. L. (1967, December). Horizontal Shear Connection in Composite Concrete Beams under Repeated Loads. *ACI Journal, 64*(12), 811-819.

Basler, E., & Witta, E. (1966). Discussion of "Connections in Precast Concrete Construction". *ACI Journal, proceedings, 63*, 1027.

Basler, E., & Witta, E. (1966). Discussion of "Connections in Precast Concrete Construction". *ACI Journal Proceedings, 63*, 1027.

Beer, F., Johnston, J. E., DeWolf, J., & Mazurek, D. (2014). *Mechanics of Materials* (7 ed.). McGaw-Hill Education.

Birkeland, H. W. (1968). Precast and Prestressed Concrete, class notes for course. *University of British Columbia*.

Birkeland, P. W., & Birkeland, H. W. (1966). Connections in Precast Concrete Construction. *ACI Journal*, 345-367.

Canadian Standards Association (CSA). (2009). *Carbon Steel bars for Concrete Reinforcement CAN/CSA G30.18-09.* Mississauga, Ontario, Canada: Canadian Standards Association.

Canadian Standards Association (CSA). (2012). *Design and Construction of Building Structures with Fiber-Reinforced Polymers CAN/CSA S806-12.* Mississauga, Ontario, Canada: Canadian Standards Association.

Canadian Standards Association (CSA). (2014). *Canadian Highway Bridge Design Code CAN/CSA-S6-14.* Mississauga, Ontario, Canada: Canadian Standards Association.

Candaian Standards Association (CSA). (2004). *Design of Concrete Structures for*

Buildings CAN/CSA A23.3-04. Rexdale, Ontario, Canada: Canadian Standards Association.

CTA 76-B4 Composite Systems Without Ties. (1976). Tacoma, Washington: Concrete Techology Associates.

European Committee for Standardization. (2004). *EN 1992-1-1 Eurocode 2: Design of concrete structures - Part 1-1: General rules and rules for buildings.*

Gaston, J. R., & Kriz, L. B. (1964, June). Connections in Precast Concrete structures - Scarf Joints. *PCI Journal, 9*(3), 37-59.

Gohnert, M. (2003). Horizontal shear transfer across a roughened surface. *Elsevier, Cement and Concrete Composites, 25*(3), 379-385.

Hanson, N. (1960). Precast-Prestressed Concrete Bridges 2.Horizontal Shear Connections. *PCA Journal, 2*(2), 38-58.

Harries, K., Zeno, G., & Shahrooz, B. (2012). Toward an Improved Understanding of Shear-Friction Behaviour. *ACI Structural Journal, 109*(6), 835-844.

Hofbeck, J., Ibrahim, I., & Mattock, A. (1969). Shear Transfer in Reinforced Concrete. *ACI Journal, 66*(2), 119-128.

Hsu, T. T., Mau, S. T., & Chen, B. (1987). Theory of Shear Transfer Strength of Reinforced Concrete. *ACI Structural Journal, 84*(2), 149-160.

Hwang, S. J., Yu, H. W., & Lee, H. J. (2000). Theory of Interface Shear Capacity of Reinfroced Concrete. *Journal of Structural Engineering, 126*(6), 700-707.

Khan, L., & Mitchell, A. (2002, February). Shear Friction Tests with High-Strength Concrete. *ACI strucutral Journal, 99*(1), 98-103.

Khan, L., & Slapkus, A. (2004). Interface Shear in High Strength Composite T-beams. *PCI Journal, 49*(4), 102-110.

Loov, R. (1978). Design of Precast Connections. *Paper presented at a seminar orgnized by Compa International Pte, Ltd*, 8 pages.

Loov, R. E., & Patnaik, A. K. (1994). Horizontal Shear Strength of Composite Concrete Beams with Rough Interfaces. *PCI Journal, 39*(1), 48-69.

Mansur, M. A., Vinayagam, T., & Tan, K. H. (2008, April). Shear Transfer across a crack in Reinforced High-Strength Concrete. *American Society of Civil Engineers, Journal of Materials in Civil Engineering, 20*(4), 294-302.

Mast, R. F. (1968, June). Auxiliary Reinforcement in Concrete Connections. *American Society ofCivil Engineers, Journal of Structural Division, 94*(ST6), 1485-1505.

Mattock, A. H. (1974, January). Shear Transfer in Concrete Having Reinforcement at an Angle to the Shear Plane. *American Concrete Institute, Special Publicatio 42*, 17-42.

Mattock, A. H. (1988, January-February). Reader Comments on "Influence of Concrete Strength and Load History on the Shear Friction Capacity of Concrete Members" by Walraven et al. *PCI Journal, 33*(1), 165-166.

Mattock, A. H. (1994, Spetember-October). Reader Comments on "Horizontal Shear Strength of Composite Concrete Beams with a Rough Interface" by Loov and Patnaik. *PCI Journal, 39*(5), 106-108.

Mattock, A. H. (2001, January-February). Shear friction and high-strength concrete. *ACI Structutral Journal, 98*(1), 50-59.

Mattock, A. H. (2001, January-February). Shear Friction and High-Strength Concrete. *ACI Structural Journal, 98*(1), 50-59.

Mattock, A. H., & Hawkins, N. M. (1972, March-April). Shear Transfer in Reinforced Concrete-Recent Research. *PCI Journal, 17*(2), 55-75.

Mattock, A. H., & Kaar, P. H. (1961, January). Precast-Prestressed Concrete Bridges, 4. Shear Tests of Continous Girders. *PCI Journal, 3*(1), 19-46.

Mattock, A. H., Johal, L., & Chow, H. C. (1975, July-August). Shear Transfer in Reinforced Concrete with Moment or Tension Across the Shear Plane. *PCI Journal, 20*(1), 76-93.

Mattock, A. H., Li, W. K., & Wang, T. C. (1976, January-February). Shear Transfer in lightweight reinforced concrete. *Precast/Prestressed Concrete Institute, PCI Journal, 21*(1), 20-39.

Mau, S., & Hsu, T. (1988, January-February). Reader Comments on "Influence of Concrete Strength and Load History on the Shear Friction Capacity of Concrete Members"

by Walraven et al. *PCI Journal, 33*(1), 166-168.

Papanicolaou, C. G., & Triantafillou, T. C. (2002, May). Shear transfer capacity along pumice aggregate concrete and high-performance concrete interfaces. *RILEM, Materials and Structures, 35*(4), 237-245.

Park, R., & Paulay, T. (1975). *Reinforced Concrete Structures.* John Wiley & Sons.

Patnaik, A. H. (2001, April). Behaviour of Composite Concrete Beams with Smooth Interface. *Journal of Structural Engineering, 127*(4), 359-366.

Paulay, T., Park, R., & Phillips, M. H. (1974). Horizontal Construction Joints in Cast-in-Place Reinforced Concrete. *ACI Special Publication SP-42: Shear in Reinforced Concrete, Vol. 2, American Concrete Institute, Detroit*, 559-611.

Pianca, F., Schell, H., & Cautillo, G. (2005). The performance of epoxy coated reinforcement: experience of the Ontario ministry of transportation. *International Journal of Materials and Product Technology, 23*(3-4), 286-308.

Randi, N. (1997). *Investigation on Transfer of Forces Between Old and New Concrete at Different Joint Roughness, PhD thesis.* Austria: University of Innsbruck.

Raths, C. H. (1977). Reader Comments on "Design Proposals for Reinforced Concrete Corbels" by Mattock, A. H. *PCI Journal, 22*(2), 93-98.

SABS 0100-1. (1992). *The Structural use of Concrete.* Pretoria: The council of South Africa Bureau of Standards.

Saemann, J. C., & Washa, G. W. (1964). Horizontal Shear Connections Between Precast Beams and Cast-in-Place Slabs. *Journal of American Concrete Institute, 61*(11), 1383-1409.

Shaikh, A. F. (1978, March-April). Proposed Revisions to Shear-Friction Provisions. *PCI Journal*, 12-21.

Shaw, D. M., & Sneed, L. H. (2014). Interface Shear Transfer of Lightweight-Aggregate Concrete Cast at Different Times. *PCI Journal*, 130-144.

Valluvan, R., Kreger, M. E., & Jirsa, J. O. (1999, July-August). Evaluation of ACI 318-95 Shear-Friction Provisions. *ACI Structural Journal, 96*(4), 473-483.

Vecchio, F. J., & Collins, M. P. (1986). The Modified Compression-Field Theory for Reinforced Concrete Elements Subjected to Shear. *ACI Journal, 83*(2), 219-231.

V-ROD. (2016). *Fiber Glass Reinforcement*. Retrieved from http://www.vrod.ca/en/Fiberglass-reinforcement/Civil-Engineering

Walraven , J., & Stroband, J. (1994). Shear Friction in High-Strength Concrete. *ACI Special Publication, 149*, 311-330.

Walraven, J. C. (1981). Fundamental analysis of aggregate interlock. *Journal of Structural Division, 107*(ST11), 2245-2270.

Walraven, J. C., & Reinhardt, H. W. (1981). Theory and Experiments on the Mechanical Behaviour of Cracks in Plain and Reinforced Concrete Subjected to Shear Loading. *Heron, 26*(1A).

Walraven, J., Frénay, J., & Pruijssers, A. (1987, January-February). Influence of Concrete Strength and Load Histrory on the Shear Friction Capacity of Concrete Members. *PCI Journal, 32*(1), 66-84.

Wight, J. K., & MacGregor, J. G. (2011). *Reinforced Concrete Mechanics and Design* (6 ed.). Prentice Hall.

Zeno, G. A. (2009). *Use of High Strength Steel Reinforcement in Shear Friction Applications, MASE thesis.* Pittsburgh, PA: University of Pittsburgh.

VITA AUCTORIS

NAME: Jehad Alkatan

PLACE OF BIRTH: Syria

YEAR OF BIRTH: 1988

EDUCATION: Damascus University, Damascus, Syria
2005-2010 B.A.Sc. in Civil Engineering

University of Windsor, Windsor, Ontario, Canada
2014-2015 Honours Certificate in Civil Engineering

University of Windsor, Windsor, Ontario, Canada
2015-2016 M.A.Sc. in Civil Engineering/Structural